

Novel Strategies for the Inhibition of Biofilm Formation on Polymer Surfaces

Von der Fakultät für Mathematik, Informatik und Naturwissenschaften
der Rheinisch-Westfälischen Technischen Hochschule Aachen
zur Erlangung des akademischen Grades
eines Doktors der Naturwissenschaften
genehmigte Dissertation

vorgelegt von

Diplom-Pharmazeutin
Carla Terenzi

aus Pescara, Italien

Berichter: Universitätsprofessor Dr. rer. nat. Hartwig Höcker
 Universitätsprofessor Dr. rer. nat. Doris Klee

Tag der mündlichen Prüfung: 18.Mai 2006

Diese Dissertation ist auf den Internetseiten der Hochschulbibliothek online verfügbar.

Danksagung

Die vorliegende Arbeit wurde auf Anregung und unter Leitung von Herrn Professor Dr. rer. nat. Hartwig Höcker am Lehrstuhl für Textilchemie und Makromolekulare Chemie der Rheinisch-Westfälisch-Technischen Hochschule Aachen in der Zeit von Januar 2002 bis Mai 2006 durchgeführt.

Mein besonderer Dank gilt Herrn Professor Dr. Hartwig Höcker für die hochinteressante Themenstellung und die wissenschaftliche Unterstützung bei der Durchführung dieser Arbeit.

Professor Dr. Doris Klee danke ich für die wissenschaftliche Betreuung und die freundliche Übernahme des Korreferats.

Ein herzlicher Dank geht an Dr. Jochen Salber, Dr. Rui Miguel Paz und Jean Heuts für das Korrekturlesen dieser Arbeit. Der gesamten Arbeitsgruppe Biomaterialien möchte ich für die stets vorhandene Hilfsbereitschaft, die zahlreiche Diskussionen, und die freundschaftliche Atmosphäre danken. Bei allen Mitarbeitern des Deutschen Wollforschungsinstituts möchte ich mich für die gute Zusammenarbeit bedanken.

Index

1	Introduction	1
1.1	Biofilm formation on artificial polymer surfaces	1
1.2	Antimicrobial strategies currently used in the treatment of infectious disease and the problem of bacterial resistance	6
1.2.1	Conventional antimicrobial therapies based on bactericides and bacteriostatics	6
1.2.2	The problem of bacterial resistance	10
1.3	Modern strategies for prevention and defense against bacterial infections.....	11
1.3.1	Different approaches to the generation of antimicrobial surfaces	11
1.3.2	Novel concepts for the generation of antibacterial surfaces interfering with the quorum sensing mechanism.....	14
1.4	Potential antagonists for QS receptors	17
1.4.1	Secondary metabolites as QS receptor antagonists	18
1.4.1.1	<i>Delisea pulchra</i> -derived halogenated furanones.....	18
1.4.1.2	Coagulase negative staphylococci-derived RIP	20
2	Aim of the thesis	23
3	Results and discussion	25
3.1	Application of 3-butyl-5-(bromomethylene)-2(5H)-furanone as QS antagonist incorporated into PDLLA films	25
3.1.1	Synthesis of 3-butyl-5-(bromomethylene)-2(5H)-furanone	25
3.1.2	Isolation, purification, and characterization of 3-butyl-5-(bromomethylene)-2(5H)-furanone	31
3.1.3	Isolation and characterization of a furanone derivatives mixture.....	33
3.2	Preliminary investigations on the inhibition of biofilm formation on PDLLA by incorporation of 3-butyl-5-(bromomethylene)-2(5H)-furanone.....	36
3.2.1	Preparation of PDLLA films containing 2-(2-bromoethyl)-2,5,5-trimethyl-1,3-dioxane and characterization of their <i>in vitro</i> release properties.....	36

3.2.2	Preparation of PDLLA films containing 3-butyl-5-(bromomethylene)-2(5H)-furanone and characterization of their <i>in vitro</i> release properties.....	39
3.3	Application of RIP as a QS antagonist immobilized on a biomaterial surface	41
3.3.1	RIP molecule synthesis by using the principles of solid-phase peptide chemistry.....	41
3.3.2	Isolation and purification of RIP	45
3.3.2.1	Ion exchange chromatography.....	45
3.3.2.2	Reverse phase medium pressure liquid chromatography	46
3.3.3	Characterization of RIP	48
3.3.3.1	Reverse phase high performance liquid chromatography	48
3.3.3.2	Matrix-assisted laser desorption ionization time of flight mass spectrometry	49
3.3.3.3	Amino acid analysis	50
3.4	Prevention of biofilm formation by covalent immobilization of a synthetic RIP on functionalized PVDF	52
3.4.1	Functionalization of PVDF surfaces	52
3.4.2	Qualitative and quantitative characterization of PVDF-g-PAAc surfaces	53
3.4.3	Covalently immobilized RIP on PVDF-g-PAAc surfaces	70
3.4.4	Evaluation of the antibacterial properties of PVDF-g-PAAc surfaces covalently modified with RIP by means of microbiological <i>in vitro</i> tests	72
3.5	Antimicrobial and antifungal PDMS with Kathon® 910 SB.....	74
3.5.1	Preparation of unloaded PDMS microspheres and PDMS microspheres loaded with 30 weight-% of Kathon® 910 SB.....	75
3.5.2	Investigation of the biocidal properties of Kathon® 910 SB-loaded PDMS microspheres	78
4	Experimental section	83
4.1	Analytic methods and equipment	83
4.1.1	Nuclear magnetic resonance spectroscopy	83
4.1.2	UV/VIS spectroscopy	83
4.1.3	Analytical reverse phase high performance liquid chromatography	83

4.1.4	Matrix-assisted laser desorption ionization time of flight mass spectrometry	84
4.1.5	Amino acid analysis	84
4.1.6	White light interferometry	85
4.1.7	X-ray photoelectron spectroscopy.....	85
4.1.8	Attenuated total reflection-infrared spectroscopy	85
4.1.9	Raman spectroscopy	86
4.1.10	Contact angle measurements	86
4.1.11	Zeta potential measurements.....	86
4.2	Chemicals and materials.....	87
4.3	Preparation of 3-butyl-5-(bromomethylene)-2(5H)-furanone.....	89
4.3.1	Preparation of diethyl 2-acetyl-3-butylbutanedioate	89
4.3.2	Preparation of 2-(2-oxopropyl)hexanoic acid (pathway A)	90
4.3.3	Preparation of 2-(2-oxopropyl)hexanoic acid (pathway B)	90
4.3.4	Preparation of 2-(1,3-dibromo-2-oxopropyl)-hexanoic acid.....	91
4.3.5	Alternative way for the preparation of 2-(1,3-dibromo-2-oxopropyl) hexanoic acid.....	92
4.3.6	Preparation of 3-butyl-5-(bromomethylene)-2(5H)-furanone.....	92
4.4	Preparation of PDLLA films loaded with active agent	93
4.5	<i>In vitro</i> release experiments.....	93
4.6	Synthesis, isolation and purification of RIP-NH ₂	94
4.6.1	Coupling of the first amino acid (Fmoc-Phe) to the resin	94
4.6.2	Determination of resin loading by Fmoc cleavage	94
4.6.3	Capping procedure	94
4.6.4	Activation of the amino acids and coupling reactions.....	95
4.6.5	Kaiser test.....	95
4.6.6	Coupling protocol for Fmoc- solid-phase peptide synthesis.....	96
4.6.7	Cleavage of RIP-NH ₂ peptide from the resin.....	96
4.6.8	Purification of RIP-NH ₂ by means of column chromatography (ion exchange chromatography and reverse phase medium pressure liquid chromatography).....	97
4.7	Modification of PVDF surfaces.....	97
4.7.1	Preparation of PVDF foils.....	97
4.7.2	Plasma treatment.....	98

4.7.3	Graft copolymerisation of acrylic acid	99
4.7.4	Quantification of the carboxyl group content of PVDF-g-PAAc surfaces by means of toluidine blue staining.....	99
4.7.5	Quantification of the carboxyl group content of PVDF-g-PAAc surfaces by means of pH-titration	99
4.7.6	Covalent immobilization of RIP-NH ₂	100
4.7.7	Quantification of immobilized model peptide YRGDS by radioactive labeling with ¹²⁵ Iodine	100
4.7.8	Evaluation of the antibacterial properties of PVDF-g-PAAc surfaces covalently modified with RIP by means of picoGreen assay	102
4.8	Preparation of microspheres	102
4.8.1	Preparation of Kathon® 910 SB-loaded PDMS microspheres and unloaded PDMS microspheres	102
4.9	Investigation of the biocidal properties of Kathon® 910 SB-loaded PDMS microspheres	103
4.9.1	Agar diffusion hole test and dilution test.....	103
5	Literature	104

Abbreviations

AAc	acrylic acid
ABC	ATP-binding cassette
AHL	N-acylated homoserine lactone
AI	autoinducer
AIP	autoinducing peptide
ASA	amino acid analysis
ATR-IR	attenuated total reflection infrared spectroscopy
BCI	biomaterial-centered infection
BSA	bovine serum albumin
ca.	circa
CV	central venous
d	day
DABCO	1,4-diazabicyclo[2.2.2]octane
DBF	dibenzofulvene
DCOIT	4,5-dichloro-N-octyl-isothiazolin-3-one
DIC	diisopropylcarbodiimide
DIPEA	N,N- diisopropylethylamine
dist.	distilled
DMF	dimethyl formamide
DNA	deoxyribonucleic acid
dsDNA	double-strained DNA
EDC	N-ethyl-N'-(3-dimethylaminopropyl)-carbodiimid- hydrochloride
e.g.	<i>exempla gratia</i>
EPS	extracellular polymer substances
et al.	<i>et alteres</i>
FDA	Food and Drug Administration
Fmoc	fluorenylmethyloxycarbonyl
HOBt	1-hydroxybenzotriazole
i.e.	<i>idest</i>
IEC	ion exchange chromatography

IEP	isoelectric point
IRE	internal reflection element
MALDI-ToF-MS	matrix-assisted laser desorption ionization -time of flight- mass spectrometry
M_t/M_0	fractional amount of the active agent released at time point t
MTBE	methyl- <i>tert</i> -butyl-ether
NHS	N-hydroxysuccinimide
NMR	nuclear magnetic resonance spectroscopy
o/w	oil in water emulsion
p.a.	pro analysis
PAAc	polyacrylic acid
PBS	phosphate buffered saline
PDLLA	poly(D,L-lactide)
PDMS	poly(dimethyl siloxane)
PEG	polyethylene glycol
PEO	polyethylene oxide
HEMA	polyhydroxyethylmethacrylat
POO•	peroxy radicals
POOH	hydroperoxides
POOP	peroxides
ppm	<i>parts per million</i>
PVA	polyvinylalcohol
PVDF	poly(vinylidene fluoride)
PVDF-g-PAAc	PVDF grafted with PAAc
QAS	3-(trimethoxysilyl)-propyldimethyloctadecylammonium chloride
QS	quorum sensing
RAP	RNA III activating peptide
R_f	ratio of fronts
RIP	RNA III inhibiting peptide
RIP-NH ₂	RNA III inhibiting peptide amide
RNA	ribonucleic acid

R _m	parameter of the surface roughness, average maximum height of the profile
RP-HPLC	reverse phase- high performance liquid chromatography
rpm	rotation per minute
RP-MPLC	reverse phase- medium pressure liquid chromatography
R _q	parameter of the surface roughness, root mean roughness
R _{ti}	parameter of the surface roughness, height of the profile
sccm	standard cubic centimetre
SEM	scanning electron microscopy
SPPS	solid phase peptide synthesis
t	time
<i>t</i> -Boc	<i>tert</i> -butyloxycarbonyl
TB	toluidine blue
TBTU	o-(benzotriazol-1-yl)-N,N,N',N'-tetrametyuronium tetrafluoroborate
TCA	trichloro acetic acid
TES	triethylsilane
TFA	trifluoro acetic acid
TLC	thin layer chromatography
TRAP	target protein of RAP
UT	urinary tract
UV/VIS	ultraviolet/visible
WIM	white light interferometry
XPS	X-ray photoelectron spectroscopy
YKPITN	RAP
YSPWTNF	RNA III inhibiting peptide
YSPWTNF-NH ₂	RNA III inhibiting peptide-amide

The abbreviations of the amino acids follow the nomenclature rules of the IUPAC-IUB-commission (*J. Biol. Chem.*, **241**, (1961), 2491; *Biochem J.*, **126**, (1972), 773)

Summary

Microbial adhesion to the surfaces of implanted biomaterial and the formation of complex biofilms at the interface between a biomaterial and the biological environment frequently result in device-associated or biofilm-related infections. These infections are extremely difficult to eradicate and are common causes of morbidity and mortality. During biofilm formation, the adherent bacterial cells metabolize nutrients, grow, divide and secrete a polysaccharide matrix, which binds the cells firmly to the surface. Once embedded in these biofilm layers, bacteria are protected against the host's immune cells and antimicrobial agents. Moreover, development of bacterial resistance to antibiotics limits the presently available therapeutic approaches. The organization of the biofilm into a complex structure is regulated by the exchange of chemical signals between the bacterial cells in a mechanism known as quorum sensing (QS). Thus, to prevent biofilm development by interfering with the QS mechanism could provide a novel approach to combat biofilm-related infections.

The aim of this work was the development of new strategies to prevent bacterial adhesion and biofilm formation on biomaterial surfaces, based on compounds that inhibit the QS mechanism. Two different anti-QS molecules were used: 3-butyl-5-(bromomethylene)-2(5H)-furanone, and the RNA III inhibiting peptide (RIP).

3-Butyl-5-(bromomethylene)-2(5H)-furanone is one of the secondary metabolites, called halogenated furanones or fimbriolides, produced by the Australian macroalga *Delisea pulchra* to protect its surface from colonization and fouling by marine organisms. In order to mimic the defense mechanism evolved by the macroalga, 3-butyl-5-(bromomethylene)-2(5H)-furanone was synthesized and incorporated into films of the commonly used biodegradable biopolymer poly(D,L-lactide) (PDLLA) (Resomer[®] 208).

The synthesis of 3-butyl-5-(bromomethylene)-2(5H)-furanone consisted of 6 reaction steps. Ethyl-2-bromohexanoate was used as starting molecule. In the first

reaction step ethyl-2-bromohexanoate was condensed with ethylacetoacetate to yield diethyl-2-acetyl-3-butylbutanedioate. Subsequently, the diester was hydrolysed and decarboxylated. The obtained γ -keto acid (2-(2-oxopropyl) hexanoic acid) was brominated. The brominated derivatives were cyclised and dehydrobrominated to give a mixture of different furanone derivatives. This mixture was purified by preparative thin layer chromatography (TLC). 3-Butyl-5-(bromomethylene)-2(5H)-furanone was obtained in a good grade of purity. The compound was analyzed by means of ^1H -NMR and UV spectroscopy. The ^1H -NMR spectrum was in agreement with literature. The UV spectrum of 3-butyl-5-(bromo-methylene)-2(5H)-furanone, measured in EtOH/H₂O (50:50, [v/v]), showed a characteristic well-defined band at $\lambda_{\text{max}} = 287 \text{ nm}$. Purification of the mixed furanone derivatives by preparative TLC yielded, beside the pure 3-butyl-5-(bromomethylene)-2(5H)-furanone, a mixture of three compounds, which could not be separated. ^1H -NMR spectroscopy demonstrated that this mixture consisted of 3-butyl-5-(dibromomethylene)-2(5H)-furanone, 4-bromo-5-(bromomethylene)-3-butyl-2(5H)-furanone, and 3-butyl-5-methylene-2(5H)-furanone.

The release kinetics of the QS inhibitor from the PDLLA films was studied. A preliminary investigation of agent-loaded PDLLA film preparations and the characterization of their *in vitro* release properties was carried out using 2-(2-bromoethyl)-2,5,5-trimethyl-1,3-dioxane as model compound. PDLLA films containing 5% [w/w] of 2-(2-bromoethyl)-2,5,5-trimethyl-1,3-dioxane and PDLLA films containing 1% [w/w] of 3-butyl-5-(bromomethylene)-2(5H)-furanone were prepared. The *in vitro* release experiments showed a diffusion controlled mechanism for both compounds. Fitted data demonstrated a release exponent of around 0.5.

RIP is a seven-amino-acids long peptide (YSPWTNF), which has been shown to be an effective inhibitor of the QS mechanisms in *Staphylococcus aureus* and *Staphylococcus epidermidis*. So far, only the use of this peptide as non-covalently bound (i.e. adsorbed) coating has been investigated, but the efficacy of covalently immobilized RIP on biomaterials has not yet been assessed. Therefore, it was

decided to synthesize RIP and to covalently attach it to the non-degradable fluorinated homopolymer polyvinylidene fluoride (PVDF).

The more stable amid form of the RIP peptide was synthesized by means of solid phase peptide synthesis (SPPS), using the fluorenylmethyloxycarbonyl (Fmoc)-protecting group strategy. The peptide was purified by ion exchange chromatography (IEC) followed by reverse phase medium pressure liquid chromatography (RP-MPLC). Reverse phase high performance liquid chromatography (RP-HPLC) demonstrated that a peptide purity of ca. 99 % was achieved. The proper composition of the peptide was confirmed by amino acid analysis. A mass profile was generated by means of MALDI-ToF-MS, two m/z values were seen, 913,438 Da (regular) and 935,456 Da (for the sodium form from the matrix).

As PVDF does not possess functional groups, which allow a surface modification, a plasma-induced graft polymerization method was applied for the activation and the functionalisation of the polymer surface. First, the samples were treated by a low-pressure MW-induced Ar-plasma. Subsequently, peroxides and hydroperoxides were generated on the surfaces by exposure to air. To functionalize the oxidized PVDF substrates acrylic acid (AAc) was graft-co-polymerized onto their surface. PVDF samples were characterized after every modification step. First of all, surface topography was characterized by means of white light interferometry. After Ar-plasma treatment no relevant modification of the topography of the surface could be determined. Graft-co-polymerization of AAc led to a strong roughness increase. The generation of hydroperoxides on PVDF surfaces after Ar-plasma treatment was proven by means of XPS, which showed an oxygen content increase and a fluorine content decrease. The successful grafting of PAAc on the plasma activated PVDF surface was demonstrated by the appearance of a strong carbonyl stretching band at 1710 cm^{-1} in the ATR-IR spectrum. After AAc grafting no fluorine could be detected by means of XPS. As a result of the introduction of carboxylic acid groups the oxygen content increased and a new photo line at 289.1 eV characteristic for the carbon in carboxyl groups was detected in the C1s-spectra. A homogeneous distribution of carboxyl groups on the PVDF-g-PAAc surface was further confirmed by Raman spectroscopy. To characterize the grafted PAAc layer under aqueous conditions contact angle

measurements, according to the captive bubble method, and zeta-potential measurements were carried out. The contact angle measurements established, that the PVDF-g-PAAc surfaces possess a strong hydrophilic nature. The zeta-potential measurements indicated, that the surface coverage of PVDF-g-PAAc with carboxylate groups is exceedingly high and has its maximum above pH 8.0. The carboxyl groups concentration on PVDF-g-PAAc was determined to be 0.42 nmol/mm² by means of UV/VIS spectrophotometry and 3 nmol/mm² by means of automated potentiometric acid-base titration.

The RIP-NH₂ peptide was coupled to the carboxyl groups of the PAAc-layer by means of the water soluble carbodiimide method. Two different concentrations of the RIP-NH₂ solution were used for the coupling reaction, 20 µg/ml and 10 µg/ml. In order to obtain information about the effective amount of RIP-NH₂ covalently attached to PVDF-g-PAAc surface, radioactive binding studies were carried out using a ¹²⁵I-labelled model peptide, YRGDS. Equivalent to the bioligand RIP-NH₂, Y(¹²⁵I)RGDS was covalently bound to the PVDF-g-PAAc surface. Three different Y(¹²⁵I)RGDS coupling solution concentrations were investigated, 10 µg/ml, 50 µg/ml, and 100 µg/ml. An amount of about 30 ng/cm² of ¹²⁵I-labelled YRGDS was detected on the PVDF-g-PAAc surface, when the 10 µg/ml peptide solution was used for the coupling reaction. This amount increased to ca. 1150 ng/cm² and 2100 ng/cm², when solutions of 50 µg/ml and 100 µg/ml of Y(¹²⁵I)RGDS were used, respectively. On the basis of these studies it could be assumed that around 30 ng/cm² of RIP-NH₂ were covalently attached to the PAAc modified PVDF surface, when the coupling reaction was performed with the 10 µg/ml bioligand solution. An amount of immobilized RIP-NH₂ between 30 ng/cm² and 1150 ng/cm² is expected for the 20 µg/ml coupling solution.

Finally, the antibacterial properties of RIP-NH₂-coated PVDF surfaces were determined *in vitro* by means of a pico-Green assay using *Staphylococcus aureus* (ATCC 29213). The obtained results demonstrated that RIP-NH₂ immobilized on PAAc-g-PVDF was able to considerably reduce bacterial adhesion. Stronger antibacterial properties were achieved, when the immobilization reaction was performed in the 10 µg/ml peptide solution. This suggested that there is an optimal effective concentration for covalently bound RIP-NH₂.

Another part of this work deals with the encapsulation of Kathon[®] 910 SB from the company ROHM AND HAAS (Germany) into poly(dimethyl siloxane) (PDMS) microspheres. Kathon[®] 910 SB possesses excellent effectiveness against a wide range of fungi and bacteria and has been specifically designed to protect silicone sealants from bacterial and fungal attack. PDMS-microspheres containing 30 weight-% of Kathon[®] 910 SB were prepared in order to assess the antibacterial and fungicidal properties of the Kathon[®] 910 SB once incorporated in this system. Kathon[®] 910 SB-loaded microspheres with a size smaller than 125 µm were synthesized according to the o/w solvent evaporation method, using Sylgrad[®] 184 from the company Dow Corning (Germany) as base material. The antibacterial and antifungal properties of the prepared microspheres were investigated by means of dilution tests and agar diffusion hole tests. Compared to the Kathon formulation, the Kathon loaded microspheres were less effective against the two bacterial strains used in the dilution test, *Staphylococcus aureus* and *Pseudomonas aeruginosa*. However, they showed a good antifungal activity in both tests.

1 Introduction

1.1 Biofilm formation on artificial polymer surfaces

The vast majority of microorganisms live in their natural environment in protective communities known as biofilms. A biofilm community can include bacteria, fungi, yeasts, protozoae and other organisms usually encased in an extracellular polysaccharide (slime) that they themselves secrete¹. It may form essentially on any environmental surface on which sufficient moisture is present, like

- on solid substrates in contact with moisture
- on soft tissue surfaces in living organisms
- at liquid air interfaces

The development of a biofilm is characterized by a series of complex and well-regulated steps. The exact molecular mechanism differs from organism to organism, but the sequence of events is similar across a wide range of them (Fig. 1).

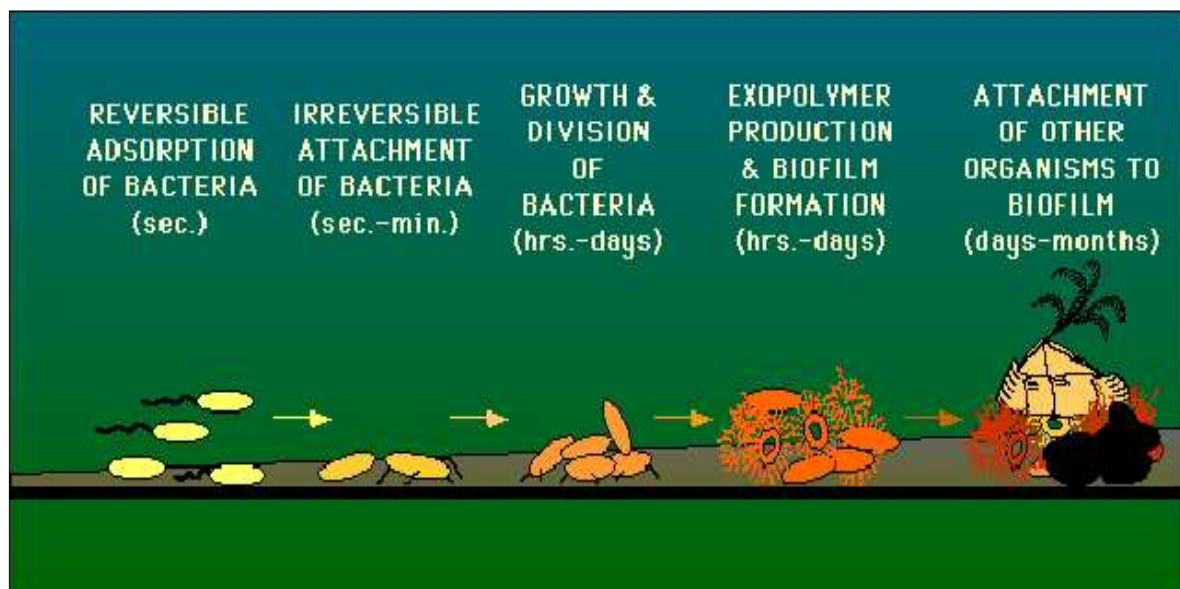


Fig. 1: Model of biofilm formation on a surface involving different steps: reversible attachment, irreversible attachment, accumulation and maturation²

The formation of a biofilm starts with the adhesion of bacteria to surfaces by effects of physical forces, such as Brownian motion, van der Waals attraction forces, gravitational forces, electrostatic and hydrophobic interactions¹. If the association between the bacterium and its substrate persists long enough, molecular-specific reactions between bacterial surface structures and substratum surfaces become predominant, transforming the reversible adsorption to a permanent and essentially irreversible attachment. Once anchored to the surface the microorganisms start growing dividing and secreting a slimy matrix, based on extracellular polymer substances (EPS), which binds the microorganisms together. EPS are biopolymers which form hydrogels with water and provide a stable structure to the biofilm. Most of these biopolymers are polysaccharides consisting of sugar such as glucose, galactose, mannose and fructose, but also traces of proteins, lipids and nucleic acids are present³. This growing biofilm serves as focus for the attachment and growth of other organisms increasing the biological diversity of the community. As shown in Fig. 2, expanded growth evolves into complex 3-D structures of tower- and mushroom shaped cell clusters all connected by water channels, that serve as a primitive circulatory system for delivery of nutrients and removal of wastes^{1,4}.

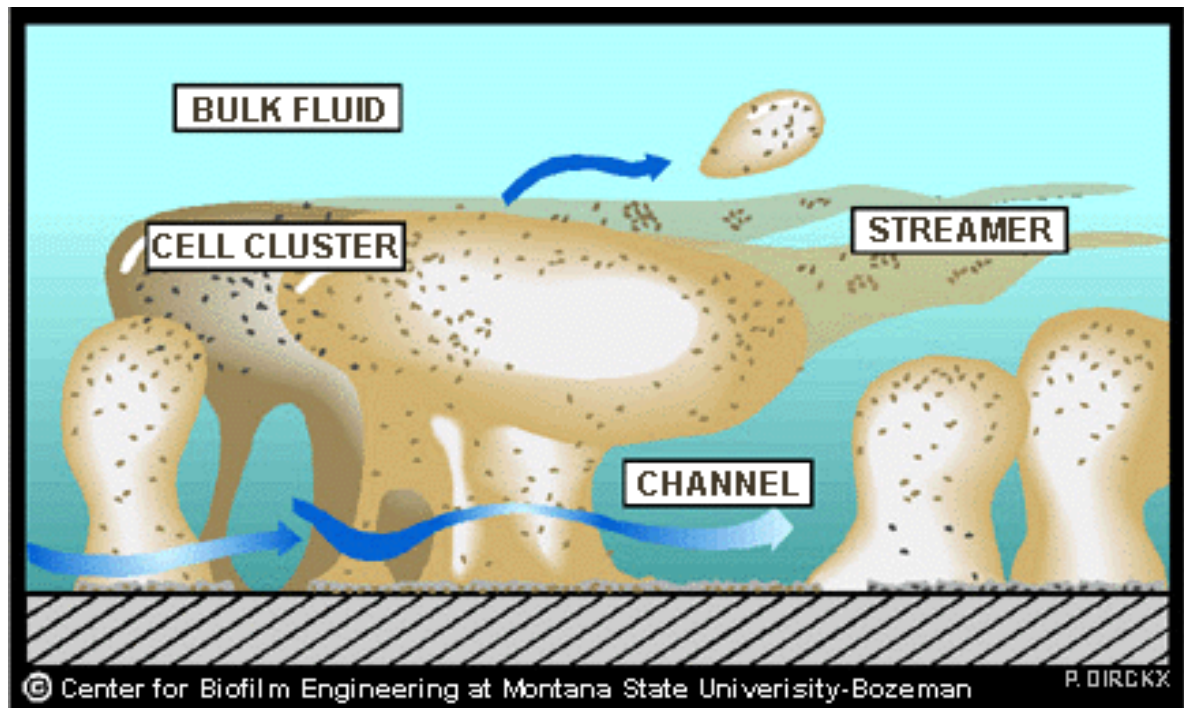


Fig. 2: Complex 3-D structure of a typical biofilm showing channels and cavities filled with nutrients and metabolites in between cell clusters

The formation of biofilms is an important survival strategy for bacterial cells. Once established, biofilm infections are rarely resolved by host defense mechanism⁵. Antibiotic therapy typically reverses the symptoms caused by planktonic cells released from the biofilm, but fails to destroy the biofilm itself⁶. It is variously estimated that bacteria within biofilms are effectively from 20-1000⁷ times to 500-5000 times⁸ less sensitive to antibiotics than planktonic microorganisms. The immediate implication of this resistance is the prolonged and high concentration levels of antibiotic treatment required. This is often medically impractical. There are different potential reasons for this reduced sensitivity:

- The slimy matrix (EPS) inhibits the penetration of antibiotics into the biofilm. The antibiotics react with the surface layers of the biofilm while letting the protected bacteria population grow unchecked, until they break out of the biofilm and spread the infections to distant locations within the host.

-
- The matrix may contain enzymes that could degrade the antibiotics, for instance β -lactamase which is active against penicilline.
 - The bacterial cells on the surface of the biofilm are phenotypically different from the cells within the biofilm matrix. The surface cells are metabolically active, they grow and divide. Little oxygen and small amounts of nutrients are available to the embedded cells, therefore they are smaller and grow slower. These bacteria are in a kind of “dormant state” that make them unsusceptible against antibiotics, but when cells in the other layers are killed, they become active and regenerate the biofilm.
 - Biofilm serves as an ion-exchange matrix within itself, thus providing more organic nutrients and also enable bacteria to counter cationic antimicrobial agents⁵.

Biofilms can be a serious health threat, especially in patients in whom artificial substrates have been introduced. Microbial infections can form on biomaterials that are totally embedded into the human body or partially exposed to the outside. *Escherichia coli*, staphylococci, and *pseudomonas* species are among the most common invading bacteria. After the biomaterial is implanted, either tissue cells or microorganisms will begin to colonize it; if tissue cells succeed in colonizing it first, the implant will most likely be successful. If bacteria colonize first, a biofilm will develop resulting often in the failure of the implant. In the late 20th century millions of patients, who received tissue and organ replacement experienced biomaterial-centered infection (BCI). The incidence of BCI varies from 4 % for hip prostheses to 100 % for urinary tract catheters after 3 weeks use (Tab. 1).

Tab. 1: Incidences of infection of different biomedical implants and devices after 3 weeks of use⁹. The incidence of infection (the probability of the microorganisms reaching the biomaterials surface) depends in which body part the material is implanted

Body site	Implant or device	Incidence of infection (%)
Urinary tract	UT catheters	10-20
Percutaneous	CV catheters	4-12
	Temporary pacemaker	4
	Short indwelling catheters	0.5-3
	Peritoneal dialysis catheters	3-5
Subcutaneous	Cardiac pacemaker	1
Soft tissue	Mammary prosthesis	1-7
	Intraocular lenses	0.13
Circulatory system	Prosthetic heart valve	1.88
	Multiple heart valve	3.6
	Vascular graft	1.5
	Artificial heart	40
Bones	Prosthetic Hip	2.6-4.0
	Total knee	3.5-4

The complications caused by BCI may vary from the dysfunction of the implanted device itself to lethal sepsis of the patient. Due to the difficult resolution of a biofilm infection, the removal of the complete implant is most often necessary at the expense of considerable costs and patient's suffering.

1.2 Antimicrobial strategies currently used in the treatment of infectious disease and the problem of bacterial resistance

1.2.1 Conventional antimicrobial therapies based on bactericides and bacteriostatics

Antimicrobial agents conventionally used in the therapy of bacterial infections, called antibiotics, can be distinguish from a clinical point of view into two different groups:

Antibiotics like penicillines and cephalosporines are bactericidal, i.e. they kill the target bacterium. Others, like macrolides, aminoglycosides, tetracyclines and gyrase inhibiting substances are bacteriostatic, i.e. they inhibit growth and reproduction of certain bacteria. Bactericidal agents are more effective, but bacteriostatic agents can be extremely beneficial since they permit the normal defenses of the host to destroy the microorganisms ¹⁰⁻¹². Therefore, the most important property of an antibiotic is its selective toxicity, meaning that the drug is highly effective against the bacterial pathogens but has little or no toxic effect on the host. The biochemical processes in bacteria are in some way different from those in host cells, and the advantage of this difference is usually exploited by the antibiotic in order to achieve a high selectivity toward bacteria.

There are five main mechanisms of action by which the antibiotics exert their bacteriostatic or bactericidal activity, they are shown schematically in Fig. 3:

- Inhibition of cell wall synthesis
- Disruption of cell membrane function
- Inhibition of protein synthesis
- Inhibition of nucleic acid synthesis
- Action as anti-metabolites

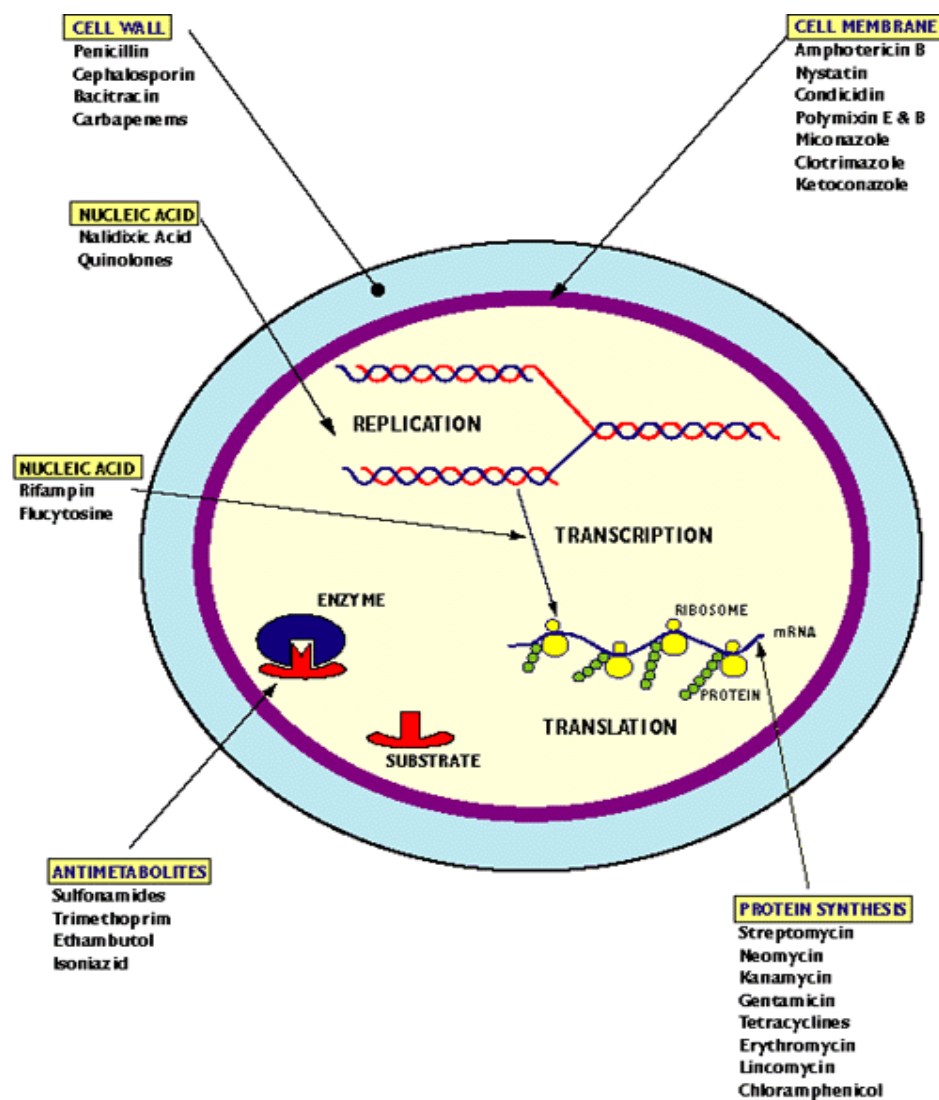


Fig. 3: Schematic overview of the interactions between different antibiotics and a bacterial cell¹³

*Inhibition of cell wall synthesis*¹⁴⁻¹⁶

An essential component of the bacterial cell wall is a specific mucopeptide called peptidoglycan. Multiple enzymes are required for peptidoglycan synthesis and attachment to the cell wall. Enzymes involved in the final stages of cell wall synthesis are called transpeptidases. β -Lactam antimicrobials, as penicillins and cephalosporins, bind to transpeptidases and inhibit peptidoglycan formation, thus interfering with cell wall synthesis. Another example of an anti-cell-wall agent is

vancomycin, a glycopeptide antimicrobial which interrupts cell wall synthesis by forming a complex with residues of peptidoglycan precursors. Loss or damage on the peptidoglycan layer destroys the rigidity of the bacterial cell wall which is essential for the survival of bacteria in hypotonic environments and therefore, result in death. Cell wall synthesis inhibitors exert their selective toxicity against bacteria because human cells lack cell wall. They are only effective against actively dividing bacteria, since this is when new cell walls are being created.

Disruption of cell membrane function^{17,18}

The cytoplasmic membrane acts as a diffusion barrier for water, ions, nutrients, and serves as transport system. The integrity of the membranes is vital to bacteria and compounds that cause their disruption rapidly kill the bacteria. However, due to the similarities in phospholipids in bacterial and eukaryotic membranes, this action is rarely specific enough to permit these compounds to have a large therapeutic application. The only antibacterial of clinical importance that acts by this mechanism is polymyxin, a cationic octapeptide that binds to negatively charged membrane phospholipids and thereby disorganizes membrane permeability^{19,20}. It is effective mainly against Gram-negative bacteria and is usually limited to topical use.

Inhibition of protein synthesis²¹⁻²³

Many antimicrobial agents owe their efficacy to the inhibition of some steps in the complex process of protein synthesis taking place in the ribosome. They take advantage of the fact that the bacterial ribosome and the eukaryotic ribosome structurally differ, achieving their selective toxicity in this way. Tetracyclines, aminoglycosides (e.g. gentamicin), macrolides (e.g. erythromycin) and chloramphenicol are the most important antimicrobials with this mode of action.

Inhibition of nucleic acid synthesis

Some antibiotics affect the synthesis of DNA or RNA, or can bind to DNA or RNA so that their message cannot be read. In both cases cell growth is blocked. Many

of these antimicrobial agents are unselective and affect host cells and bacterial cells alike. Therefore, their therapeutic application is limited. One special class of nucleic acid synthesis inhibitors, the fluoroquinolones²⁴, and another different compound, called rifampicine²⁵, show a higher selectivity against prokaryotes and are still used as therapeutics.

Action as antimetabolites

Many antimicrobial agents are competitive inhibitors of essential metabolites or growth factors which are needed in bacterial metabolism. These types of antimicrobial agent are referred to as antimetabolites or growth factor analogs, since they are designed to specifically inhibit an essential metabolic pathway in the bacterial pathogen. At chemical level, competitive inhibitors are structurally similar to bacterial growth factors and metabolites, but they do not fulfill their metabolic function in the cell²⁶. Some are bacteriostatic and some are bactericidal. Their selective toxicity is based on the premise that the bacterial pathway does not occur in the host. Sulfonamides and trimethoprim are antimetabolites that interfere with folate metabolism in the bacterial cell by competitively blocking the biosynthesis of tetrahydrofolate, which is necessary for the final synthesis of DNA, RNA and bacterial cell wall proteins²⁷.

1.2.2 The problem of bacterial resistance

One of the main problems related to the use of antibiotics is the ability of bacteria to become resistant to them. There are four basic biochemical mechanisms by which bacteria resist the bactericidal or bacteriostatic effects of antimicrobials:

- 1) Alteration of the antimicrobial's target receptor molecule in the bacteria.
- 2) Decreasing the accessibility of the antimicrobial to the target by altering the entry of the antimicrobial into the cell or increasing the removal of the antimicrobial from the cell.
- 3) Destruction or inactivation of the antimicrobial.
- 4) Generation of a new metabolic pathway by the bacteria, that is not inhibited by the antimicrobial^{28,29}.

The development of bacterial resistance results from changes in the genome of bacteria. Two mechanisms are independent factors in producing resistant microbes. One is driven by principles of natural selection: a spontaneous mutation in the bacterial chromosome imparts resistance to a member of the bacterial population; antimicrobials destroy the susceptible bacteria but permit the resistant mutant to grow and proliferate. The second mechanism in producing resistant microbes is the exchange of genes between strains and species^{30,31}. Thus, a previously susceptible bacterial strain may become equipped with genes to resist a specific class, or even multiple classes of antimicrobials. The combined effects of fast growth rates, high concentrations of cells, genetic processes of mutation and selection, and the ability to exchange genes, are responsible for the extraordinary rates of adaptation and evolution that can be observed in bacteria. For these reasons bacterial resistance to antimicrobials takes place very rapidly and represents a serious concern in pharmacotherapy.

1.3 Modern strategies for prevention and defense against bacterial infections

1.3.1 Different approaches to the generation of antimicrobial surfaces

In recent years, a series of different approaches have been used to develop biomaterial surfaces onto which bacteria cannot attach, grow and colonize. The most important ones can be summarized as follow:

- Surfaces with non-covalently bound antimicrobial agents
- Surfaces with covalently immobilized antimicrobial agents
- Surfaces with bacteria repellent properties
- Polymer matrices loaded with antibiotics
- Antimicrobial polymers

Surfaces with non-covalently bound antimicrobial agents

Immersion of a medical device into antimicrobial solutions might be one of the simplest methods for loading antimicrobial agents onto its surface. This method has already been examined for antibiotics such as rifampicin, ciprofloxacin, tobramycin and certain cephalosporins³². The main problem associated to this technique is that biomaterials generally have a limited affinity for such agents, and the majority of the drug will be present in the outermost layer of the biomaterial surface. Consequently, the limited concentration of drug that can be incorporated may be insufficient for a prolonged antimicrobial effect³². Drug loading of biomaterials has been enhanced by precoating their surfaces with a connective coating, wherein the interaction between the antimicrobial agent and the connective coating is facilitated by electrostatic interaction. This coating technology has found wide application in biomaterial science. For example, polyurethane catheters coated with ethylenediaminetetraacetate and minocycline showed potential in reducing recurrent vascular catheter-related bacteraemia.³³ In

vitro tests of silver-coated polyurethane used as biliary stent demonstrated a reduced bacteria adherence of 10 to 100 fold.³⁴ A coating of ciprofloxacin-containing liposomes sequestered in polyethylene glycol (PEG) hydrogel seemed to significantly reduce bacterial adhesion to silicone catheter material³⁵; to mention some examples reported in the literature.

Surfaces with covalently immobilized antimicrobial agents

Antimicrobial agents have been covalently attached to polymeric medical devices in order to achieve a permanent coating and a prolonged antimicrobial effect. Unfortunately only a limited number of antimicrobials can be used, because the active sites are frequently masked by covalent attachment. Good results in preventing biofilm centered infection have been achieved by attaching certain functional groups with antimicrobial effect, e.g. quaternary ammonium groups to the surface of the biomaterial. Silicon rubber with covalently coupled 3-(trimethoxysilyl)-propyldimethyloctadecylammonium chloride (QAS) showed antimicrobial properties against adhering bacteria, both *in vitro* and *in vivo*³⁶. Polyurethanes with quaternary ammonium groups demonstrated an efficient prevention of bacterial adhesion and colonization³⁷. However, quaternary ammonium compounds have been shown to be toxic to human cells as well³⁸.

Surfaces with bacteria repellent properties

To prevent device-related infections increasing efforts have focused on developing biomaterials with anti-adhesive properties. By modifying a polymer surface with highly hydrated and close-packed chain-like molecules, such as polyethylene oxide (PEO) or polyacrylamides, anti-adhesive properties can be obtained. The hydrated chains provide a sterically hindered barrier that minimizes non-covalent interactions and reduces bacterial adhesion³⁹. An alternative approach for minimizing bacterial adhesion is to prepare polymers with negative surface charges⁴⁰. Most bacteria carry a net negative surface charge at physiological conditions. Therefore, negatively charged biomaterial surfaces discourage adhesion, while positively charged surfaces promote it.

Polymer matrices loaded with antibiotics

A widely used method for preparing devices, that are intrinsically bacteria infection-resistant, is the incorporation of an antimicrobial agent into the polymer matrix at the polymer synthesis stage or at the device manufacturing stage. The aim is to develop biomaterials which release the antimicrobial agent into the surrounding medium in a controlled manner, thereby preventing bacterial colonization. Ciprofloxacin-loaded polyurethane demonstrated to have bactericidal properties⁴¹. Rifampicin was incorporated into silicone in an attempt to prevent infection of cerebrospinal fluid shunts with some success⁴². Numerous are the examples of antimicrobial agents incorporated into biodegradable polymers such as polyglycolides and polylactides. This approach may offer a new direction for medical device design, due to the bi-functionality of the system, providing both controlled release of antimicrobial agents and controlled degradation of the surface of the device with removal of adherent bacteria³². A disadvantage of the direct incorporation of antimicrobial agents into polymer matrices is a possible reduction of the mechanical properties of the polymer which are essential to ensure an optimal performance of the medical device in the patient's body³².

Antimicrobial polymers

The covalent linkage of an antibacterial agent to a monomer prior to polymerization provides a method of producing perhaps the most resilient drug-polymer. However, the selection of therapeutic agents or active groups with chemistry that is compatible with the synthetic reaction scheme constitute a limit to this approach. Antibacterial polymers with quaternary ammonium salts, bis-guanidine groups, quaternary pyridinium salts, phosphonium salts and sulfonium salts have been synthesized⁴³.

1.3.2 Novel concepts for the generation of antibacterial surfaces interfering with the quorum sensing mechanism

The problem of bacterial resistance to antimicrobial agents currently used in conventional therapy and the difficulty to eradicate already established biofilms emphasize the need to find new strategies for combating biofilm-associated infections. It has been found that a critical role in the formation of mature and differentiated biofilm structures is played by the bacterial cell-to-cell communication system, known as quorum sensing (QS). QS is a mechanism by which bacteria regulate the expression of specific genes in response to population density⁴⁴. Using this intercellular communication system bacteria can sense, if there is a large enough number of cells to start the biofilm formation. The mechanism is based on self-generated signal molecules called autoinducers (AI). In general, each bacterial cell produces a basal level of AI, which move in and out of cell membranes through diffusion mechanism or active transportation⁴⁵. The concentration of the extracellular AI increases proportionally to the bacterial cell density. At a threshold population density, described as a bacterial “quorum”, the accumulated signaling compounds interact with cellular receptors, which control the expression of a set of specific target genes⁴⁶ (Fig. 4). QS-controlled genes encode for proteins that play a crucial role in biofilm development, for instance they are involved in the building of the extra-cellular matrix or in the irreversible adhesion of the bacteria onto the surfaces. It has been observed that *Pseudomonas aeruginosa* mutants, deficient in the production of QS-signaling molecules, form abnormal biofilms⁴⁷. Beside biofilm maturation, a large number of other specialized processes are reported to be regulated by density-dependent signaling molecules including antibiotic production, bioluminescence, genetic competence, sporulation, swarming motility and virulence⁴⁸. However, a more centralized role for QS is to regulate cellular adaptation to changing environmental conditions. As environmental conditions often change rapidly, bacteria need to respond quickly in order to survive. These responses include adaptation to available nutrients, defense against other microorganisms which may compete for the same nutrients and the avoidance of toxic compounds potentially dangerous to the bacteria. First described in two species of marine bioluminescent bacteria, *Vibrio harveyi* and *Vibrio fischeri*^{49,50}, QS is now known to be widespread among

both Gram-positive and Gram-negative bacteria. Many Gram-positive bacteria make use of small post-translationally processed peptides as QS-signals⁵¹. These peptides are usually secreted by ATP-binding cassette (ABC) transporters. Some interact with membrane bound sensor kinases that transduce a signal across the membrane, others are transported into the cell by oligopeptide permeases, where they then react with intracellular receptors. The specific interaction between the signaling molecule and their target induce a phosphorylation cascade that ends with the activation of cognate response regulator protein.

In contrast to Gram-positive bacteria, the vast majority of Gram-negative bacteria utilize diffusible N-acylated homoserine lactone (AHL) molecules. This mode of QS is mediated by proteins belonging to the LuxI- and LuxR-families. LuxI-type proteins direct the AHL synthesis, while LuxR-type proteins function as transcriptional regulators, which are capable to bind AHL signal molecules. Once formed, the AHL-regulator complex stimulates expression of the target genes⁴⁷. Different bacterial species may produce different AHLs, which vary in length (from C₄ to C₁₄) and substitution of the acyl chain⁵², but contain the same homoserine lactone moiety². In some cases a single bacterial species can have more than one QS system and therefore uses more than one signal molecule. Preferential binding of an AHL by its cognate LUXR-type protein guarantees a high degree of selectivity and complexity so that the bacterium may respond to each molecule in a different way.

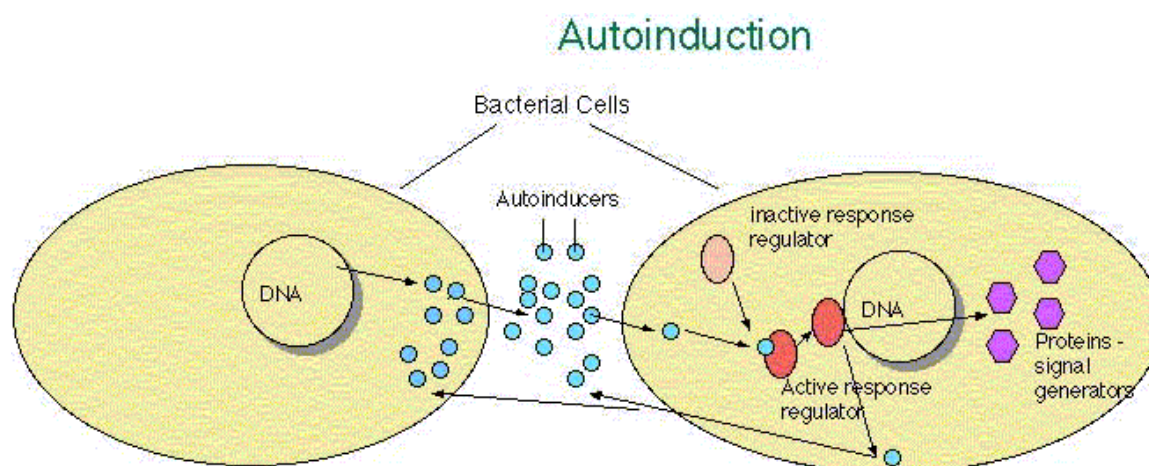


Fig. 4: QS mechanism in bacterial cells based on the production of AI molecules. Accumulation of AI occurs in a cell-density-dependent manner until a threshold level is reached. At this time the AI binds to and activates the response regulator protein, which in turn induces gene expression⁵¹

The discovery that a wide spectrum of organisms uses QS to control biofilm development and in general the expression of the genes which causes disease, makes it an attractive target for antimicrobial therapy. Strategies designed to block QS of bacterial pathogens may represent new approaches for the prevention of infectious diseases.

1.4 Potential antagonists for QS receptors

Various strategies could be developed in order to interfere with the QS circuitry. For example, interrupting the autoinducers' biosynthetic pathway and shutting down autoinducers' synthesis, perhaps through the use of analogs of their precursors, would be a highly effective means of blocking the QS cascade. Another possible way could be the employing of compounds that inactivate the signaling molecules. However, the most promising strategy for interrupting the QS mechanism is based on the use of signaling molecule analogs. AI and protein receptors have a unique specificity for one other. Noncognate AI typically only weakly activate or may inhibit receptor protein activation altogether. Therefore, analogs that bind to but do not activate receptor proteins could act as antagonist to prevent autoinducers' binding, which in turn would shut down the QS cascade. QS receptor antagonists have been found to exist in nature, examples are the secondary metabolites produced by a seaweed (*Delisea pulchra*) and an heptapeptide, called RNA III inhibiting peptide (RIP), isolated from culture supernatants of coagulase negative staphylococci. These compounds (secondary metabolites) of absolutely different classes may find large application as new biofilm-inhibiting and antibacterial therapeutics. The concept that they attenuate bacterial virulence by interfering with the cell-to-cell communication systems, rather than by killing bacteria (bactericidals) or by inhibiting their growth (bacteriostatics) is very attractive. The use of such antipathogenic agents is in fact far less likely to pose a selective pressure for development of resistant mutants, than the application of classical antimicrobial therapies.

1.4.1 Secondary metabolites as QS receptor antagonists

1.4.1.1 *Delisea pulchra*-derived halogenated furanones

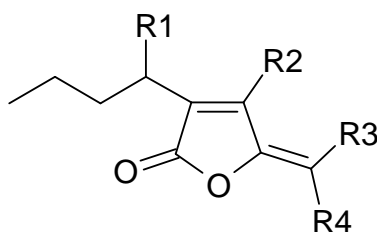
In the marine environment, many organisms have developed specific defensive strategies to protect themselves against bacterial colonization and biofilm formation. For instance, *Delisea pulchra* (Fig. 5), a red macroalga indigenous to the south-eastern coast of Australia, produces a range of structurally related metabolites – called halogenated furanones or fimbriolides – which possess strong antifouling and antimicrobial properties⁵³.



Fig. 5: Red colored macro-alga *Delisea pulchra* indigenous to the south-eastern coast of Australia

These compounds are encapsulated in vesicles in gland cells in the seaweed, which provides a mechanism for delivery of the metabolites to the surface of the alga at concentrations which discourage a wide range of prokaryote and eukaryote fouling organisms^{54,55}. The red alga produces more than 20 different fimbriolides⁵⁶, which share a common 3-butyl-5-(halo)methylene-2(5H)-furanone

skeleton, but differ in the number and the nature of the halogen substituents and the presence or absence of oxygen functionality in the butyl side-chain (Fig. 6).



R1 = H, OH or OAc

R2, R3, R4 = are H or halogen

Fig. 6: Structure of the secondary metabolites produced by *Delisea pulchra*

Because of their structural similarities to AHLs (Fig. 7), the signaling molecules used by Gram-negative bacteria, fimbriolides affect the interaction between AHLs and the putative regulatory protein (LuxR or LuxR homologue) by competitively binding to the receptor site⁵⁷. It has also been demonstrated that the binding of the furanones to LuxR protein causes conformational changes that enlist the furanone-LuxR complex into rapid proteolytic degradation⁵⁸. Thus, *Delisea pulchra* metabolites inhibit transcriptional activation of genes, which encode the QS phenotype by a double mode of action, occupying the AHL binding site of LuxR and decreasing the cytoplasmic concentration of the regulatory protein.

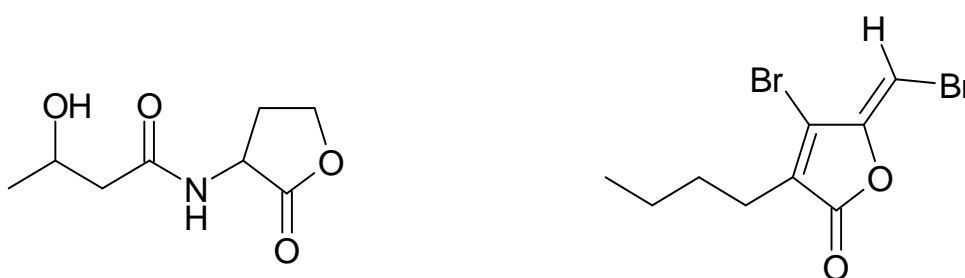


Fig. 7: Structures of a AHL produced by *Vibrio harveyi* (left) and a brominated furanone produced by *Delisea pulchra* (right)

More recently, it has been found that furanones can also interfere with a species-unspecific communication system that is probably based on

furanone-related compounds as well^{59,60}. This species-unspecific QS is used by both Gram-positive and Gram-negative bacteria⁶⁰. As a consequence, these agents inhibit the expression of QS controlled behavior including virulence factors production and biofilm formation, in a wide range of microorganisms. It has been observed that halogenated furanones do not interfere with the initial attachment of the bacteria to the substratum, instead, interrupting their communication system, they affect the architecture of the biofilm and enhance the process of bacterial detachment, leading to a loss of bacterial biomass.

Beside the antimicrobial properties the halogenated furanones exhibit other interesting features for potential applications in medicine and biomaterial science. These compounds are not cytotoxic to human cells and do not initiate an acute inflammatory response, neither *in vitro* nor *in vivo*⁶¹. They maintain their activity and stability even after a sterilization process⁶² and moreover, as already mentioned in paragraph 1.4, they are unlikely to induce bacterial resistance. Indeed, in a million years of evolution, no natural resistance to these furanones has been developed by bacteria in nature.

1.4.1.2 Coagulase negative staphylococci-derived RIP

RIP is a peptide consisting of seven amino acids, originally isolated from culture supernatants of coagulase negative staphylococci, suggested to be *Staphylococcus warneii* or *Staphylococcus xylosus*. The sequence of RIP was identified as Tyr-Ser-Pro-X-Thr-Asn-Phe (YSPXTNF), where X can be a Cys, a Trp, or a modified amino acid⁶³. This peptide has been shown to be an effective inhibitor of the QS mechanisms in *Staphylococcus aureus* and *Staphylococcus epidermidis*, which are major causes of infection related to biofilm formation on medical devices. So far, two QS systems related to *Staphylococcus aureus* and *Staphylococcus epidermidis* have been described. The first one is based on the autoinducer RNA III activating peptide (RAP) and its target protein TRAP. The second is composed of the peptide AIP (autoinducing peptide) and its receptor AgrC. As cells proliferate and the colony grows, the cells secrete RAP. When RAP reaches a threshold concentration, it induces the phosphorylation of its target protein TRAP. TRAP protein induces bacteria adhesion, through an yet unknown

mechanism, and stimulates the synthesis of AIP and AgrC. AIP itself down-regulates the phosphorylation of TRAP, leading to reduced cell adhesion, and induces the phosphorylation of its receptor AgrC. This leads to the production of the regulatory RNA molecule RNA III, that induces toxin synthesis^{64,65}. Because of the similarity in sequence between the NH₂-terminated sequence of RAP Tyr-Lys-Pro-Ile-Thr-Asn (YKPITN) and RIP (YSPXTNF), RIP competes with RAP concerning the phosphorylation of TRAP. This results in reduced bacterial adhesion and consequently in prevention of biofilm formation. Additionally, the production of RNA III is minimized, which results in a suppression of toxin synthesis^{63,64}(Fig. 8).

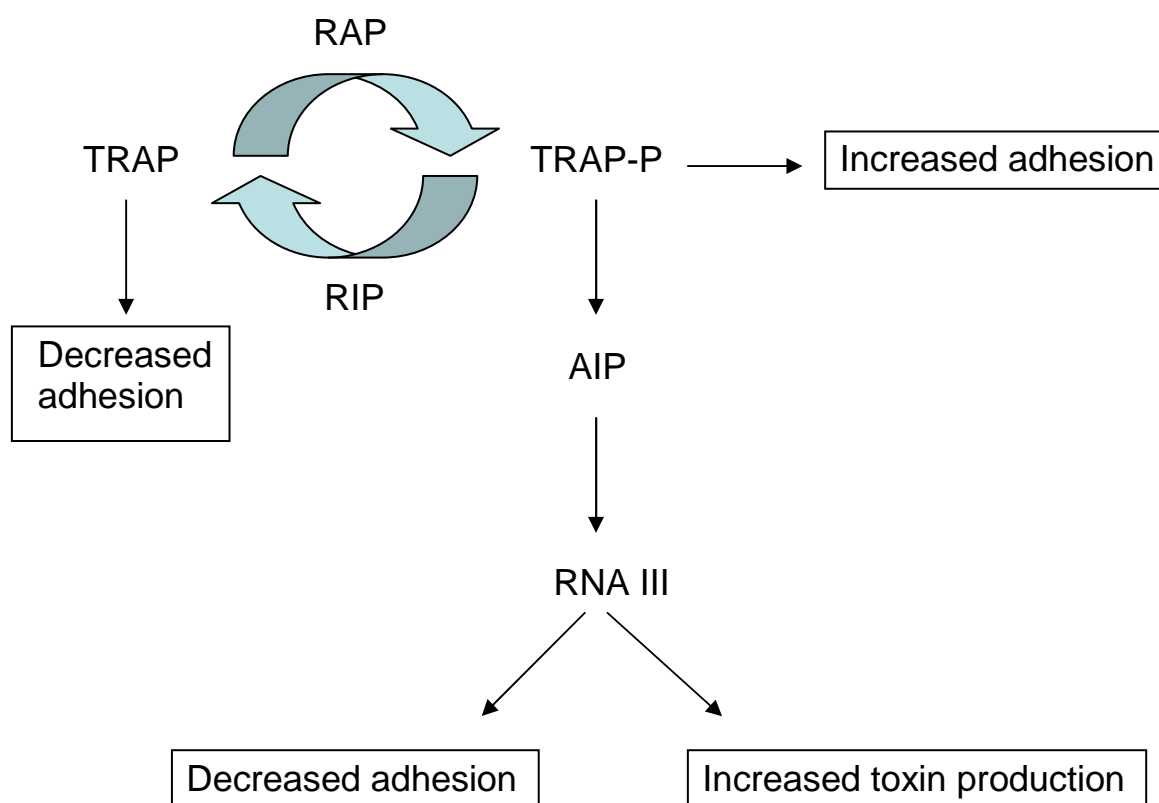


Fig. 8: Schematic overview of the effects of RAP and RIP peptide on the regulation of bacterial adhesion and subsequent toxin production of *Staphylococcus aureus* and *Staphylococcus epidermidis*

TRAP is a highly conserved receptor protein among staphylococci. For instance, the sequence of TRAP in *Staphylococcus epidermidis* has 76 % identity to that of TRAP in *Staphylococcus aureus*. This suggests, that RIP can be used as global

suppressor of adherence, biofilm formation and finally infection by different staphylococcal strains⁶⁶.

RIP was synthesized in its amide form as YSPWTNF-NH₂ and has been shown to be highly stable and extremely effective in suppressing *Staphylococcus aureus* infections *in vivo*, including cellulites, septic arthritis, keratitis, osteomyelitis, and mastitis⁶⁴. In *in vitro* studies, RIP-NH₂ inhibited bacterial adherence to epithelial cells and reduced adherence and biofilm formation on polystyrene, polyurethane and silicone, which were loaded by immersion in a peptide solution⁶⁵. Further *in vivo* experiments were carried out to test, whether the inhibition of bacterial cell-to-cell communication by RIP-NH₂ is sufficient to eliminate medical device-associated infections by staphylococci. Grafts previously soaked in solutions of RIP, saline, and inactive RIP analogue, respectively, were implanted into rats, and subsequently bacteria like *Staphylococcus aureus* and *Staphylococcus epidermidis* were injected into the implants as well. As a model for parental surgical prophylaxis, some of the rats were also treated with intraperitoneally injected RIP. The infected control groups (i.e. rats that had received either saline-soaked grafts or inactive RIP analogue-soaked grafts) demonstrated evidence of graft infection. In contrast, all rats in the RIP-soaked graft group and the RIP-injected group exhibited strongly reduced bacterial load. All rats in the RIP-soaked graft group, which were also administered RIP intraperitoneally, demonstrated no evidence of graft infection, indicating 100% protection. It is noteworthy, that none of the rats showed clinical evidence of drug-related adverse effects⁶⁷. This suggests, that RIP can be used to coat medical devices for prevention of bacterial colonization and subsequent infection.

2 Aim of the thesis

Biofilm-related infections are serious complications connected to the use of medical devices, which often result in morbidity and mortality. Currently available therapeutic approaches are often ineffective in fighting bacterial biofilm formation and fail to eradicate infections. There are two main reasons for this failure: the ability of bacteria encased in the biofilm matrix to be more resistant to treatment compared to planktonic bacteria and development of bacterial resistance to antimicrobial agents. The discovery of an interbacterial communication system, called quorum sensing, regulating biofilm maturation and bacterial virulence, opens new opportunities to interfere with the development of biofilms and overcome the problem of biofilm related infections on medical devices.

The aim of this work is the development of new strategies to reduce or to prevent completely biofilm formation on biomaterial surfaces. These strategies are based on the employment of two QS inhibitors: the 3-butyl-5-(bromomethylene)-2(5H)-furanone, which is one of the secondary metabolites produced by the red alga *Delisea pulchra* and the heptapeptide RIP.

The first strategy is focused on the incorporation of 3-butyl-5-(bromomethylene)-2(5H)-furanone into a polymeric system in order to mimic the defense mechanism evolved by the marine alga. A commonly used biodegradable biomaterial, poly(D,L-lactide) (PDLLA), has been selected as a model matrix for loading with synthesized QS antagonist 3-butyl-5-(bromomethylene)-2(5H)-furanone. One main task is to reproduce and optimize the synthesis of this *Delisea pulchra* metabolite. Another aim is to improve the isolation, purification and analysis of the different furanone derivatives, produced during synthesis. The next step is to load the biomaterial matrices using mixtures of PDLLA and the antagonist 3-butyl-5-(bromomethylene)-2(5H)-furanone. Finally, the antagonist release kinetics from the polymer are studied.

The second strategy is focused on covalent immobilization of RIP as an anti-biofilm coating for a non-degradable polymer as poly(vinylidene fluoride)

(PVDF). The RIP peptide's amid form is synthesized by solid phase peptide synthesis (SPPS) using fluorenylmethyloxycarbonyl (Fmoc) protecting group strategy. After isolation, purification and complete characterization, the peptide is covalently coupled to the PVDF surface. Therefore, the surface of the polymer has to be activated and functionalized by means of Ar-plasma and subsequent thermally induced graft-co-polymerization of acrylic acid (AAc). Carboxyl groups of the immobilized AAc are then used to covalently immobilize the RIP-NH₂ peptide by water soluble carbodiimide chemistry. Each step of the immobilization sequence is followed by means of X-ray photoelectron spectroscopy (XPS), attenuated total reflection infrared spectroscopy (ATR-IR), Raman spectroscopy, contact angle measurement according to the captive bubble method and zeta potential measurement. The carboxyl groups' concentration, generated on the polymer surface, is determined using UV/VIS photometry and a newly established potentiometrically monitored titration method. Radioactive binding studies are performed in order to ascertain the amount of RIP immobilized on the polymer surface. Finally, the ability of RIP-coated PVDF to inhibit bacterial adhesion and biofilm formation is estimated *in vitro* by means of a pico-Green assay and using *Staphylococcus aureus*.

In addition to the above mentioned areas of basic research on the development of new strategies for inhibition of bacterial adhesion and biofilm formation on biomaterials, a study of more practical application has been carried out in cooperation with an industrial partner. Kathon® 910 SB, a formulation from the company ROHM AND HAAS (Germany), is used to protect silicone sealants from bacterial and fungi contaminations. Therefore, Kathon®910 SB is incorporated into poly(dimethyl siloxane) (PDMS) matrices. The loading conditions and the release properties are analyzed and improved in a continuous loop feedback process. Finally, Kathon® 910 SB samples are investigated in *in vitro* experiments.

3 Results and discussion

3.1 Application of 3-butyl-5-(bromomethylene)-2(5H)-furanone as QS antagonist incorporated into PDLLA films

The issue, that people become much older in the western industrial countries and the increasing problem of multi-morbidity underscore the need for development of a new implant and medical device generation. They have to stay in the patient's body for a longer period of time and be characterized by a higher antibacterial activity, a broader range of effectiveness, and higher durability. The inhibition of biofilm formation by interfering with the QS system seems to be a smart strategy^{2,45,47,51,68}. If QS of bacteria sitting on surfaces can be inhibited, one may be able to eliminate implant-centered infections. Structurally related halogenated furanones, produced by the red alga *Delisea pulchra*, have been shown to be effective inhibitors of the QS mechanism in a wide range of Gram-negative and Gram-positive bacteria, as discussed in detail in chapter 1. Therefore, a major aim of this study was the synthesis of 3-butyl-5-(bromomethylene)-2(5H)-furanone, one of the anti-QS furanone compounds produced and secreted by *Delisea pulchra*, and its incorporation into PDLLA.

3.1.1 Synthesis of 3-butyl-5-(bromomethylene)-2(5H)-furanone

In spite of their biological significance and their potential for biomedical application, there is still no general method suitable for large-scale synthesis of halogenated furanones. The few reported synthesis protocols turned out to be difficult to reproduce, particularly when regarding the isolation and purification of the target compound 3-butyl-5-(bromomethylene)-2(5H)-furanone⁶⁹⁻⁷¹ (Fig. 9).

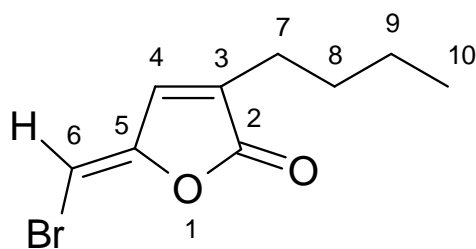
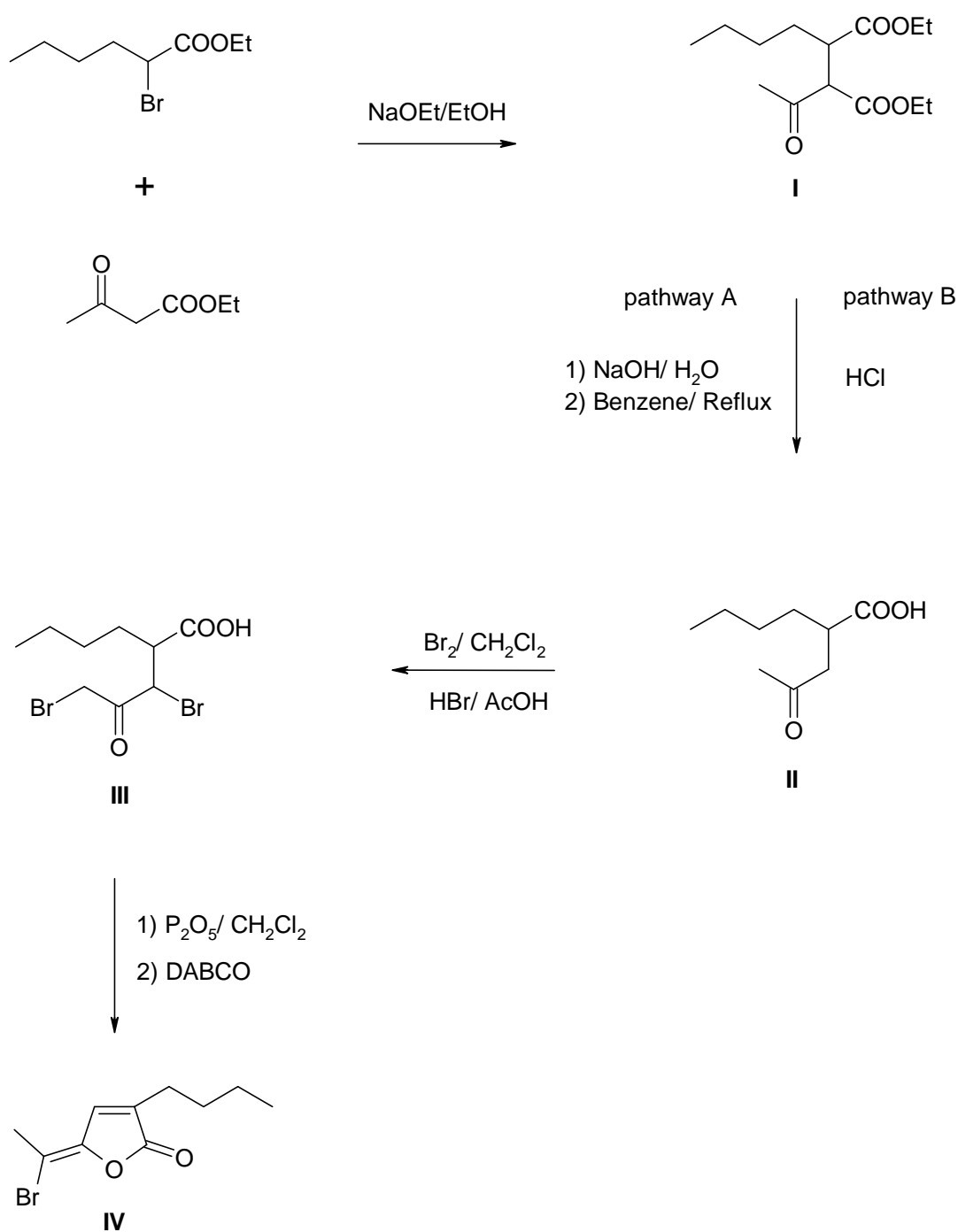


Fig. 9: Molecular structure of the QS antagonist 3-butyl-5-(bromomethylene)-2(5H)-furanone

In consideration of a continuously increasing global interest in biofilm inhibiting mimetics, the optimization of the target-oriented synthesis, isolation, and purification of furanone derivatives of the complex mixture excreted by *Delisea pulchra* was tackled. Simultaneously, the group of Prof. Griesser (Ian Wark Research Institute, University of South Australia) started working on the improvement of the synthesis of such furanone derivatives.

3-Butyl-5-(bromomethylene)-2(5H)-furanone was prepared following the 6-step synthesis sequence, illustrated in Scheme 1.



Scheme 1: Synthesis of 3-butyl-5-(bromomethylene)-2(5H)-furanone, a 6-step reaction scheme

As already published, the use of ethyl-2-bromohexanoate as starting molecule for the synthesis was considered. In the first reaction step ethyl-2-bromohexanoate was condensed with ethylacetoacetate to yield diethyl-2-acetyl-3-

butylbutanedioate (**I**, Scheme 1). Subsequently, the diester was hydrolysed and decarboxylated. The obtained γ -keto acid (**II**, Scheme 1) was brominated and after that the brominated derivatives were cyclised and dehydrobrominated to give a final mixture of different furanones.

The condensation of ethyl-2-bromohexanoate with ethylacetoacetate was carried out with sodium ethanolate suspended in absolute ethanol. In order to achieve a better diester yield, *in situ* prepared sodium ethanolate was used. The crude product was purified by column chromatography using petroleum/ethyl acetate (1:4, [v/v]) as the mobile phase. ^1H -NMR spectroscopy revealed, that the diester (**I**, Scheme 1) was obtained as an erythro and threo mixture (Fig. 10) (yield 55 %). The proton adjacent to the β -keto ester group appears as two doublets at δ 3.87 and δ 3.92 ppm, each with coupling constants J of about 10 Hz, which is typical for isomeric compounds; moreover the acetyl protons appear as two singlet at δ 2.26 and δ 2.3 ppm. The ratio of the diastereoisomers can be obtained from the integration of the above mentioned signals (1.6:1). The presence of the erythro-threo mixture was further confirmed by thin layer chromatography (TLC), the two diastereoisomers have in fact different retention times R_f ($R_{f1}=0.48$ and $R_{f2}=0.55$; mobile phase: petroleum/ethyl acetate (1:4, [v/v])).

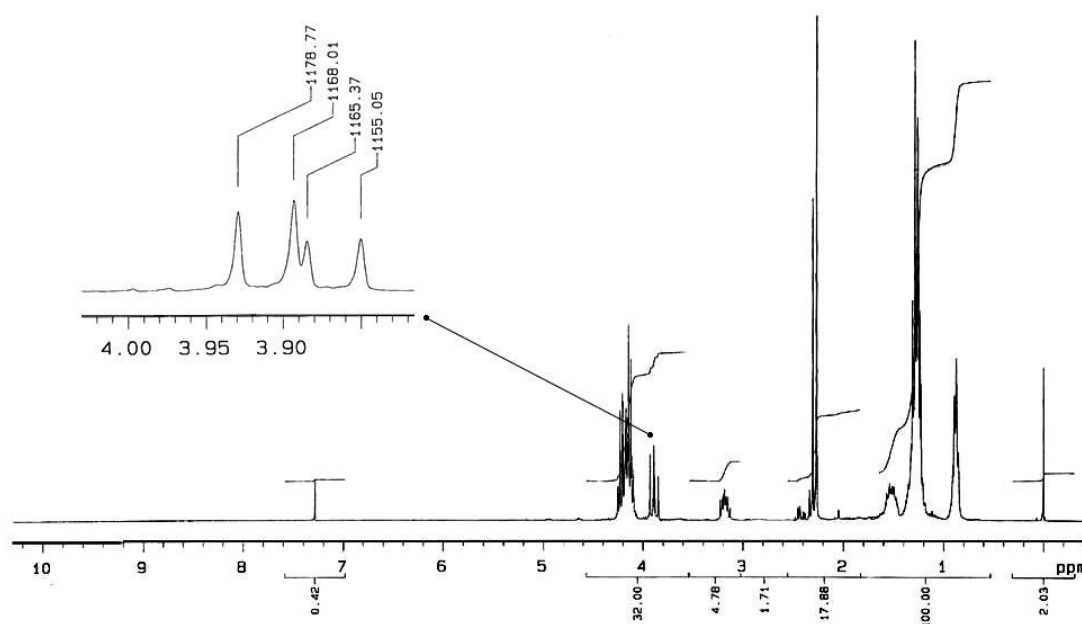


Fig. 10: ^1H -NMR spectrum of diethyl-2-acetyl-3-butylbutanedioate (I, Scheme 1) in CDCl_3 , which reveals the presence of an erythro-threo mixture as demonstrated in the magnified section

Hydrolysis of the diester (I, Scheme 1) was accomplished, as described in literature^{68,70} (pathway A, Scheme 1), with a sodium hydroxide solution (1.25 M). Subsequently, the diacid was isolated from the reaction mixture by acidification with sulfuric acid (2.0 M). The γ -keto acid (II, Scheme 1) was obtained in good yield (87%) by refluxing the crude diacid for 1 h. The decarboxylation reaction was carried out in two different solvents, toluene and benzene, and a better result was achieved when benzene was used (87 % yield versus 80 % yield). Additionally, a good yield (90 %) of the γ -keto acid (II, Scheme 1) was achieved using the alternative pathway (pathway B, Scheme 1), performing the hydrolysis and the decarboxylation of the diester in a single step by treatment with concentrated hydrochloric acid.

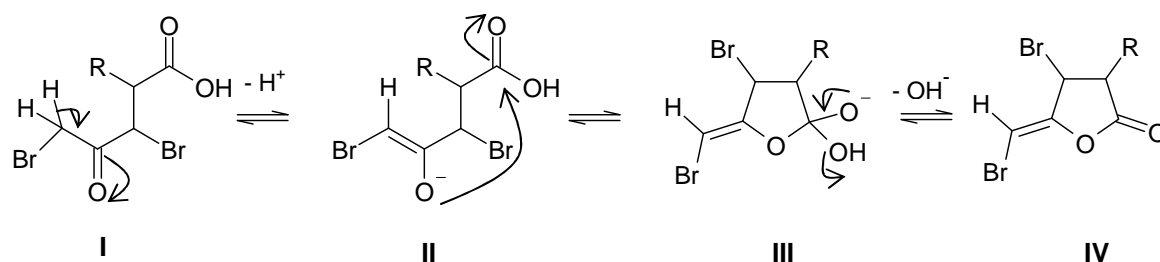
To prepare the 2-(1,3-dibromo-2-oxopropyl)hexanoic acid (III, Scheme 1), the 2-(2-oxopropyl) hexanoic acid (II, Scheme 1) was treated with two equivalents of bromine in chloroform in the presence of a catalytic amount of hydrobromic acid. The bromination proceeds by the formation of the enol-form promoted by the

hydrobromic acid, followed by enol reacting with the halogen. All hydrogens adjacent to the keto group can react with bromine, so that a complex mixture of different mono-, di- and tri-bromo-derivatives was obtained. The brominated products turned out to be extremely difficult to separate and none of the purification methods used permits the isolation of the desired 2-(1,3-dibromo-2-oxopropyl)hexanoic acid (**III**, Scheme 1). No separation was achieved with column chromatography using ethyl acetate/hexane (1:4, [v/v]) as the mobile phase. To perform column chromatography a series of different mobile phases was investigated by TLC, but all trials failed. Additionally, reverse phase-medium pressure liquid chromatography (RP-MPLC) was performed to separate the complex mixture of more or less brominated intermediates, but the method also turned out to be an inadequate technique for their purification. Furthermore, anion exchange chromatography could not be applied since the brominated derivatives were unstable at alkaline pH values under which the chromatography has to be performed.

In order to achieve a more selective bromination of 2-(2-oxopropyl)hexanoic acid (**II**, Scheme 1), an alternative synthetic strategy was attempted. Bromine was added very slowly (over a period of 4 h) to a solution of 2-(2-oxopropyl)hexanoic acid (**II**, Scheme 1) in diethyl ether, keeping the temperature at -5°C ⁷². Even under these reaction conditions a mixture of brominated compounds difficult to separate was generated. Short-path ball-tube distillation was performed in the attempt to isolate the 2-(1,3-dibromo-2-oxopropyl)hexanoic acid (**III**, Scheme 1) without achieving positive results.

Due to the enormous separation difficulties, the mixed brominated keto acids, derived from the reaction of 2-(2-oxopropyl)hexanoic acid (**II**, Scheme 1) with bromine in the presence of hydrobromic acid, were used as such in the following reaction step. The brominated keto acids were efficiently converted into tetrahydro-2(5H)-furanones by treatment with phosphorus pentoxide. Scheme 2 illustrates the cyclisation mechanism of 2-(1,3-dibromo-2-oxopropyl)hexanoic acid promoted by P_2O_5 . It acts in two different ways. First, it catalyses the deprotonation in α -position to the keto-group to give a carbanion (**I**, Scheme 2) and the enolate (**II**, Scheme 2), respectively. The enolate (**II**, Scheme 2) is able to undergo cyclisation to give a five-membered ring (**III**, Scheme 2), which reacts

finally under dehydrogenation supported again by P_2O_5 to yield the tetrahydro-2(5H)-furanones (**IV**, Scheme 2).



Scheme 2: Proposed mechanism for the cyclisation of 2-(1,3-dibromo-2-oxopropyl)hexanoic acid to 4-bromo-3-butyl-5-(bromomethylene)-2(5H)-furanone promoted by P_2O_5

The crude brominated tetrahydro-2(5H)-furanones were subsequently dehydrobrominated to yield the corresponding furanones, by treating them with the organic nitrogen-base 1,4-diazabicyclo[2.2.2]octane (DABCO) (Scheme 1).

3.1.2 Isolation, purification, and characterization of 3-butyl-5-(bromomethylene)-2(5H)-furanone

The synthetic route followed for the preparation of 3-butyl-5-(bromomethylene)-2(5H)-furanone yielded a mixture of products with high structural similarity, whose separation turned out to be very complex. Preparative TLC performed using ethyl acetate/hexane (1:10, [v/v]) as the mobile phase, even though being a time consuming method, enabled the isolation of the desired brominated furanone (**IV**, Scheme 1) in a good grade of purity. Purification of the mixed furanone derivatives by preparative TLC yielded, beside the pure 3-butyl-5-(bromomethylene)-2(5H)-furanone, a mixture of three compounds, which could not be separated. 3-Butyl-5-(bromomethylene)-2(5H)-furanone was analyzed by 1H -NMR and UV-spectroscopy. The NMR data for 3-butyl-5-(bromomethylene)-2(5H)-furanone (Fig. 11) were in agreement with those in literature⁶⁹⁻⁷¹. The compound showed a singlet at δ 7.07 ppm which is assigned to H4 of the

furanone ring (Fig. 9) the singlet at δ 5.98 ppm is characteristic for the proton of the exocyclic double bond while the signals that appear at δ 2.35 ppm, δ 1.58 ppm, δ 1.36 ppm and δ 0.93 ppm are assigned to the butyl side-chain.

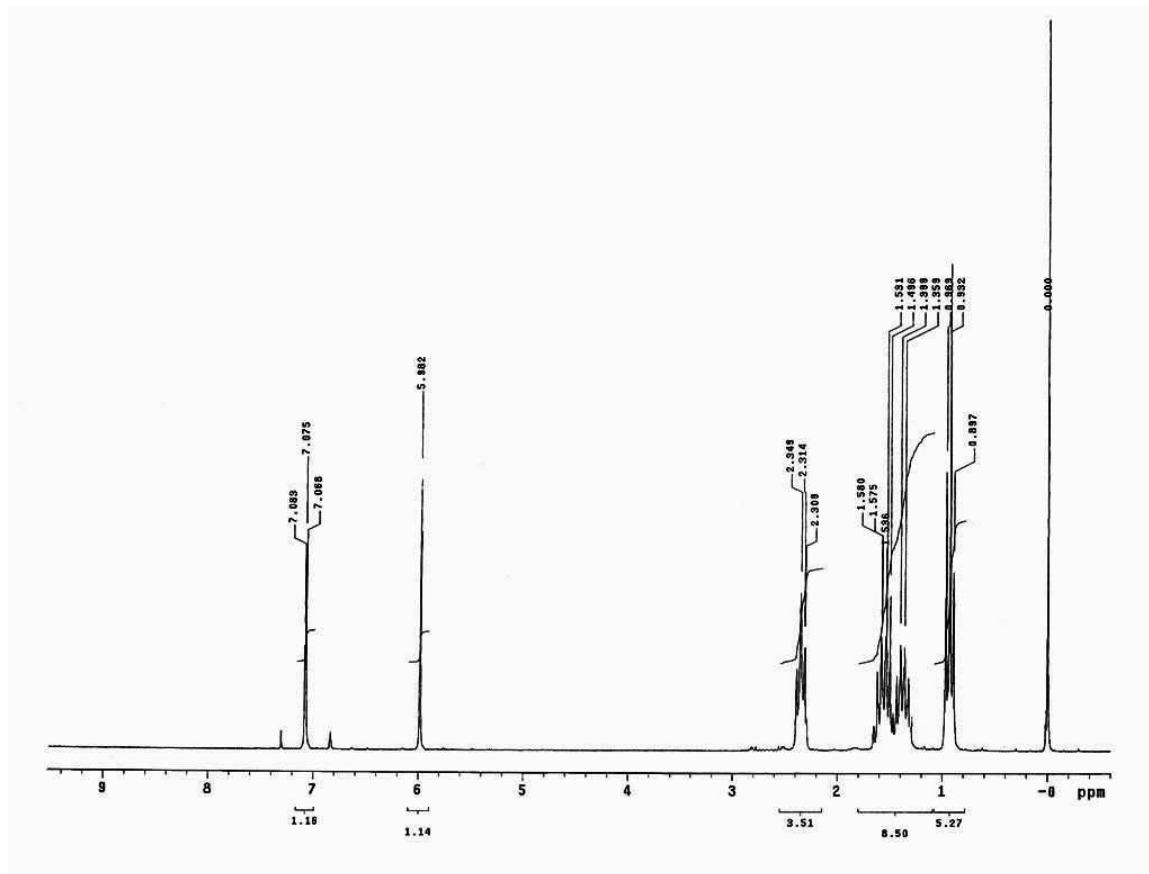


Fig. 11: ¹H-NMR spectrum of 3-butyl-5-(bromomethylene)-2(5H)-furanone in CDCl₃

The UV spectrum of 3-butyl-5-(bromomethylene)-2(5H)-furanone, measured in EtOH/H₂O (50:50, [v/v]), showed a characteristic well-defined band at λ_{max} = 287 nm (Fig. 12).

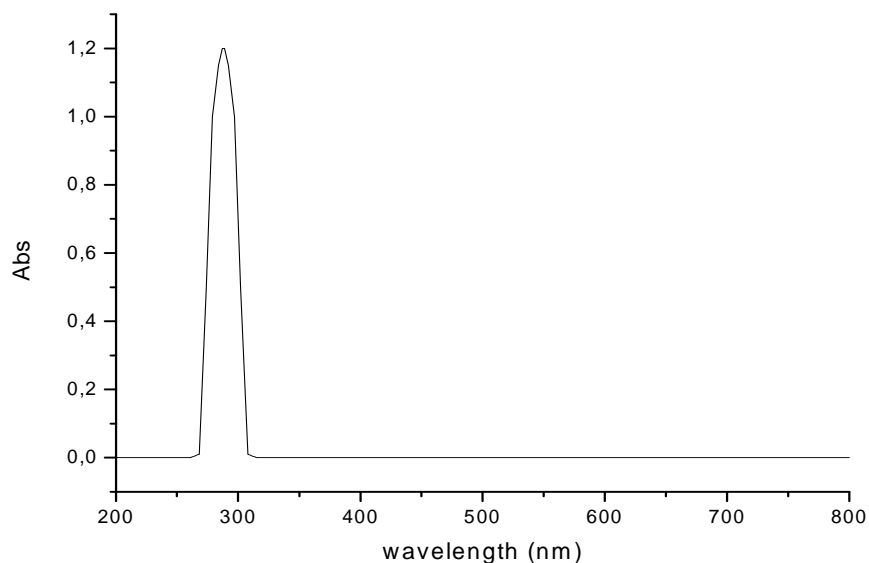


Fig. 12: UV spectrum of 3-butyl-5-(bromomethylene)-2(5H)-furanone in EtOH/H₂O (50:50,[v/v])

3.1.3 Isolation and characterization of a furanone derivatives mixture

The mixture of furanone derivatives, observed as a second band characterized by a lower retention time in preparative TLC compared to the target product 3-butyl-5-(bromomethylene)-2(5H)-furanone, was also analyzed by means of ¹H-NMR spectroscopy. The spectrum, shown in Fig. 13, demonstrates that this mixture consists of 3-butyl-5-(dibromomethylene)-2(5H)-furanone, 4-bromo-5-(bromomethylene)-3-butyl-2(5H)-furanone, and 3-butyl-5-methylene-2(5H)-furanone (Fig. 14).

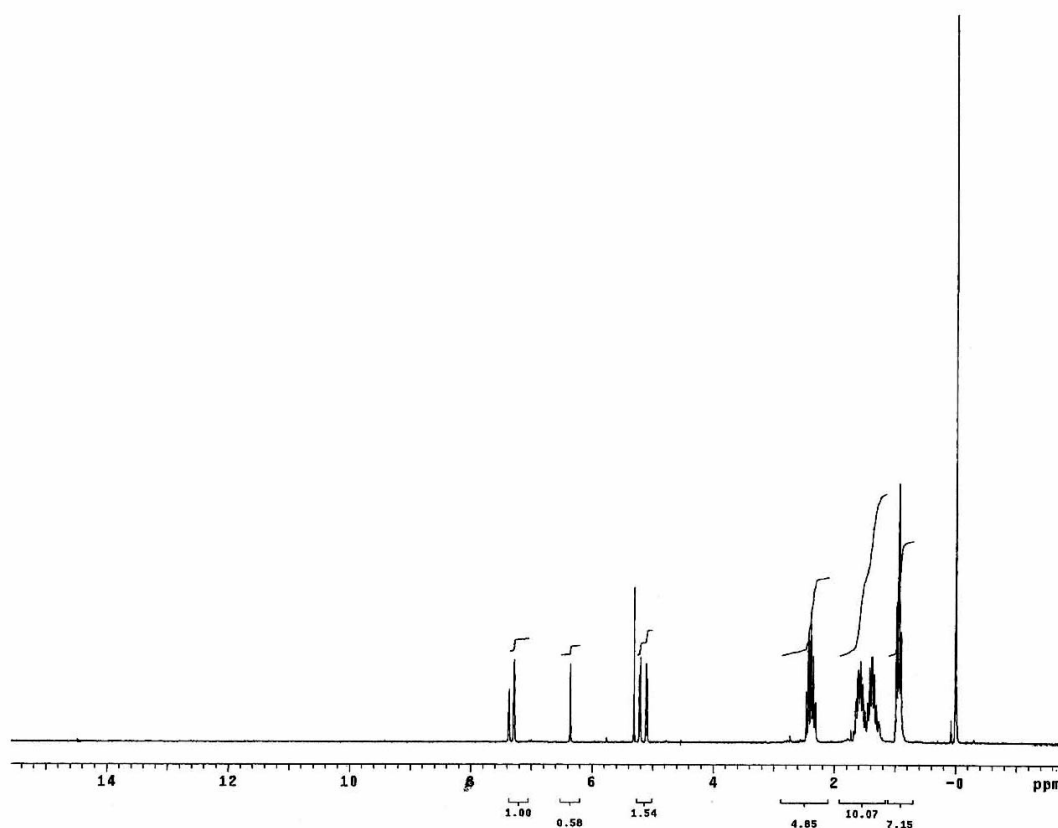


Fig. 13: ^1H -NMR spectrum in CDCl_3 of the mixture of 3 furanone compounds: 3-butyl-5-(dibromomethylene)-2(5H)-furanone, 4-bromo-5-(bromomethylene)-3-butyl-2(5H)-furanone and 3-butyl-5-methylene-2(5H)-furanone

The singlet at δ 7.38 ppm corresponds to the H4 of the furanone ring of 3-butyl-5-(dibromomethylene)-2(5H)-furanone (**I**, Fig. 14). The singlet at δ 6.36 ppm is assigned to the proton at the exocyclic double bond of the 4-bromo-5-(bromomethylene)-3-butyl-2(5H)-furanone (**II**, Fig. 14). the signal at δ 7.3 ppm is assigned to the H4 of the furanone ring of 3-butyl-5-methylene-2(5H)-furanone (**III**, Fig. 14) and the signals at δ 5.29 and δ 5.12 to the exocyclic double bond protons of 3-butyl-5-methylene-2(5H)-furanone (**III**, Fig. 14).

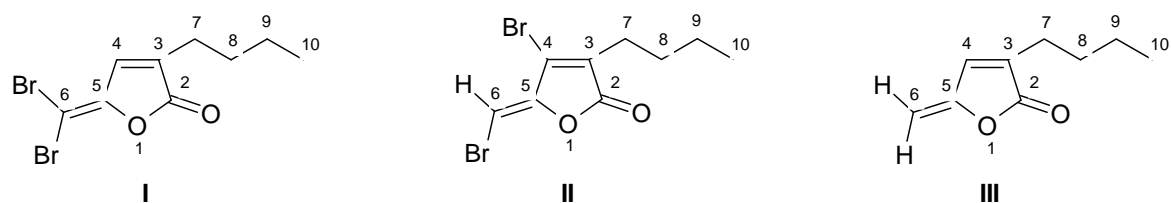


Fig. 14: Molecular structures of different furanone derivatives isolated as a mixture during the synthesis described in Scheme 1:

(I) 3-butyl-5-(dibromomethylene)-2(5H)-furanone, (II) 4-bromo-5-(bromomethylene)-3-butyl-2(5H)-furanone, and (III) 3-butyl-5-methylene-2(5H)-furanone

3.2 Preliminary investigations on the inhibition of biofilm formation on PDLLA by incorporation of 3-butyl-5-(bromomethylene)-2(5H)-furanone

Researchers of the University of South Wales in Sydney (Australia) observed, that the surface of macroalga (seaweed) *Delisea pulchra* was relatively free of bacterial colonization⁵³. This prompted an in-depth investigation of the defense mechanism against marine bacteria evolved by the alga. It has been determined that *Delisea pulchra* produces QS-antagonist molecules, called fimbriolides or halogenated furanones (see paragraph 1.4.1.1). These compounds reside in vesicles in the seaweed gland cells and are released at the algae's surface, where they prevent bacterial adhesion and biofilm formation.

The objective of this study was to mimic the defensive strategy of *Delisea pulchra* developing a biomaterial, which would continuously release the QS-antagonist, 3-butyl-5-(bromomethylene)-2(5H)-furanone, at their surface. PDLLA, one of the most commonly used biodegradable polymers, was selected as a model matrix for loading with the synthesized QS-antagonist. To prepare 3-butyl-5-(bromomethylene)-2(5H)-furanone loaded PDLLA films, mixtures of the halogenated furanone and the polymer were used. Preliminary investigations on the preparation of agent-loaded PDLLA films and the characterization of their *in vitro* release properties were carried out using 2-(2-bromoethyl)-2,5,5-trimethyl-1,3-dioxane as model compound.

3.2.1 Preparation of PDLLA films containing 2-(2-bromoethyl)-2,5,5-trimethyl-1,3-dioxane and characterization of their *in vitro* release properties

Prior to studying the release kinetic of 3-butyl-5-(bromomethylene)-2(5H)-furanone from PDLLA (Resomer® R 208) films, the release behavior of a model compound was investigated. 2-(2-Bromo-ethyl)-2,5,5-trimethyl-1,3-dioxane (Fig. 15) was selected as model molecule, due to its similarity in size, chemical structure and hydrophilic/hydrophobic properties with the antibacterial molecule.

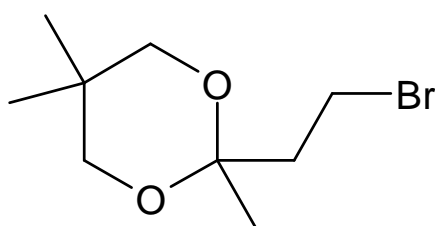


Fig. 15: Structure of 2-(2-bromoethyl)-2,5,5-trimethyl-1,3-dioxane used as a model compound for 3-butyl-5-(bromomethylene)-2(5H)-furanone intended for the emulation of controlled release systems based on PDLLA

The 2-(2-bromoethyl)-2,5,5-trimethyl-1,3-dioxane and the 3-butyl-5-(bromomethylene)-2(5H)-furanone have a molecular weight of 237 Da and 230 Da, respectively. Like the halogenated furanone, the model compound is an oil, has a cyclic structure and contains a bromine atom. Both molecules are insoluble in water and have good solubility in ethanol and methylenechloride.

PDLLA films containing 5% [w/w] of 2-(2-bromoethyl)-2,5,5-trimethyl-1,3-dioxane were produced. The prepared films were circular with a diameter of 24 mm and a thickness of 12 μm . To prepare them, the 2-(2-bromoethyl)-2,5,5-trimethyl-1,3-dioxane model substance and the polymer were dissolved in chloroform, the resulting solution was poured onto glass plates and the solvent was allowed to evaporate.

In vitro drug release studies were performed in triplicate; the experiments were carried out in deionized water under perfect sink conditions in a shaker incubator at 37 $^{\circ}\text{C}$. At defined time points the amount of active agent released was determined by UV/VIS spectrophotometry.

In Fig. 16 the release of 2-(2-bromoethyl)-2,2,5-trimethyl-1,3-dioxane from PDLLA containing 5% [w/w] 2-(2-bromo-ethyl)-2,2,5-trimethyl-1,3-dioxane is shown, where the fraction of released compound (M_t/M_0) is cumulatively plotted versus time.

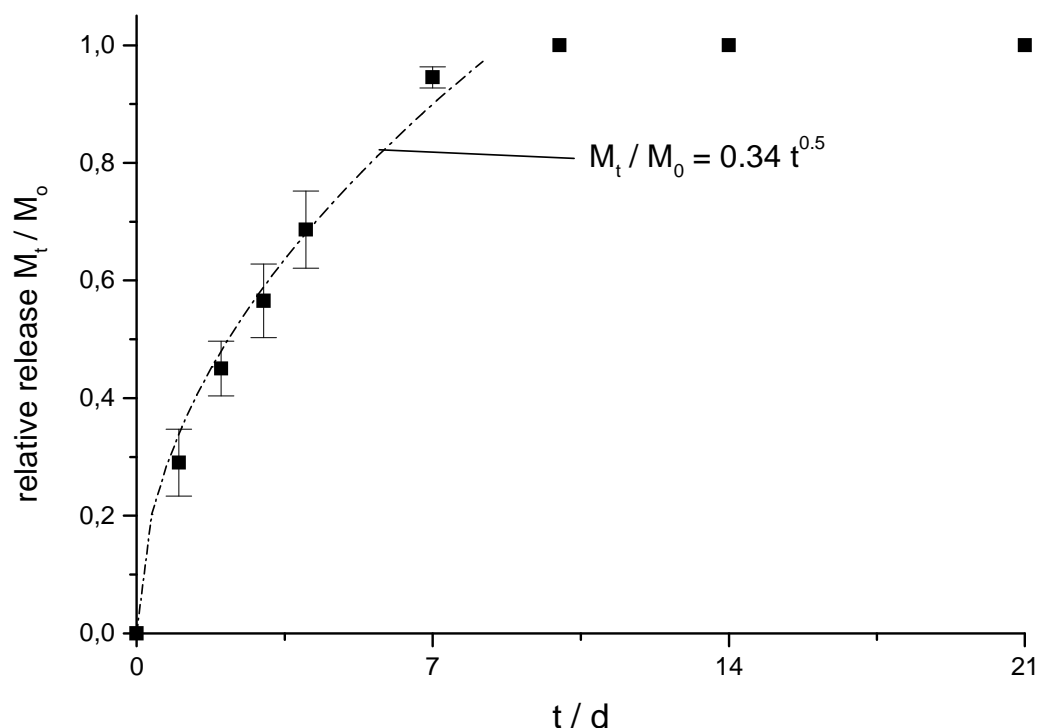


Fig. 16: Relative, cumulative release M_t/M_0 of 2-(2-bromoethyl)-2,2,5-trimethyl-1,3-dioxane from PDLLA films containing 5% [w/w] 2-(2-bromoethyl)-2,2,5-trimethyl-1,3-dioxane. The release experiments were carried out in deionized water at 37 °C under perfect sink conditions ($n = 3$)

The release profile shows, that within the first 7 days 95% of the incorporated 2-(2-bromoethyl)-2,2,5-trimethyl-1,3-dioxane was released from the films. Later time points showed no significant release. The fit describes a system according to the model for diffusion controlled systems. The model applied to describe the release, is based on a linear dependence between the fractional amount released and the square root of time (eq. 1). The diffusional exponent is $n = 0.5$ and matches the Case I – Transport mechanism for diffusional controlled systems^{73,74,75}.

$$M_t/M_0 = k_{kin} \cdot t^n \quad (\text{eq. 1})$$

M_t/M_0 : fractional amount released

k_{kin} : kinetic constant

n : diffusional exponent

$n = 0.5$ diffusion controlled release mechanism (Case I – Transport)

$0.5 < n < 1$ anomal or non Fickian diffusion (Case II – Transport)

For the release profile fit time points within the fractional release amount $M_t/M_0 < 0.8$ were used.

3.2.2 Preparation of PDLLA films containing 3-butyl-5-(bromomethylene)-2(5H)-furanone and characterization of their *in vitro* release properties

PDLLA films containing 1% [w/w] of 3-butyl-5-(bromomethylene)-2(5H)-furanone (Fig. 17) were prepared.

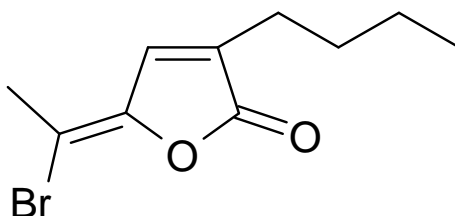


Fig. 17: Structure of the QS antagonist 3-butyl-5-(bromomethylene)-2(5H)-furanone

The prepared films had a diameter of 15 mm and a thickness of 12 μm . They were characterized in terms of *in vitro* release behavior as described for the model compound 2-(2-bromoethyl)-2,2,5-trimethyl-1,3-dioxane.

The PDLLA/3-butyl-5-(bromomethylene)-2(5H)-furanone system has a lower release rate than the model system PDLLA/2-(2-bromoethyl)-2,2,5-trimethyl-1,3-dioxane. It showed a continuous sustained release over the observed period of

75 days. 60 % of the incorporated furanone was released within the investigated time (Fig. 18).

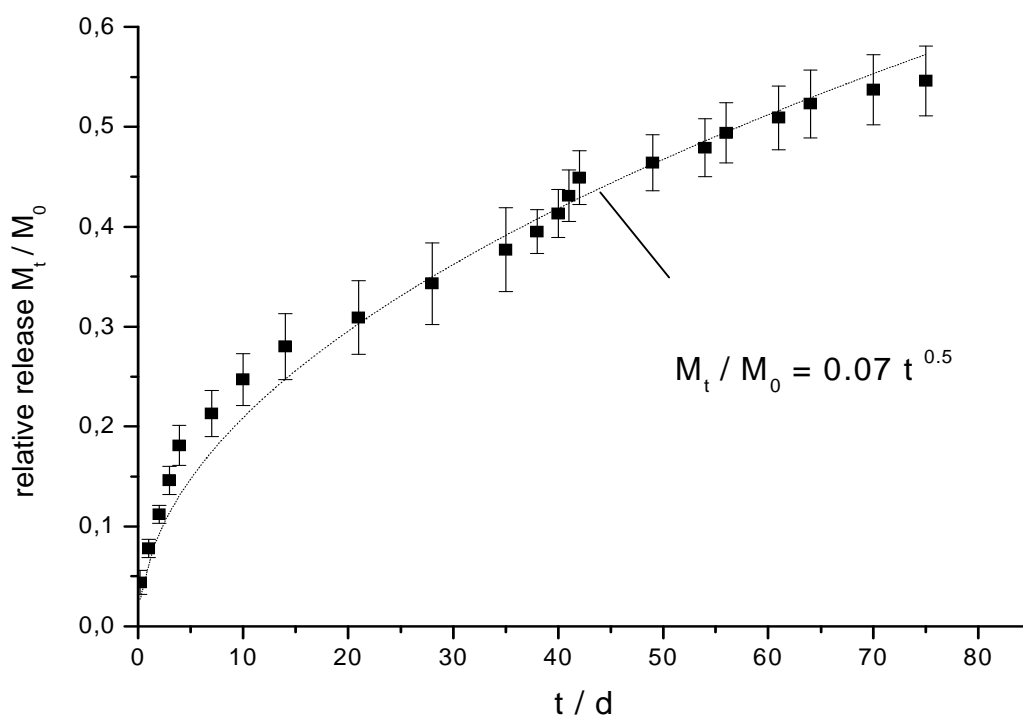


Fig. 18: Relative, cumulative release M_t/M_0 of 3-butyl-5-(bromomethylene)-2(5H)-furanone from PDLLA films containing 1% [w/w] furanone. The release experiments were carried out in deionized water at 37 °C under perfect sink conditions (n = 3)

The fit describes a system according to the model for diffusion controlled systems (eq. 1). A diffusion controlled release mechanism of 3-butyl-5-(bromomethylene)-2(5H)-furanone from the PDLLA films over the investigated time period can therefore be assumed.

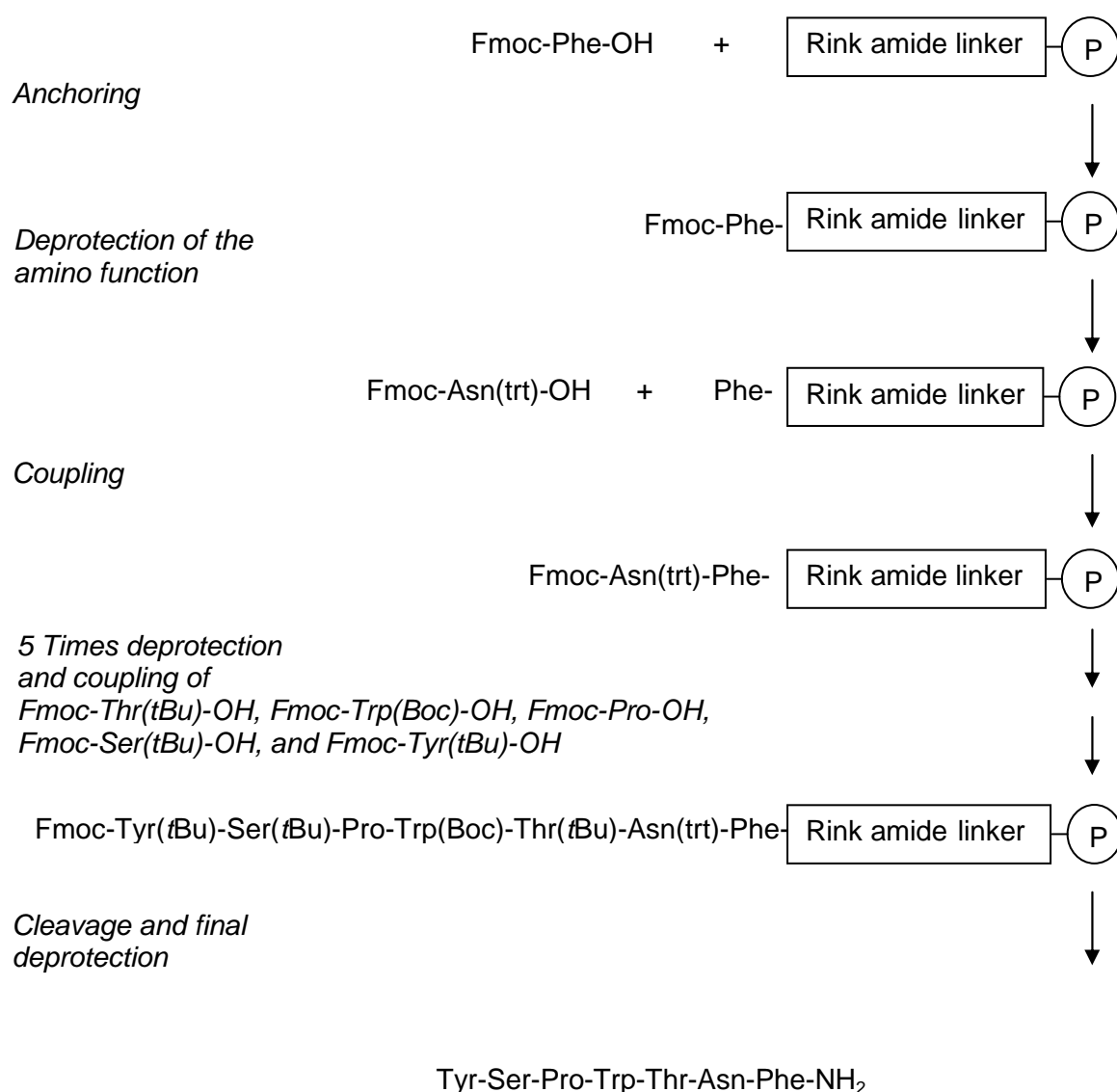
3.3 Application of RIP as a QS antagonist immobilized on a biomaterial surface

The prevention of biofilm development by using antagonists of QS receptors is becoming a more and more attractive strategy^{2,45,47,51,68}. RIPs, a new class of anti-QS peptides with the primary structure YSPXTNF, are predicted to have a high potential for inhibiting bacterial adhesion and biofilm formation. So far, only the use of these peptides as non-covalently bound (e.g. adsorbed) coatings has been investigated, but the effectiveness of covalently immobilized RIPs on biomaterials is not yet assessed. Therefore, it has been decided to synthesize a RIP molecule and to attach it covalently to a non-degradable polymer.

3.3.1 RIP molecule synthesis by using the principles of solid-phase peptide chemistry

RIP molecules, isolated from supernatants of coagulase staphylococci, are not commercially available and therefore have to be synthesized. Since the natural peptides YSPXTNF, differing at the position X, are carboxy-terminated, they are sensitive towards enzymatic degradation. RIP peptide with Trp (W) at the position X, was then synthesized in its more stable amide form, as suggested in literature⁶³. The preparation of the peptide was carried out by the method of the solid-phase peptide synthesis (SPPS), introduced by R. B. Merrifield in 1963. The fundamental premise of SPPS involves the sequential addition of α -amino and side-chain protected amino acid residues to a solid support, the resin. The resin is a synthetic polymer bearing reactive groups. These groups react with the terminate carboxylic groups of the N- α -protected amino acids, thereby covalently binding them to the polymer. Subsequently, the protecting group of the α -amino group can be removed and a second N- α -protected amino acid can be coupled to the attached amino acid. These steps are repeated until the desired sequence is obtained. At the end of the synthesis a different reagent is applied to cleave the bond between the C-terminal amino acid and the polymer resin. The detached peptide molecules can then be isolated from solution. Side-chain protecting groups are often chosen in such a way that they can be cleaved simultaneously

with the detachment of the peptide from the resin (Scheme 3). The great advantage of solid phase synthesis is the elimination of intermediate purification steps, such as crystallization or lengthy chromatographic operations. Since the peptide is bound to an insoluble support, any unreacted reagent left at the end of each coupling step can be removed by a simple wash procedure, greatly decreasing the time required for the synthesis. The general steps of SPPS are described in more detail elsewhere⁷⁶⁻⁸¹.



Scheme 3: General scheme of the synthesis of the amide form of RIP (YSPWTNF-NH₂) by means of SPPS. (P) denotes the polymeric support, (Rink amide linker) is the anchoring group, (Fmoc) is the temporary protecting group, and (*t*Bu), (Boc), and (trt) are the side-chain protecting groups

To synthesize the RIP peptide Fmoc/*tert*-butyl chemistry was used. The fundamental characteristic of Fmoc/*tert*-butyl strategy, is its orthogonality. While base labile 9-fluorenylmethyloxycarbonyl (Fmoc) groups are adopted for α -amino protection, the side chains are protected with *tert*-butyl or trityl based groups which can be cleaved, together with the resin linkage, by trifluoro acetic acid (TFA). The amino acids serine, tyrosine, and threonine were incorporated in their *tert*-butyl-N- α -Fmoc protected form, which is very common for these residues⁷⁷. For the incorporation of asparagine and tryptophan the trityl-protected derivative Fmoc-Asn(trt)OH and the *tert*-butyloxycarbonyl- (Boc) protected derivative Fmoc-Trp(Boc)OH were used, respectively. The advantages of the application of *t*-Boc as side protecting group for tryptophan and the trityl protecting group to block the free amide side chain on the asparagine are widely discussed in literature⁸²⁻⁸⁴. In order to reduce unwanted side reactions at the amino acid side chains, scavengers as triethylsilane (TES) and tryptamine were added to the cleavage solution. To prepare the peptide in its amide form a resin functionalized with an appropriate Rink amide linker, 4-(2',4'-dimethoxyphenyl-Fmoc-aminomethyl)-phenoxymethyl-polystyrene, was used. The linker is shown in Fig. 19.

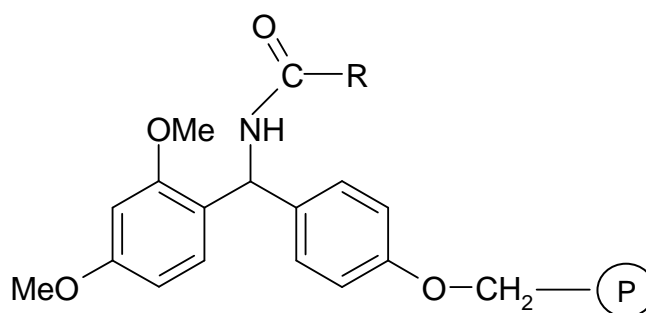


Fig. 19: Rink amide linker attached to the resin (P) and to a peptide (R) used for the preparation of the amide form of the RIP peptide (YSPWTNF-NH₂)

3.3.2 Isolation and purification of RIP

Side reactions may take place during the building of the peptide sequence and especially during the cleavage process. Therefore, it is necessary to separate the target peptide from the resin and the generated by-products. Then in a final step peptide molecules are purified to a final purity of more than 98 % by reverse phase- high performance liquid chromatography (RP-HPLC) and analyzed.

3.3.2.1 Ion exchange chromatography

After the cleavage procedure the clear reaction mixture was mixed with an excess of methyl-*tert*-butyl-ether (MTBE) to precipitate the target peptide as well as all peptide by-products. Subsequently, the suspension was centrifuged. After a few re-suspension steps with fresh MTBE and subsequent centrifugation to remove the scavengers and all other low molecular organic impurities, the precipitate was dissolved in a buffer solution (10 % [v/v] isopropanol in 0.01 M NaH₂PO₄·2H₂O, pH 3). In the first purification step the mixture was fractionated by cation exchange chromatography. At a pH-value of 3.0 most peptide molecules should be positively charged. In Fig. 20 the chromatogram of the separation of the SPPS reaction mixture with a sulfopropyl-modified and dextrane-based (SP-Sephadex)

cation exchange material is shown. As described by the red line in the chromatogram a linear sodium chloride gradient from 0 - 0.5 M was used.

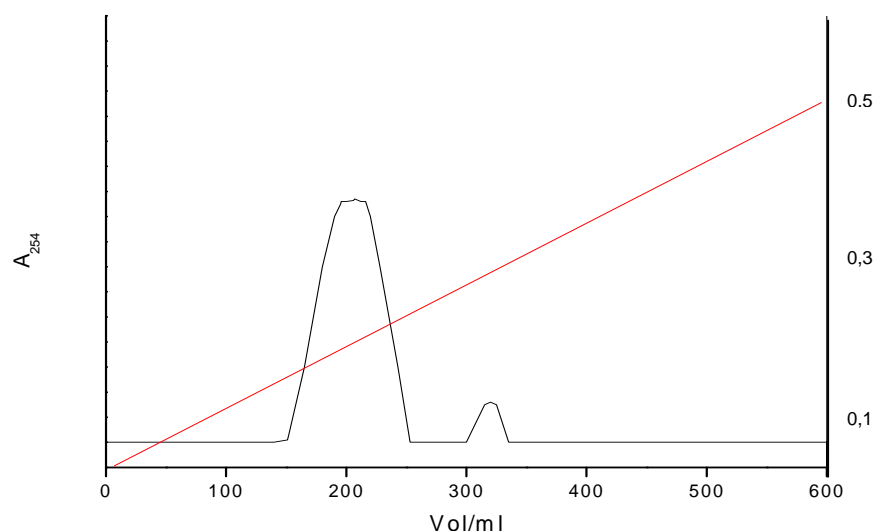


Fig. 20: Ion exchange chromatography (IEC) of the crude peptide performed with a cationic SP-Sephadex column (pH 3.0, gradient: 0 - 0.5 M NaCl). The first peak contained the target peptide

3.3.2.2 Reverse phase medium pressure liquid chromatography

After all fractions of the main part of the first peak of the ion exchange chromatography (IEC) procedure were collected, a final separation by RP-MPLC was performed. As reverse phase material C_{18} -modified silica was used. A linear gradient of 5-30 % [v/v] isopropanol in 0.1 % [v/v] aqueous TFA was applied over a period of 3 h. The RP-MPLC-chromatogram shows one wide band (Fig. 21).

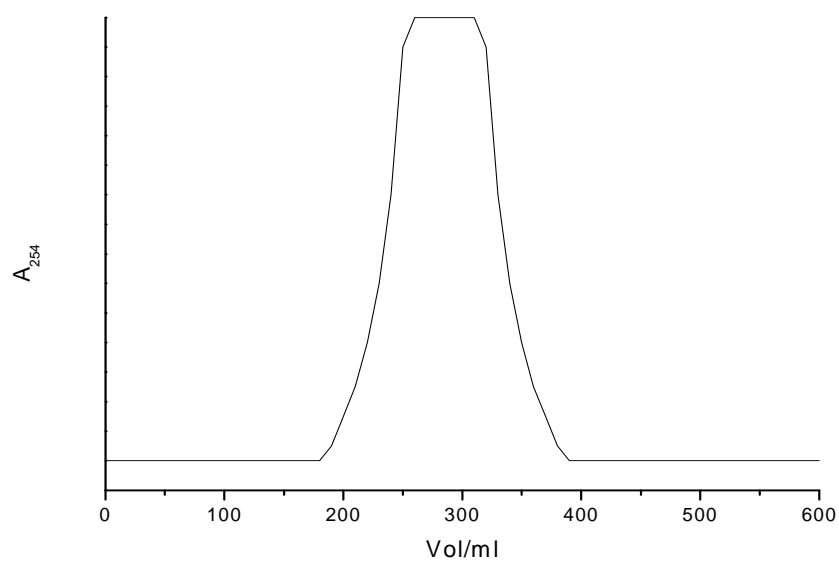


Fig. 21: RP-MPLC of the first IEC fraction using a linear gradient of 5-30 % [v/v] isopropanole in 0.1 % [v/v] TFA at a flow rate of (3 ml/min). A C_{18} -column was applied

Only the fractions of the central part of the band were used for subsequent quality control by RP-HPLC, matrix-assisted laser desorption ionization time of flight mass spectrometry (MALDI-TOF-MS), and amino acid analysis (ASA).

3.3.3 Characterization of RIP

3.3.3.1 Reverse phase- high performance liquid chromatography

The purity of the synthesized peptide YSPWTNF-NH₂ was confirmed by RP-HPLC (Fig. 22). The RP-HPLC run was performed on a C₁₈ column applying a gradient of 10-40 % [v/v] acetonitrile in 0.1 % [v/v] TFA for 20 min (at 1 ml/min) and monitoring at 210 nm. Only one peak was observed and a 99 % purity of the target peptide was obtained.

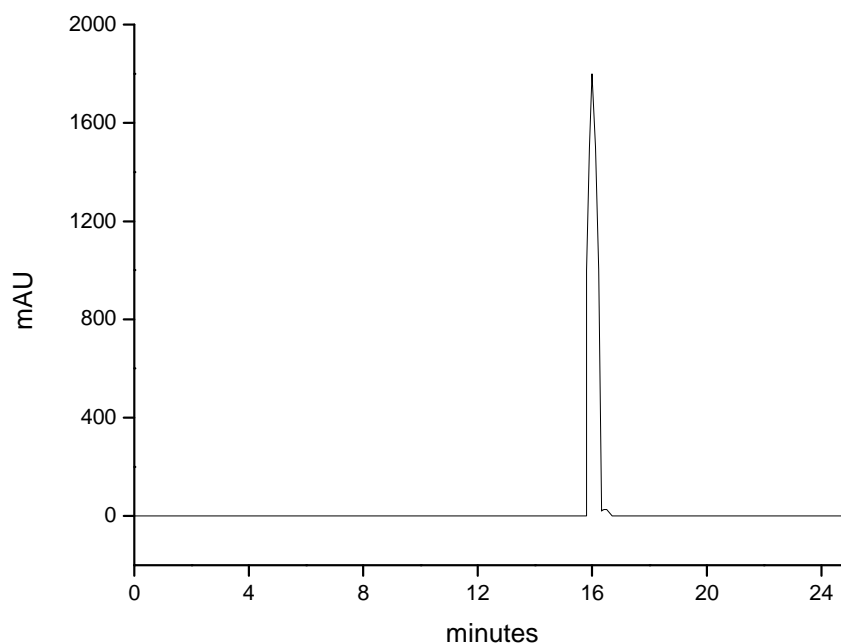


Fig. 22: RP-HPLC chromatogram of the synthesized peptide YSPWTNF-NH₂. The chromatography run was carried out on a C₁₈ column. A linear gradient of 10-40 % [v/v] acetonitrile in 0.1 % [v/v] TFA was used. The flow rate was 1 ml/min

3.3.3.2 Matrix-assisted laser desorption ionization -time of flight- mass spectrometry

MALDI-TOF Mass Spectroscopy has rapidly evolved as an effective technique for the mass analysis of a wide variety of biooligomers and biopolymers, including peptides, proteins, carbohydrates, and nucleic acids^{85,86}.

By isolating the analyte molecules in an appropriate matrix (4-hydroxy- α -cyano cinnamic acid) and irradiating the sample with a high-intensity, pulsed laser beam, it is possible to generate intact, gas-phase ions of high molecular weight analytes. One of the most successful applications of MALDI-TOF-MS has been in the area of peptide and protein analysis^{87,88,89}. The discovery of appropriate matrix compounds⁹⁰⁻⁹³ and the refinement of sample preparation procedures⁹⁴⁻¹⁰⁰ have made it possible to routinely acquire high-quality mass spectra of individual peptides and proteins. Moreover, the MALDI technique is generally applicable to a wide variety of peptides and proteins with no apparent limitations imposed by the size or structure (primary, secondary, or tertiary) of the sample.

In practice, the MALDI-TOF-MS analysis of multicomponent peptide mixtures is complicated, because the different peptide and protein components of a mixture can experience preferential desorption and/or ionization in the MALDI process¹⁰¹⁻¹⁰⁴. In some mixtures, signal suppression effects can be so severe that certain peptides and protein analytes are not detected in the presence of others. Such discrimination effects are severely limiting to MALDI applications, which involve the analysis of complex peptide mixtures. On the other hand, MALDI-TOF-MS technique is a very sensitive method to indirectly detect the purity grade of a peptide.

Since RIP peptide is a highly active QS antagonist, it is very important to determine peptide purity after synthesis and to characterize the obtained compound as exactly as possible. Therefore, MALDI-TOF-MS technique was used to analyze the synthesized YSPWTNF-NH₂. In Fig. 23, the MALDI-TOF mass spectrum of the synthesized peptide is presented. The m/z values 913.432 Da and 935.456 Da correspond to the molecular mass of Rip YSPWTNF-NH₂ and to the molecular mass of its sodium adduct, respectively. The remaining peaks are impurities or fragments.

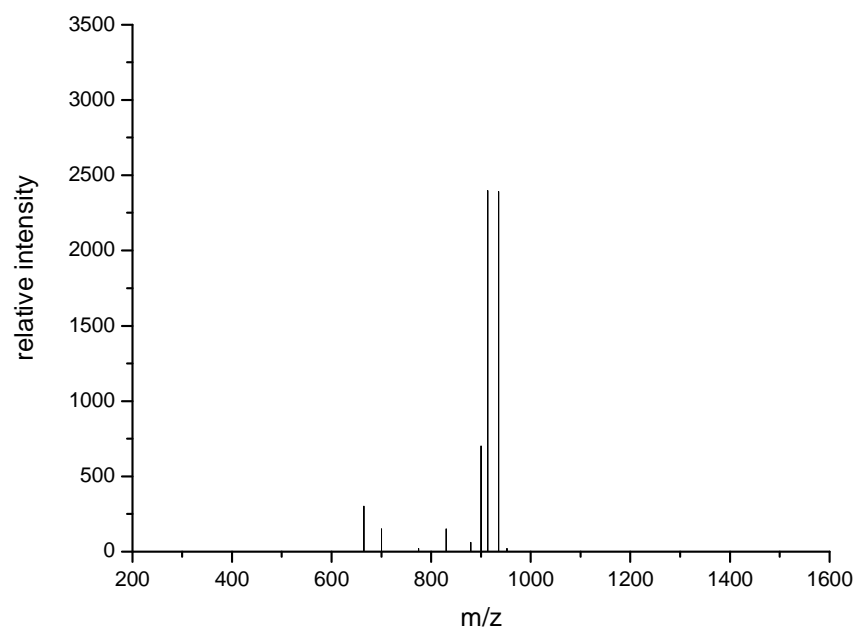


Fig. 23: MALDI-TOF mass spectra of the QS antagonist RIP (mol. Mass = 913,438 Da) and its sodium adduct (mol. Mass = 935,456 Da), purified by IEC and RP-MPLC, which was obtained by using a conventional dried-droplet sample preparation

3.3.3.3 Amino acid analysis

ASA is the suitable method to provide detailed information regarding the relative amino acid composition, which gives a characteristic profile of the target peptide. Tab. 2 compares the calculated relative amino acid composition with the analyzed one.

Tab. 2: Calculated and analyzed relative amino acid composition of the RIP peptide YSPWTNF-NH₂

Amino acid	N _{calc}	N _{ana}
Tyr	1.0	1.09
Ser	1.0	0.89
Pro	1.0	0.96
Thr	1.0	0.90
Asn	1.0	0.98
Phe	1.0	1.07

Trp can not be determined by total hydrolysis and subsequent amino acid analysis

The ASA confirmed the proper molar ratio of the amino acids in the synthesized peptide. The relative amino acid composition of the synthesized peptide is in agreement with the calculated relative amino acid composition of YSPWTNF-NH₂.

3.4 Prevention of biofilm formation by covalent immobilization of a synthetic RIP on functionalized PVDF

Polymers used for medical devices, so-called biomaterials, should fulfill some key requirements. They should possess the mechanical and physical properties, which allow them to replace defect tissues, organ parts or complete organs like heart valves, blood vessels, tendons, ligaments, etc. Furthermore, since they are interfacing biological systems, they should not be cytotoxic, immunogenic and unable to initiate an inflammatory response. Different agents can be responsible for an inflammatory reaction, for example physical stress (mechanics, heat, cold), chemicals and microorganisms (bacteria, fungi, and viruses). In order to prevent bacterial infection and consequently inflammation during and after surgery, permanent antibacterial strategies have to be adopted. The strategy used in this study is based upon the inhibition of biofilm formation on artificial surfaces by the irreversible coupling of the QS antagonist RIP YSPWTNF-NH₂ to the surface. As the investigated polymer PVDF does not possess functional groups, which allow a surface modification, a plasma-induced graft polymerization method was applied to activate and functionalize the polymer surface. AAc was polymerized onto the surface of Ar-plasma activated PVDF. The bioligand RIP-NH₂ was then immobilized to the prepared carboxy-functionalized PVDF-g-PAAc surface by EDC/NHS strategy.

3.4.1 Functionalization of PVDF surfaces

Surface modification of PVDF was carried out on melt-pressed foils prepared in-house, using PVDF granulate certified by the American Food and Drug Administration (FDA) as medical grade. Fig. 24 shows the modification step sequence. First the foils were treated with low-pressure Microwave-induced Ar-plasma. Subsequently, peroxides and hydroperoxides were generated on the surface by exposure to air. To functionalize the oxidized PVDF substrates AAc was graft-co-polymerized onto them. The PAAc grafting was thermo-initiated.

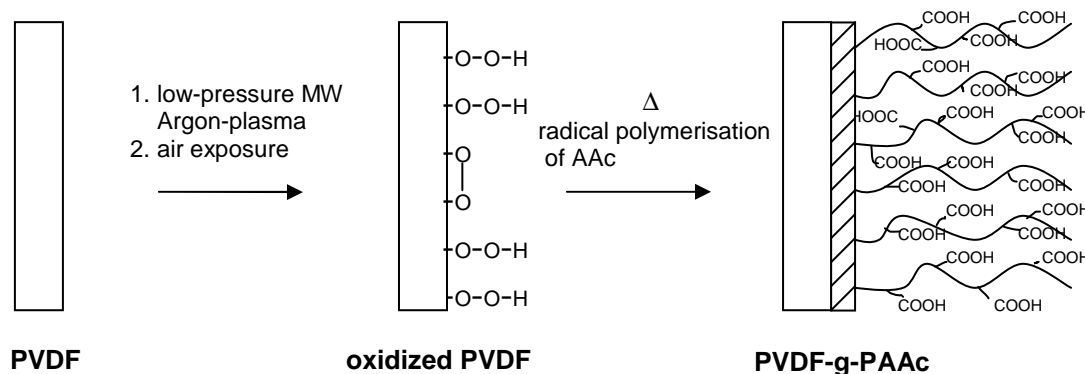


Fig. 24: Graft-co-polymerisation of AAc on melt-pressed PVDF foils

PVDF samples were analyzed after every modification step. First of all, the surface topography was characterized by means of white light interferometry (WIM) to evaluate surface roughness. The surface chemistry of unmodified, activated, and PVDF-g-PAAc was determined. Different surface sensitive techniques were used to prove a successful grafting of PAAc. XPS was performed, as well as ATR-IR, and FT-Raman spectroscopy. Additionally, the physical properties of the PAAc hydrogel coatings, like wettability and surface charge, were measured. Additionally to all these qualitative and semi-quantitative analytics, the carboxyl group content of the PVDF-g-PAAc surfaces was quantified by means of UV/VIS spectrophotometry and potentiometric titration.

3.4.2 Qualitative and quantitative characterization of PVDF-g-PAAc surfaces

The development of implants, prostheses, and medical devices with permanent coatings to inhibit bacterial adhesion, requires a thorough study of the effects of polymer surface properties on adhesion and growth of bacteria. The adhesion and proliferation of different bacteria types on various surfaces depends on polymer surface characteristics like wettability and charge^{105,106}. Wettability is a very important surface property, especially in biomedical applications. It can be manipulated directly e.g. by changing the surface topography. Therefore, an

analysis of the topography of different PVDF surfaces was carried out by means of WIM.

Before a detailed description of the analyzed PVDF surface topography, some aspects of surface profiling have to be mentioned and elucidated. There are more than 200 different surface-texture parameters, and most of them are meant to separate good data from unwanted data by manipulating the determined surface profile in a particular way. Surface texture refers to the locally limited deviations of a surface from the smooth ideal geometry of the part. The deviations can be categorized on the basis of their general patterns, as already done by Schaffer¹⁰⁷. His description of surface characteristics is briefly outlined here, starting with the consideration of a theoretically smooth flat surface. If this surface has a small hollow in its middle part, it is still smooth but curved. Two or more equidistant hollows produce a wavy surface. As the spacing between such waves decreases, the resulting surface would be considered flat but rough. Surfaces having the same height of irregularities are described as wavy, curved, or rough, according to the spacing of these irregularities. Additionally, surface texture includes closely spaced random roughness irregularities and more widely spaced repetitive waviness irregularities. Therefore, the American National Standard B46.1-1985 defines it as the repetitive or random deviation from the nominal surface that forms the 3D topography. As such, it includes roughness, waviness, lay, and flaws (Fig. 25).

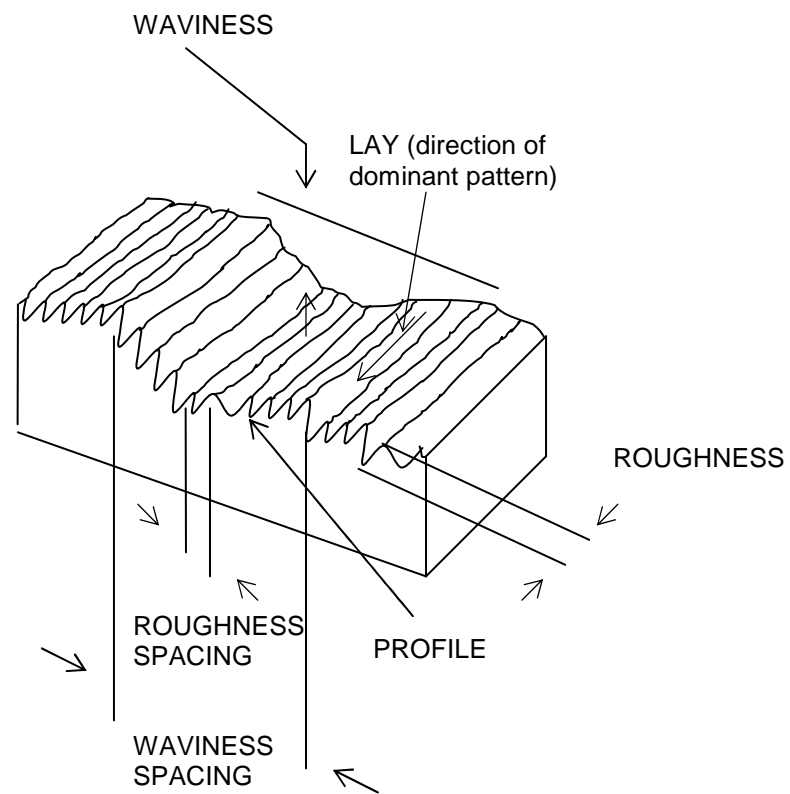


Fig. 25: Demonstration of surface characteristics, explanation of surface texture parameters, listing and defining commonly used terminology

PVDF substrates, used in this study, were prepared by a melt-pressing process. Fig. 26 shows the obtained results.

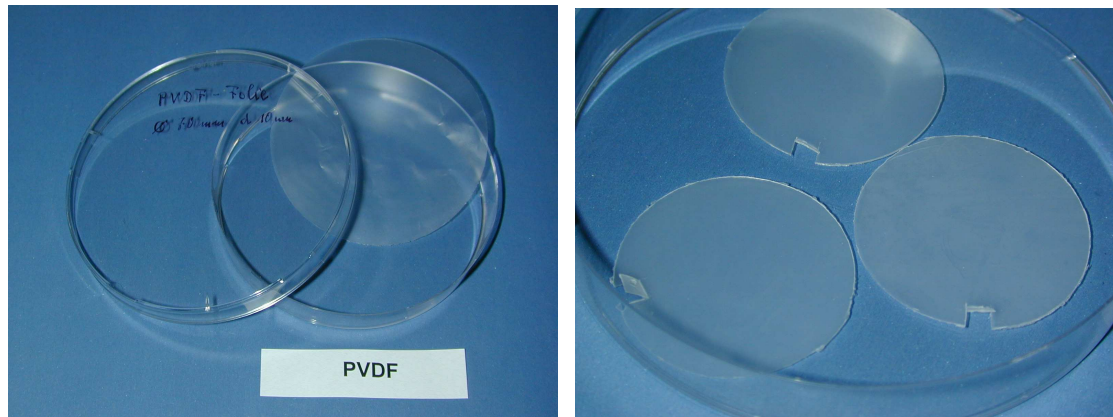


Fig. 26: Photographs of differently sized melt-pressed foils, made out of medical grade PVDF granulate

The following Figure (Fig. 27) describes the topography of melt-pressed PVDF foils, before and after PAAc grafting onto their surface, analyzed by WIM.

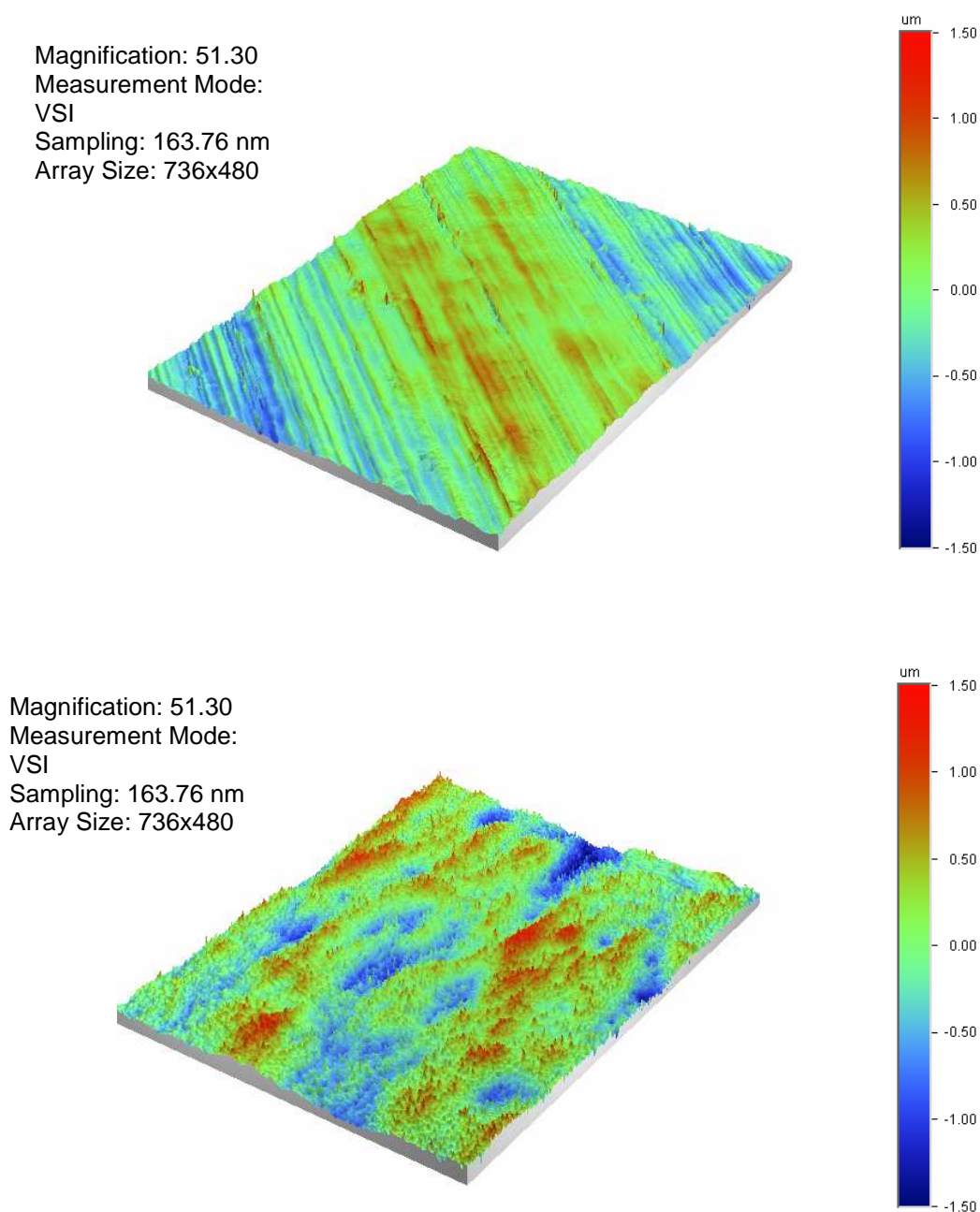


Fig. 27: WIM analysis of PVDF foils manufactured by a melt-pressing process. The PVDF surface (a) is textured and is characterized by an R_q of 320 nm and an R_{tm} of 2 μm . WIM analysis of PVDF-g-PAAc (b) demonstrates a loss of texture after PVDF surface modification with Ar-plasma and thermally initiated grafting of PAAc; the R_q and the R_{tm} of the PVDF-g-PAAc surface are 420 nm and 3 μm , respectively

WIM analysis of PVDF surfaces, which were melt-pressed between aluminium foils, always demonstrated a dominant pattern of heightened and deepened lines following one direction. The root mean roughness R_q , a parameter which specifies the average of all heights in a defined length or area (here the area is $740\ \mu\text{m} \times 480\ \mu\text{m}$), was estimated to be 320 nm. R_{tm} , average maximum height of the profile, is the average of the successive values of R_{ti} , calculated over the evaluation length and is another important parameter, characterizing the topography of a material's surface. Here, R_{tm} was measured to be $2\ \mu\text{m}$.

After Ar-plasma treatment, no significant change concerning the values of R_q and R_{tm} was determined. The plasma activation parameters for PVDF, used in this work, were optimized to generate a maximum of surface radicals and minimize surface etching. Subsequently, the graft-co-polymerization of AAc led to some important surface topography changes. R_q was analyzed to be 420 nm, which is an increase of 100 nm. Additionally, a change of R_{tm} from 2 to $3\ \mu\text{m}$ was measured, which demonstrates that the average maximum height, the vertical distance between the highest and lowest points of the PVDF surfaces, has increased tremendously after the PAAc grafting. The increase of the R_q value demonstrates, that the grafting of PAAc to the PVDF surfaces was successful. Furthermore, the increase of the vertical distance between the highest and lowest points of the PVDF-g-PAAc surface, in comparison to the unmodified PVDF surface, indicates that an activation of the original textured PVDF surface was mainly created on top of the surface protrusions. Such areas are stronger exposed to the plasma than the surface depression areas. Consequently, the subsequent grafting process was also localized on the most exposed surface areas. This was also observed in previous atomic force microscopy experiments¹⁰⁸. In conclusion, the homogeneous modification of a textured polymer surface as described here, is strongly limited by different parameters, including R_q and R_{tm} of the treated material surface, plasma quality, and the average acceleration distance of the electrons, ions, and molecular ions.

Wettability is not only influenced by topographical aspects, but also by elemental composition and chemical structure of the material surface. Therefore, it is necessary to analyze also the chemistry of the PVDF surface before and after modification. The different PVDF surfaces were investigated by surface sensitive

spectroscopic techniques, with different information depths. The methods used were XPS and ATR-IR.

Semi-quantitative information about the outermost (10 nm) surface layer of PVDF and PVDF-g-PAAc was obtained by means of XPS. The modification of melt-pressed PVDF foils by Ar-plasma and subsequent graft-co-polymerisation of AAc was reflected in clear alterations of the surface elemental composition. XPS data showing the elemental composition, as well as different carbon species, are listed in Tab. 3.

Tab. 3: Untreated and modified PVDF, characterized by means of XPS for elemental composition, binding energy and ratios of carbon (C1s), oxygen (O1s), nitrogen (N1s), fluorine (F1s) and other species

Element	BE	PVDF _{theor}	PVDF _{mp}	PVDF 60 s, Ar	PVDFgPAAc
	eV	Atom-%	Atom-%	Atom-%	Atom-%
Carbon C1s		50.0	46.4	58.3	79.3
<u>C</u> -H, <u>C</u> -C	285.0	-	-	22.1	66.3
<u>C</u> -O, <u>C</u> H ₂ -CF ₂	286.5	25.0	23.9	15.5	-
O- <u>C</u> =O	289.1	-	-	6.6	13.0
CH ₂ - <u>C</u> F ₂	290.9	25.0	22.5	14.1	-
Oxygen O1s C- <u>O</u> , C- <u>O</u> -C	532.5	-	1.5	10.7	20.5
Nitrogen N1s C- <u>N</u>	399.7	-	-	-	-
Fluorine F1s C- <u>F</u> ₂	688.0	50.0	52.1	31.0	-
Others	-	-	-	-	0.2

Theoretically, PVDF should only be composed of the elements carbon, hydrogen and fluorine. Therefore, the ratio of carbon and fluorine detected by XPS analysis should be 1:1. The unmodified melt-pressed PVDF foils were instead composed of 46.4 atom-% carbon and 52.1 atom-% fluorine and additionally of 1.5 atom-% of oxygen. After 60 s Ar-plasma treatment, the oxygen

content of the PVDF surface increased to 10.7 atom-%. Such an increase is caused by the reaction between carbon radicals generated by Ar-plasma species on the PVDF surface and oxygen in air. This leads to the formation of peroxy radicals ($\text{ROO}\bullet$), which can recombine to peroxides (ROOR), hydroperoxides (ROOH), acids, alcohols or ketones¹⁰⁹. Tab. 3 shows an acid carbon increase from 0 atom-% in untreated PVDF to 6.6 atom-% after Ar-plasma treatment and air exposure. The subtraction of this value and of the original 1.5 atom-% oxygen of untreated PVDF from the 10.7 atom-% gives a final oxygen content of 2.6 atom-%. Assuming that this oxygen value completely corresponds to ROOR and ROOH , a homogeneous PAAc-grafting based only on the subsequent thermal decomposition of such species is not probable. However, there is another important value, which has increased significantly. After Ar-plasma treatment ca. 22 atom-% of aliphatic carbon were detected. Previously it was observed, that ionizing radiation is able to form stable alkyl radicals in semi crystalline polymers like PVDF¹¹⁰⁻¹¹³. Hence, it can be assumed that plasma treatment also initiates alkyl radical formation, for instance due to the abstraction of fluorine and/or hydrogen. This explains that the fluorine value decreases after plasma treatment from 52.1 atom-% to 31.0 atom-%. Additionally, alkyl radicals are also generated by C-C-bond scission. An overall radical content of approximately 23.7 atom-% should be enough for the subsequent thermally initiated free radical polymerization of AAc. Indeed, the XPS data of Tab. 3 shows an oxygen increase of ca. 10 atom-% from 10.7 to 20.5 atom-%. Moreover, a carboxy-carbon value of 13 atom-% was observed after PAAc grafting. Further confirmation of the successful PAAc grafting is the missing fluorine signal in XPS. Lastly, this indicates that the PAAc coating layer thickness has to be a minimum of 10 nm. Obviously, a diffuse hydrogel like structure is only formed, if the surface is in contact with an aqueous medium. Otherwise, a normal surface structure like other hydrophilic materials as glass, oxidized PVDF, cellulose and polyhydroxyethylmethacrylate (PHEMA) would result. Therefore, to examine whether a material exhibits a diffuse hydrogel like structure, the analysis should be performed with the surface immersed in an aqueous solution. Moreover, investigations under aqueous conditions are particularly important for gel-like biomaterials used in contact with blood or other body fluids. From this point of view, physical means such as XPS, Auger spectroscopy, and scanning electron

microscopy (SEM) are not adequate techniques for the surface characterization of biomaterials. Unfortunately, there are very few methods available for the analysis of diffuse hydrogel-like structures, e.g. ATR-IR spectroscopy, Raman spectroscopy, contact angle measurements by Wilhelmy balance and captive bubble method, zeta potential measurements and quantification of COOH-groups by means of UV/VIS spectrophotometry and potentiometric titration.

Since it has been estimated by XPS, that the thickness of the PAAc layer of PVDF-g-PAAc samples is more than 10 nm under high vacuum conditions, it is necessary to evaluate layer thickness under normal conditions. ATR-IR spectroscopy was therefore carried out, using a Germanium (Ge) crystal as an internal reflection element (IRE). The spectrum is shown in Fig. 28. The successfully grafted PAAc chains were identified by the appearance of a strong carbonyl stretching band, with its maximum at 1710 cm^{-1} . The maximum of the light penetration depth of the spectrometer in ATR mode is ca. 300 nm at 1710 cm^{-1} . This indicates a grafted PAAc layer thickness of at least 300 nm at room temperature and normal humidity (50 % relative humidity).

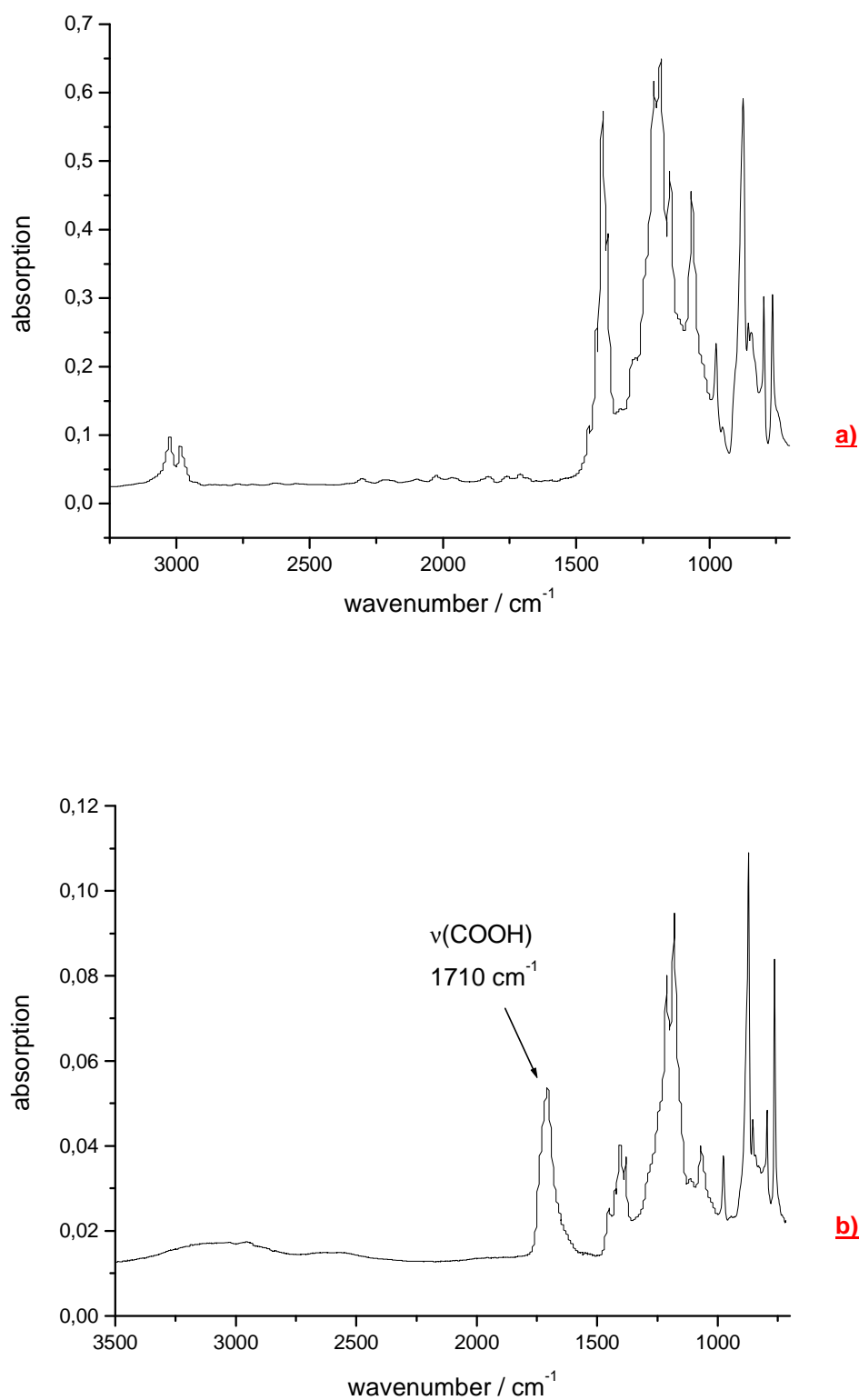


Fig. 28: ATR-IR spectra of unmodified PVDF (a) and PAAc grafted PVDF (b)

In addition to XPS and ATR-IR spectroscopy, Raman spectroscopy was carried out to prove the homogeneous grafting of circular PVDF-g-PAAc foils of 22 mm diameter. PVDF-g-PAAc samples were analyzed by scanning the surfaces. A comparison between the Raman spectra of unmodified and PAAc modified PVDF samples is shown in Fig. 29.

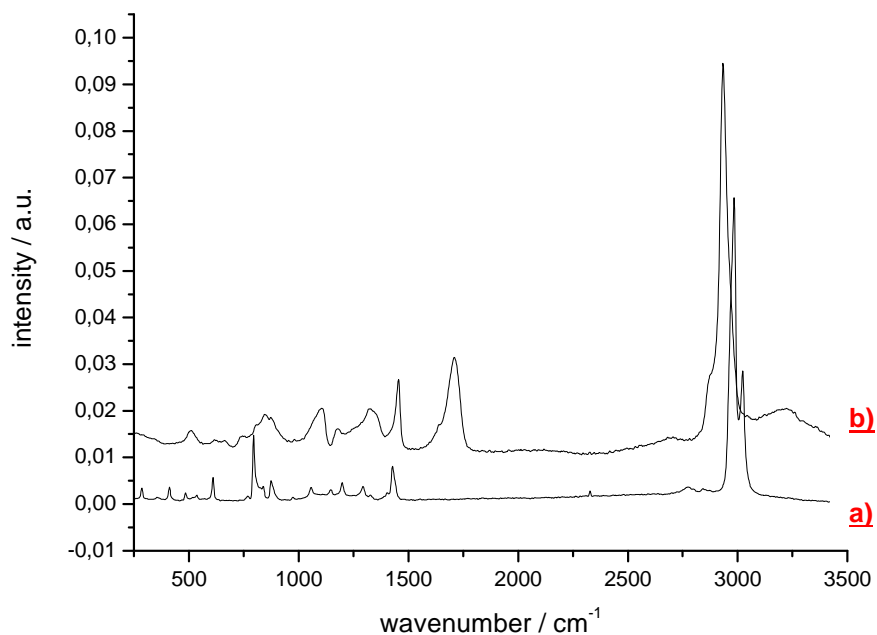


Fig. 29: Raman spectra of unmodified PVDF (a) and PVDF-g-PAAc (b)

Both ATR-IR and Raman spectroscopy demonstrated a homogeneous distribution of carboxy groups on the PVDF-g-PAAc sample surface. In the Raman spectra the characteristic carbonyl signal of the carboxy group is less prominent than in the infrared spectra. The penetration depth of the Nd: Yag-laser, with an excitation line at 1064 nm, is higher and the depth resolution z is lower than those of the ATR-IR spectrometer, when measuring with a Ge-IRE.

Since the PVDF-g-PAAc surfaces have been produced for use in aqueous solutions, for the covalent immobilization of the bioligand RIP as well as for their investigation in microbiological tests, it is very important to assess the properties of the hydrogel PAAc coating in its swollen state. One method to characterize the

grafted PAAc layer under aqueous conditions is to measure its contact angle by the captive bubble method. Results are shown in Fig. 30.

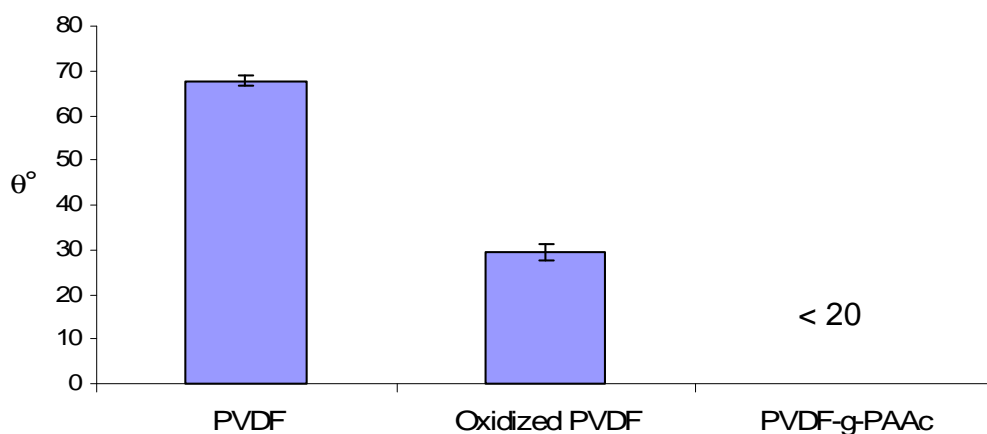


Fig. 30: Captive bubble method contact angle measurements of PVDF, oxidized PVDF (after 60 s Ar-plasma treatment), and PVDF-g-PAAc. All Measurements are taken after 24 h incubation in demineralized water

The significant contact angle decrease after Ar-plasma treatment is in agreement with the XPS data shown in Tab. 3. After PAAc grafting onto the PVDF surface contact angles could not be measured by captive bubble method because of the strong surface hydrophilicity increase. These results are consistent with the previously determined spectroscopic data.

A very powerful analytical method for studying the surface/water interface are zeta-potential measurements, these are related to electrokinetic phenomena. Briefly, the zeta-potential is the electric potential at the shear plane located at the zone from which ions are displaced by a flowing electrolyte solution. The surface, which is in contact with the electrolyte, is believed to determine which ions are released from the slipping plane. In addition, the zeta-potential is closely related to the potential of the surface, which contains chemically adsorbed ions¹¹⁴.

There are several methods for determining the zeta-potential of a surface. For the characterization of biomaterials, which are in continuous contact with an aqueous environment, streaming potential measurements are usually used¹¹⁵.

Fig. 31 describes the pH-dependence of the zeta-potential for uncoated and PAAc-g-PVDF.

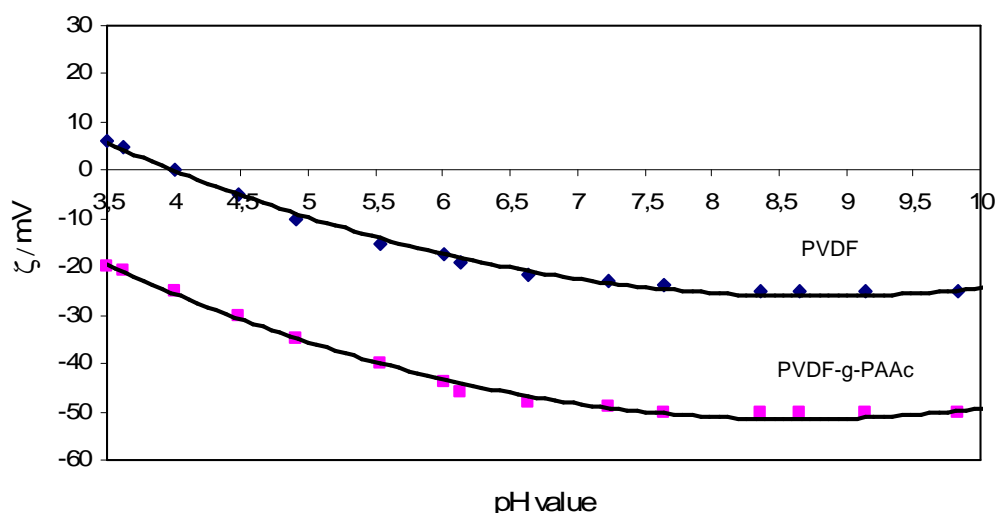


Fig. 31: pH Dependence of the zeta-potential for ♦ PVDF and ■ PVDF-g-PAAc

As is shown in Fig 31 the surface modification effect can be clearly recognized from the zeta-potential measurements. The isoelectric point (IEP) of pure PVDF is located at pH 4, below pH 4 the zeta-potential is positive and at higher pH values it is negative. After AAc grafting a strong IEP shift is observed. The zeta-potential vs. pH curves further indicate, that the surface coverage of PVDF-g-PAAc with carboxylate groups is exceedingly high and has its maximum above pH 8.0. The zeta potential-pH dependence of PVDF-g-PAAc is very similar to the values measured for AAc grafted poly(vinyl alcohol)¹¹⁶.

To measure surface charge change in dependence of pH is very important for the optimization of biomolecule coupling under aqueous conditions. Furthermore, such investigations are useful for the evaluation of the stability of the hydrogel layer stability. In the case of covalent binding of peptides or proteins via their N-terminus to the carboxyl groups of PVDF-g-PAAc optimal coupling results

are achieved at pH 8.4. At this pH value most of the carboxyl groups and the amino groups of the peptide are deprotonated.

Surface sensitive spectroscopic techniques like XPS, ATR-IR, or Raman spectroscopy are not suitable for the quantification of the carboxylic functions. In case of XPS the disadvantages are a detection limit of only 0.1 %, poor spatial resolution, difficulties in quantification associated with matrix matching and surface contamination (a particular part of the surface may not be representative for the rest of the surface or the bulk). Also one should take into account that XPS is a semi-quantitative method, which only provides the ratio of carboxylic groups in relation to other elements present in the surface. Unfortunately, ATR-IR spectroscopy shows different molar absorption coefficients of carboxyl functions.

Therefore, the carboxyl group content of the PVDF-g-PAAc surface was determined by two analytical methods: automated potentiometric acid-base titration and UV/VIS spectrometric back-titration.

Automated potentiometric acid-base titration was performed by immersing PVDF-g-PAAc films into a titrated sodium hydroxide solution. Aliquots of this solution were then titrated with hydrochloric acid (Fig. 32).

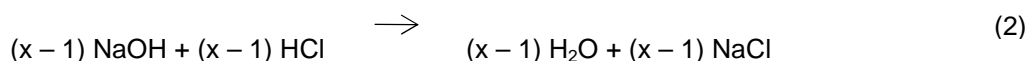
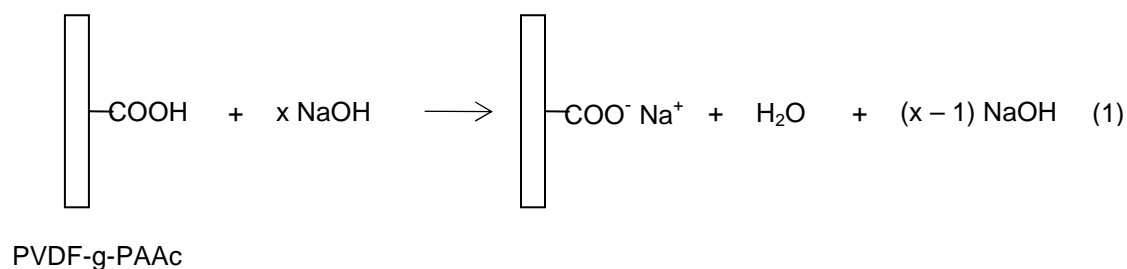


Fig. 32: (1): Deprotonation of carboxylic acid groups of PVDF-g-PAAc by titrated sodium hydroxide solution (Titrisol®). (2) Back-titration of NaOH excess with HCl

This back-titration permits an accurate carboxy group determination into the μmolar range (Fig. 34). UV/VIS spectrometric back-titration was carried out by means of toluidine blue (TB) according to the method of Kang *et al.*¹¹⁷ (Fig. 33).

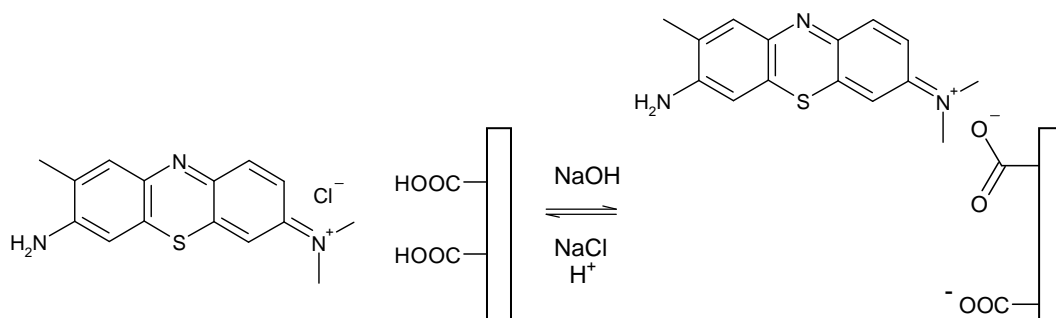


Fig. 33: Interaction between PVDF-g-PAAc and TB

Fig. 34 shows the results from by automated potentiometric acid-base titration and UV/VIS spectrometric back-titration using TB.

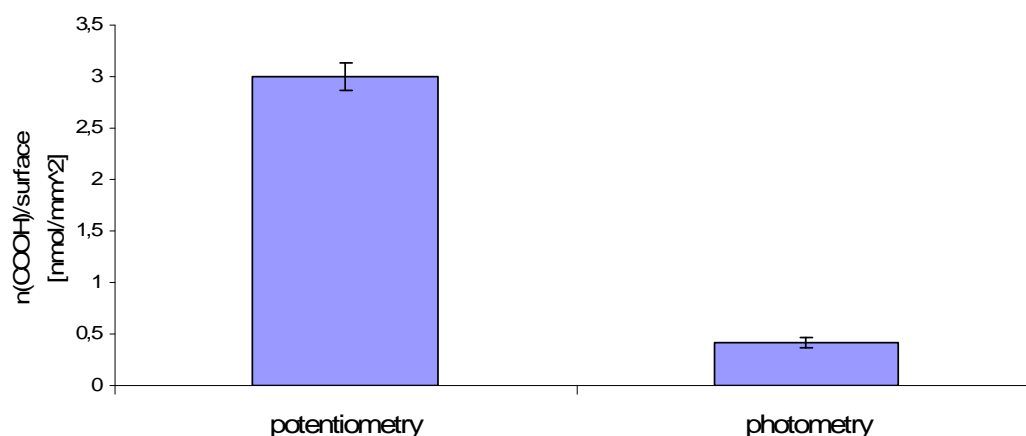


Fig. 34: Comparison of the carboxyl group content on PVDF-g-PAAc surfaces from automated potentiometric acid-base titration and UV/VIS spectrometric back-titration with TB

The carboxyl group content of PVDF-g-PAAc was estimated to be ca. 3 nmol/mm² from automated potentiometric acid-base titration and 0,5 nmol/mm² from UV/VIS spectrometric back-titration.

The different results obtained from the photometric and the potentiometric method are a consequence of the smaller dimensions of the hydroxide ions compared to the TB molecules (Fig. 35).

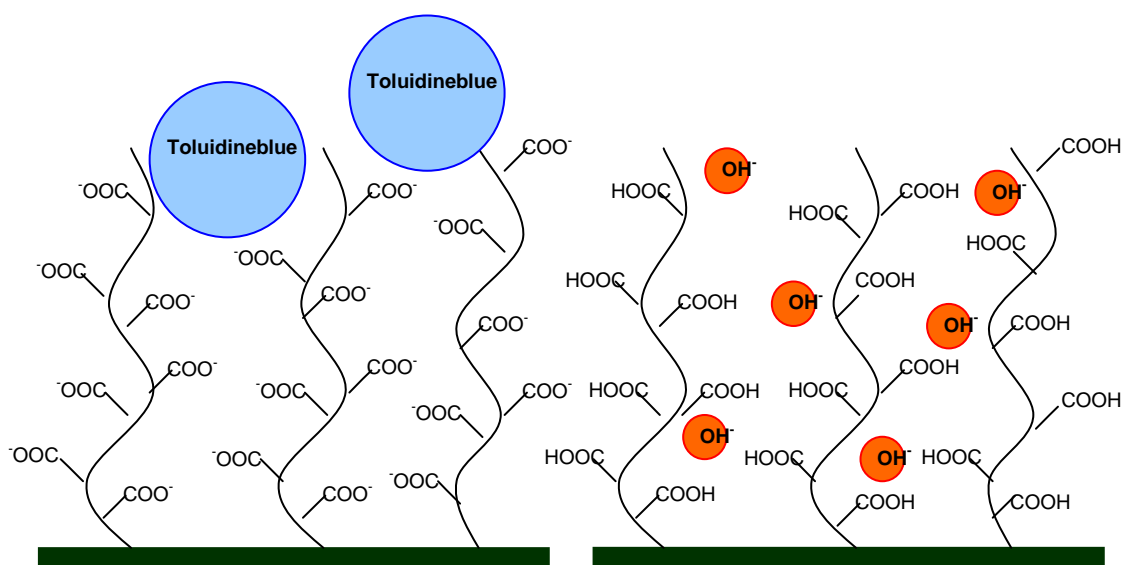


Fig. 35: Interaction between TB (left) molecules and hydroxide ions (right) with the carboxy groups of the grafted PAAc hydrogel layer. Due to their molecular dimensions, TB molecules are limited to interacting only with the outermost PAAc hydrogel layer, the hydroxide ions instead can infiltrate the PAAc chains

As depicted in Fig. 35, the TB molecules react only with the functional groups on the outermost PAAc hydrogel layer; the hydroxide ions instead are able to penetrate between the PAAc chains, thereby reacting with a higher number of carboxy groups in relation to TB.

3.4.3 Covalently immobilized RIP on PVDF-g-PAAc surfaces

The created carboxy-functionalized PVDF-g-PAAc surface was subsequently used to immobilize the bioligand RIP-NH₂ by an EDC/NHS strategy^{118,119} (Fig. 36).

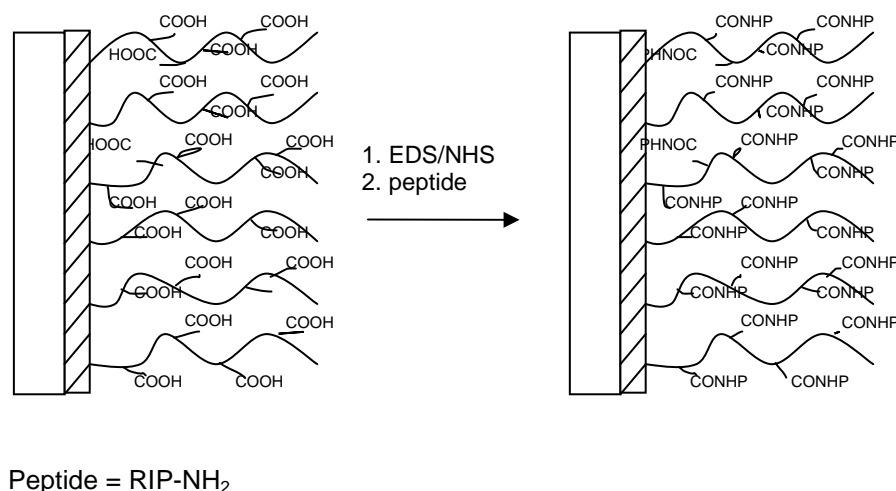


Fig. 36: Immobilization of RIP-NH₂ peptide to the PVDF-PAAc surface by EDC/NHS strategy

Two different coupling concentrations of the RIP-NH₂ solution were employed for the covalent immobilization, 20 µg/ml and 10 µg/ml. In order to obtain information about the effective amount of RIP-NH₂ covalently attached to the PVDF-g-PAAc surface, radioactive binding studies were carried out using a ¹²⁵I-labelled model peptide, (Tyr-Arg-Gly-Asp-Ser) YRGDS. This peptide was selected on account of its higher stability, compared to RIP, during labeling, isolation and purification.

Equivalent to the bioligand RIP-NH₂, Y(¹²⁵I)RGDS was covalently bound to PVDF-g-PAAc surface by EDC/NHS strategy. Three different Y(¹²⁵I)RGDS coupling solution concentrations were investigated, 10 µg/ml, 50 µg/ml, and 100 µg/ml. The amount of radioactive labeled peptide immobilized to the PVDF-g-PAAc surface was obtained by measuring the γ-radiation intensity. The results of these experiments are shown in Fig. 37.

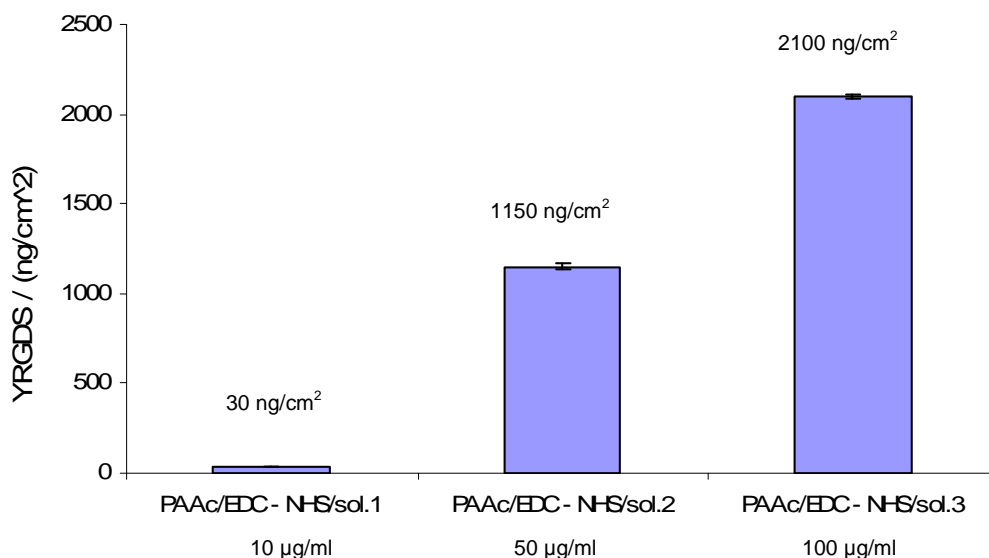


Fig. 37: Quantification of the amount of radiolabelled Y(¹²⁵I)RGDS peptide immobilized on PVDF-g-PAAc surfaces, when coupling reactions were carried out with 10 µg/ml, 50 µg/ml, and 100 µg/ml peptide solutions

As seen in Fig. 37 an amount of about 30 ng/cm² (0.05 nmol/cm²) of ¹²⁵I-labelled YRGDS was detected on the PVDF-g-PAAc surface, when a 10 µg/ml peptide solution was used for the coupling reaction. This amount increased to ca. 1150 ng/cm² (2 nmol/cm²) and 2100 ng/cm² (4 nmol/cm²), when solutions of 50 µg/ml and 100 µg/ml of Y(¹²⁵I)RGDS were used, respectively. From these results it can be assumed that around 30 ng/cm² of RIP-NH₂ were covalently attached to the PAAc modified PVDF surface, when the coupling reaction was performed in the 10 µg/ml bioligand solution. An amount of immobilized RIP-NH₂ between 30 ng/cm² and 1150 ng/cm² is expected for the 20 µg/ml coupling solution.

The comparison between the carboxy group content of the PVDF-g-PAAc surfaces and the concentration of radioactive labelled model peptide Y(¹²⁵I)RGDS covalently immobilized to the carboxy groups of the grafted PAAc by EDC/NHS method demonstrates that the PAAc provides an average surface carboxy group concentration, which is 300 times higher than the concentration of covalently

immobilized peptide. There is a big difference between the amount of surface functional groups and that of finally coupled bioligand, although a range of coupling concentrations from 16 nmol (10 µg/ml) to 160 nmol (100 µg/ml) was high enough to modify a lot of PAAc chain carboxy groups. The explanation of this phenomenon should be the same as that used for the interaction of TB molecules with PAAc. Also the concentration of surface bound TB is ca. 13 times higher than that of the peptide. Therefore another explanation has to be found. The use of an active ester to increase the reactivity of carboxy groups in aqueous solutions is a widely used technique. The *in situ* synthesized succinimidyl ester is relatively unstable under aqueous conditions. Thus, only molecules which are able to penetrate very fast into the PAAc hydrogel layer will be able to react with active ester groups on the PAAc chains, which are closely located to the grafted chain ends. If the diffusion of potential reaction partners is too low the succinimidyl esters will decompose. Here, the used peptide with a molecular weight of 600 and sterically hindered side chains probably reacts faster with the highly reactive succinimidyl ester groups on the outermost parts of the PAAc chains, than it is able to penetrate into the diffuse PAAc layer.

3.4.4 Evaluation of the antibacterial properties of PVDF-g-PAAc surfaces covalently modified with RIP by means of microbiological *in vitro* tests

The antibacterial properties of RIP-NH₂-coated PVDF surfaces were estimated *in vitro* by means of a pico-Green assay using *Staphylococcus aureus* (ATCC 29213). The pico-Green assay is a quantitative assay for double-strained DNA (dsDNA) quantification, based on the measurement of fluorescence due to the interaction of pico-Green dye with dsDNA^{120,121}. The detection of the amount of dsDNA present on modified and unmodified PVDF surfaces provides indirect information about the number of adherent bacterial cells.

As shown in Fig. 38, almost the same amount of dsDNA, ca. 25 ng/ml, was detected on PVDF and PVDF-g-PAAc surfaces. After immobilization of RIP to PVDF-g-PAAc, by using a 20 mg/ml peptide coupling solution, about 16 ng/ml of nucleic acid were detected. A stronger decrease of the dsDNA amount, to ca.

6 ng/ml, which corresponds to a stronger reduction of *Staphylococcus aureus* adhesion, was achieved when the immobilization reaction was performed in a 10 µg/ml peptide solution.

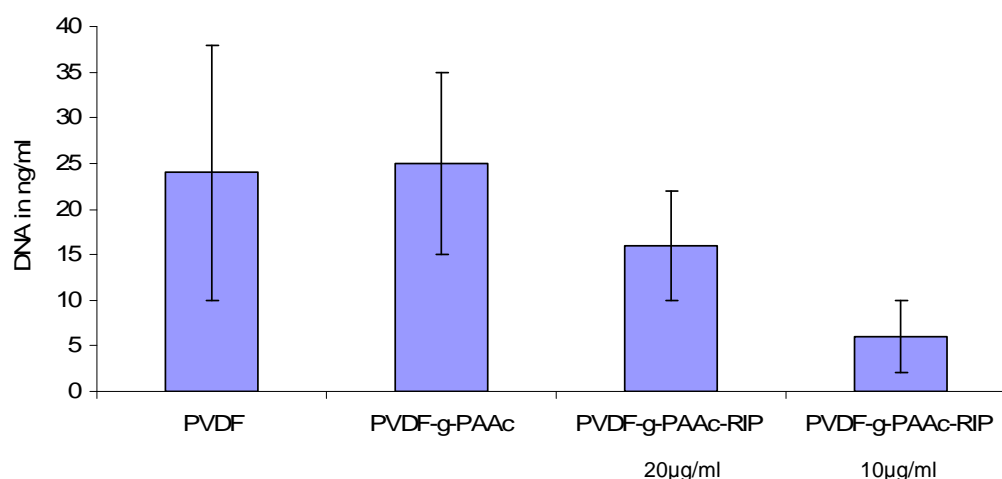


Fig. 38: Results of the pico-Green assay carried out to estimate the adhesion of *Staphylococcus Aureus* on PVDF, PVDF-g-PAAc, PVDF with immobilized RIP-NH₂ using two different concentrations of the peptide (20 µg/ml and 10 µg/ml) for the coupling reaction

The obtained results demonstrate, that RIP-NH₂ immobilized on PAAc-g-PVDF was able to reduce bacterial adhesion; they further suggest, that there is an optimal concentration for the effectiveness of the covalently bound RIP-NH₂, as it has been reported in literature for the free peptide⁶⁵.

It is well known, that receptors can become less sensitive to their ligands when exposed to a high ligand concentration. Moreover, a long term stimulation or high ligand concentration elicit an internalization of the receptor followed by degradation. This mechanism is called "down regulation"^{122,123,124}. Therefore, a treatment with a high concentration of an agonist or antagonist frequently results in a decrease of the cellular response. The stronger antibacterial properties of PVDF-g-PAAc covalently modified with a lower amount of RIP-NH₂ might be explained by the complex regulation mechanisms of the receptor activity.

3.5 Antimicrobial and antifungal PDMS with Kathon® 910 SB

Formulations containing isothiazolinone compounds, as bioactive components, are usually known by the commercial name of Kathon®. They have a broad spectrum of activity against bacteria, yeast and fungi and they are widely used as biocide in a variety of applications: in cosmetics, household cleaning products, metal working fluids, latex paint emulsions, printing inks, cooling water, paper industry and textiles^{125,126}.

Kathon® 910 SB from ROHM and HAAS (Germany) containing 1 weight-% of 4,5-dichloro-N-octyl-isothiazolin-3-one (DCOIT) (Fig. 39) in *o*-xylol has been specifically developed to protect silicone sealants from bacterial and fungi contaminations, which are responsible for undesired effects such as discoloration, degradation, odor, loss of stability or viscosity, pH change and gas generation. The active component, DCOIT, shows excellent efficiency against many bacteria and a whole range of commonly encountered fungal contaminants, including *aspergillus*, *alternaria* and *candida* species. In addition to its broad spectrum of effectiveness Kathon® 910 SB has other advantages. Due to its very low water solubility, leaching from silicone sealants is minimal and therefore a long term protection is provided. Moreover it has favorable environmental properties, since the low active component concentration, which is released into the environment during application, degrades rapidly to essentially non toxic compounds. Another product based on the same active ingredient, SEA-NINE® 211, is used in anti-fouling paints for naval applications and has received the EPA Green Challenge Award for environmental friendly chemistry, based on the fact that degradation products have been identified as non-toxic, non cumulating simple organic acid derivates. A complete risk assessment on the solvent of the formulation shows that this is also non toxic and biodegradable at release concentration level.

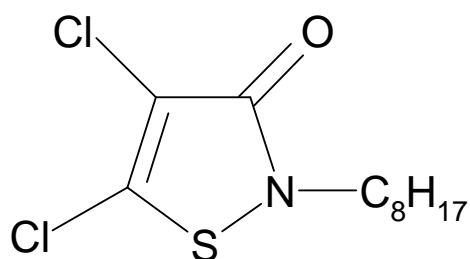
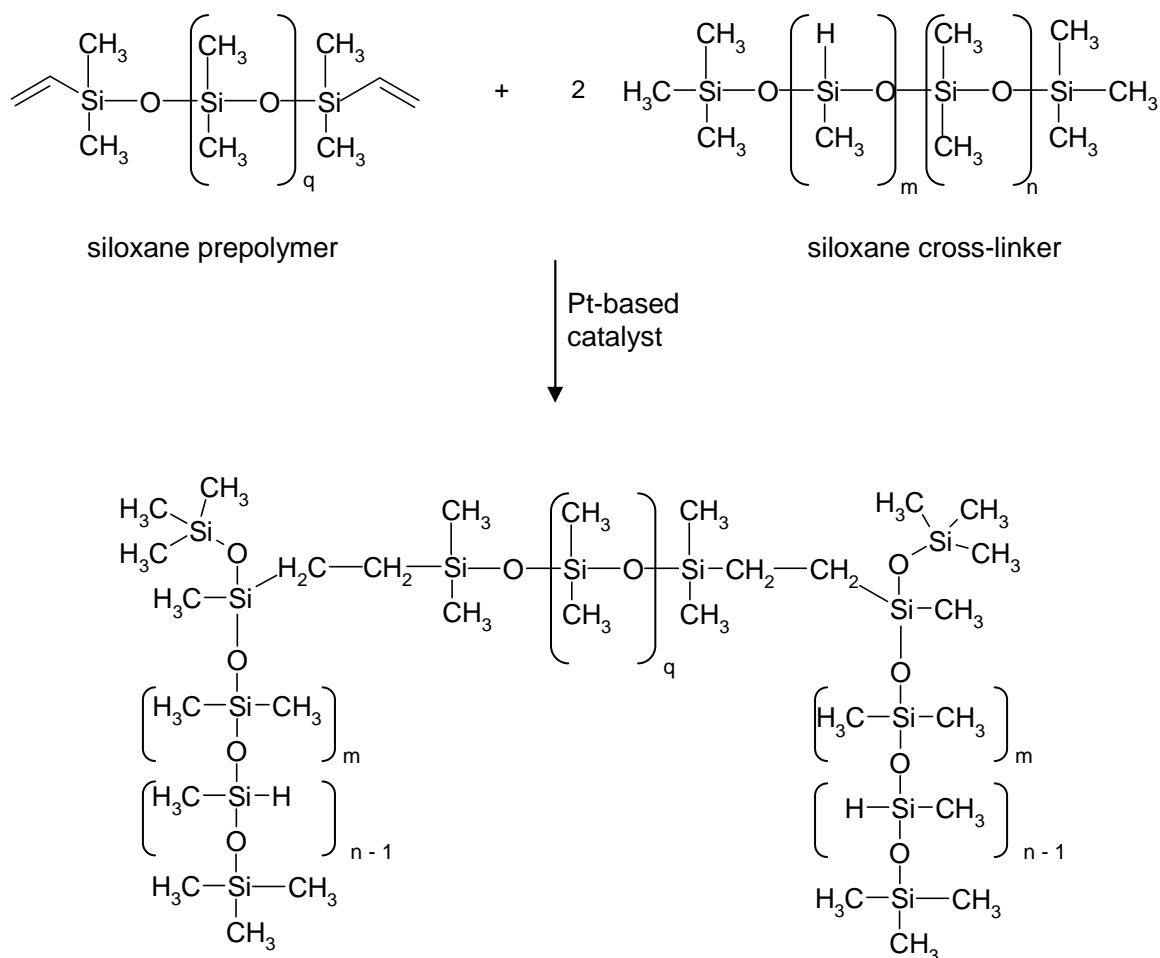


Fig. 39: Structure of 4,5-dichloro-N-octyl-isothiazolin-3-one (DCOIT), active ingredient of the formulation Kathon® 910 SB

PDMS microspheres containing 30 weight-% of Kathon® 910 SB were synthesized in order to assess the antibacterial and antifungicidal properties of Kathon® 910 SB, once incorporated in a PDMS system. To this purpose both dilution tests and agar diffusion hole tests were performed. Unloaded PDMS microspheres were used as control during these tests.

3.5.1 Preparation of unloaded PDMS microspheres and PDMS microspheres loaded with 30 weight-% of Kathon® 910 SB

For the preparation of PDMS microspheres, containing 30 weight-% of Kathon® 910 SB, a commercially available Sylgard® 184 PDMS elastomer-kit, from Dow Corning (Germany), was used as base material. The kit consists of two liquid parts: component A, a vinyl terminated siloxane prepolymer with a platinum-based catalyst and component B, a methylhydrogen siloxane cross-linking agent. The generation of the PDMS elastomer is based on an addition reaction (hydrosilylation) between the two components. Multiple reaction sites on both the prepolymer and the crosslinking oligomers allow for three-dimensional crosslinking. The reaction is catalysed by the platinum complex, it occurs at room temperature and can be accelerated at elevated temperature (up to 145°C). One advantage of this PDMS elastomer preparation method is that practically no by-products are generated. The general process is showed in Scheme 4.



Scheme 4: Schematic illustration of the addition reaction between the vinyl terminated siloxane prepolymer and the siloxane cross-linker

Sylgard® 184 PDMS microspheres containing 30 weight-% of Kathon® 910 SB with a size below 125 µm, were prepared according to the oil in water (o/w) solvent evaporation method^{127,128,129}, which is schematically illustrated in Fig. 40.

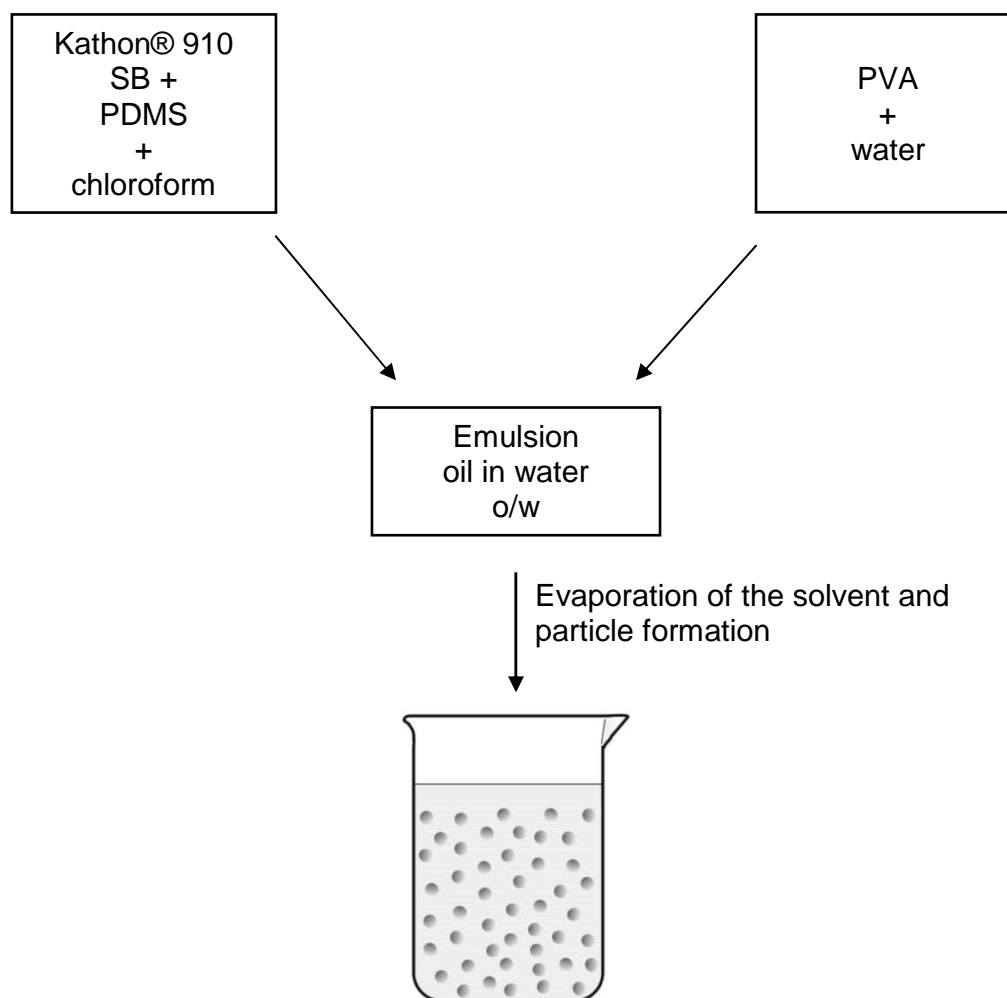


Fig. 40: Schematic illustration of the o/w solvent evaporation method used to prepare PDMS microspheres containing 30 weight-% of Kathon®

First, Kathon® 910 SB and Sylgard® 184 (component A and component B) were dissolved in chloroform. This oil phase was then mixed and emulsified with an aqueous phase containing polyvinylalcohol (PVA) as emulsion stabilizer. Once the oil/water emulsion was formed, the solvent was removed under reduced pressure in order to achieve polymer precipitation and microsphere formation. Finally, the microspheres loaded with Kathon® 910 SB were recovered by filtration, washed and dried.

Like the Kathon®-loaded PDMS microspheres the unloaded PDMS microspheres were prepared using Sylgard® 184 as base material by the o/w solvent evaporation method.

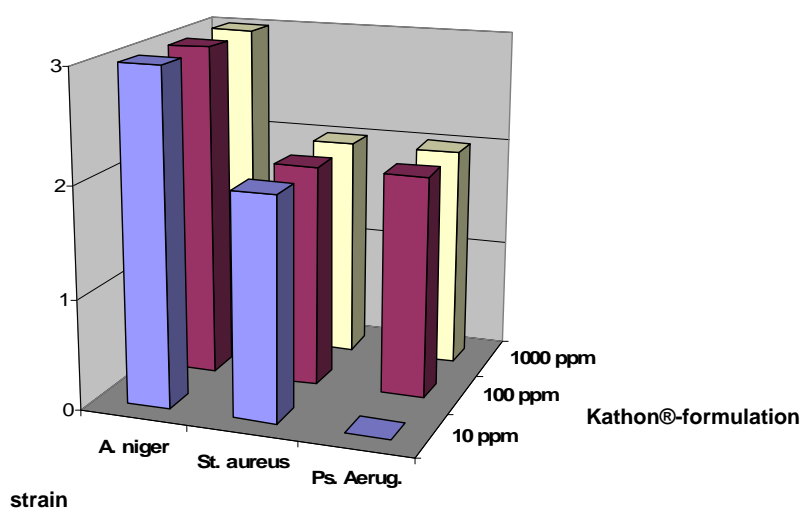
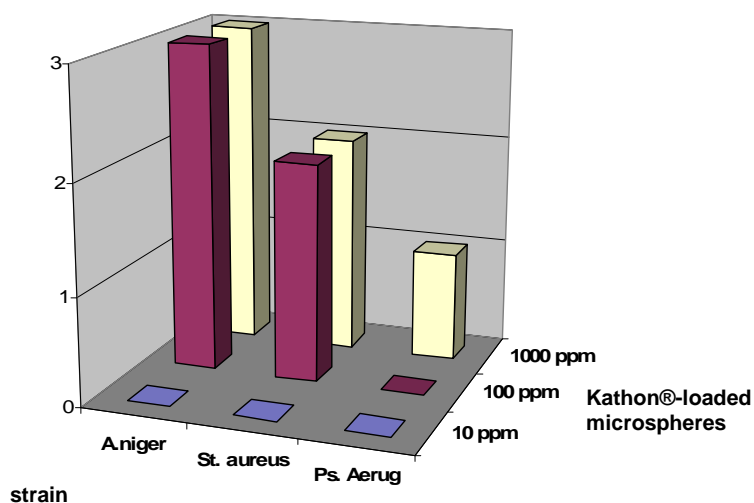
3.5.2 Investigation of the biocidal properties of Kathon® 910 SB-loaded PDMS microspheres

Dilution test and agar diffusion hole test were performed in order to investigate the antibacterial and antifungal properties of Kathon® 910 SB-loaded PDMS microspheres.

Dilution test

The test was carried out with two bacteria strains, *Staphylococcus aureus* (K 3212 DSM 799) and *Pseudomonas aeruginosa* (K1111 DSM 939), and one fungi strain, *Aspergillus niger* (K 7440 DSM 1975).

Three differently concentrated solutions (10 ppm, 100 ppm and 1000 ppm) of Kathon®-loaded microspheres and of Kathon® formulation were prepared and incubated with the bacteria and fungi strains. The turbidity of the bacterial suspension, which is a quantitative parameter of the efficiency of the bioactive component being tested, was photometrically determined. The samples incubated with *Aspergillus niger* were visually evaluated. Values obtained from the Kathon®-loaded PDMS microspheres were compared to those obtained from the Kathon® formulation. Results are shown in Fig. 41.



Legend to diagrams 3a and 3b

Growth	Inhibition	Number
No growth	100%	3
Strong inhibition	$\geq 50\%$	2
Inhibition	$\geq 10\%$	1
No effect	0%	0

Fig. 41: Results of the dilution test for Kathon®-loaded PDMS microspheres (a) and for Kathon®-formulation (b)

At 10 ppm the Kathon®-formulation completely inhibits the growth of *Aspergillus niger* and strongly reduces the growth of *Staphylococcus aureus* but does not show any activity against *Pseudomonas aeruginosa*. At the same concentration the Kathon®-loaded PDMS microspheres are not effective against any of the tested organisms. At 100 ppm the Kathon®-formulation inhibits the growth of the *Pseudomonas aeruginosa* for over 50%, whereas the loaded microspheres are still not active against this bacteria strain but as the Kathon®-formulation they are effective against *Staphylococcus aureus* and completely inhibit the growth of *Aspergillus niger*. At a concentration of 1000 ppm the loaded PDMS microspheres inhibit ca. 10% of *Pseudomonas aeruginosa* growth; no increase in antibacterial activity against *Staphylococcus aureus* was measured.

Agar diffusion hole test

The Agar diffusion hole test was used to determine the fungicidal activity of Kathon® 910 SB-loaded PDMS microspheres. *Aspergillus niger* (K 7444) and *Cladosporium cladosporioides* (K 8310) were used for the test.

The test is based on the following principle: An agar culture medium inoculated with the relevant test strain is poured into plates and allowed to harden. Holes are punched out of the agar and the antimicrobial or antifungal agent being examined is placed into them. During the incubation time the agent diffuses from the application site into the surrounding agar, and a growth inhibition zone will occur if the organism is susceptible to the agent. The inhibition zone size is a measure for the activity of the compound being tested (Fig 42).

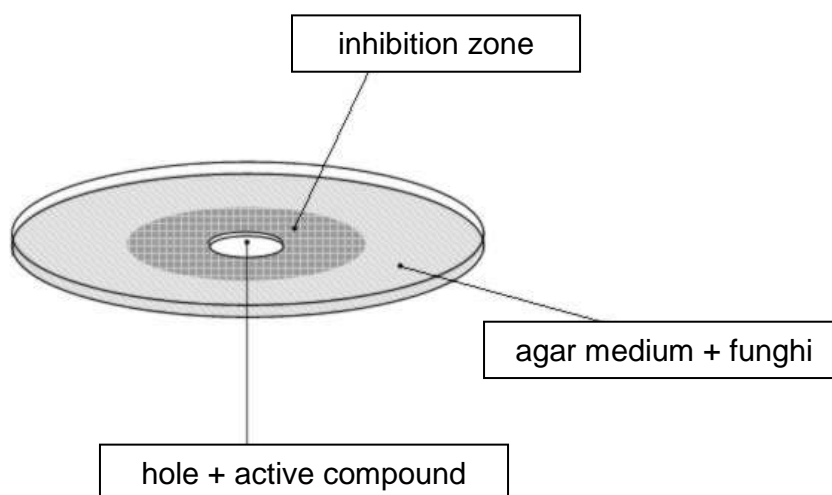


Fig. 42: Model of the agar diffusion hole test

The test was performed with PDMS microspheres containing 30 weight-% of Kathon® 910 SB and also with unloaded PDMS microspheres to have a negative control. Results are shown in Fig. 43.

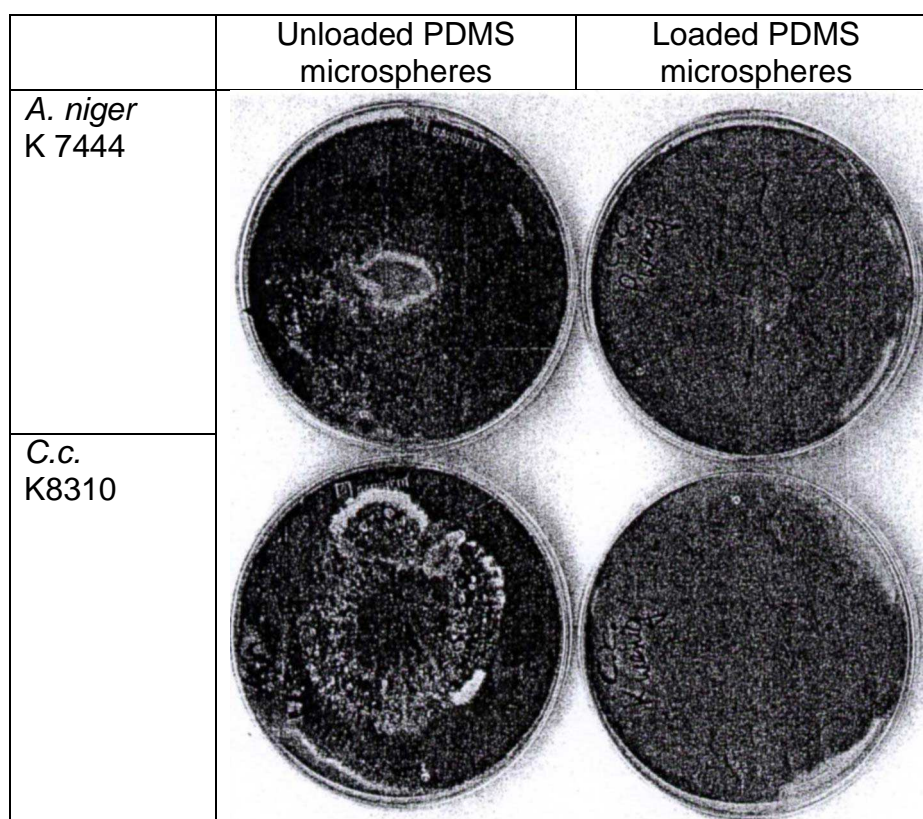


Fig. 43: Agar diffusion hole test investigating the fungicidal activity of Kathon® 910 SB-loaded PDMS microspheres toward *Aspergillus niger* (K 7444) and *Cladosporium cladosporioides* (K 8310)

The Kathon® 910 SB containing PDMS microspheres produced an inhibition zone with a diameter of circa 10 mm for both *Aspergillus niger* (K 7444) and *Cladosporium cladosporioides* (K 8310), showing to be effective against both organisms. Additionally, it has to be taken into account that the size of the inhibition zone also depends on the diffusion properties of the Kathon® 910 SB incorporated into the PDMS microspheres.

4 Experimental section

4.1 Analytic methods and equipment

4.1.1 Nuclear magnetic resonance spectroscopy

Proton nuclear magnetic resonance (^1H -NMR) and carbon-13 nuclear magnetic resonance (^{13}C -NMR) measurements were recorded on a VXR 300 spectrometer from Varian Associates (USA) or on an AMX 300 spectrometer from Bruker (USA). ^1H -NMR spectra were recorded at 300 MHz and ^{13}C -NMR spectra at 75 MHz. All the spectra were obtained in deuterated chloroform (CDCl_3) with tetramethylsilane as an internal standard.

4.1.2 UV/VIS spectroscopy

UV spectra were measured on a dual beam Lambda EZ210 UV/Vis spectrometer from Perkin Elmer (Germany). The spectra were recorded with a resolution of 0.5 nm and a wavelength scan-speed of 100 nm/min. The resulting information was analyzed using PESSW software version 1.2 Revision E.

4.1.3 Analytical reverse phase high performance liquid chromatography

Analytical RP-HPLC chromatography was performed on an Agilent 1100 Series apparatus from Bruker-Franzen Analytik GmbH (Germany). The resulting Data was analyzed by means of Chemstation A.09.03 software.

Each RP-HPLC run was performed on a Nucleosil 100-5 C_{18} column ($d = 0,4$ cm, $L = 25$ cm) from C&S Chromatography Service GmbH (Germany). A gradient of 10-40 % [v/v] acetonitrile in 0.1 % [v/v] TFA for 20 min at a flow rate of 1 ml/min

was applied. The elution solvents were filtered and degassed prior to use. For each run 100 µl of the peptide solution in acetonitrile/water (1:1, [v/v]) were injected. The eluted peptide was detected at 210 nm.

4.1.4 Matrix-assisted laser desorption ionization time of flight mass spectrometry

MALDI-ToF spectra were obtained by means of a BRUKER BIFLEXTM III MALDI time-of-flight mass spectrometer from Bruker-Franzen Analytik (Germany), equipped with a nitrogen laser (337 nm wavelength and 3 ns pulse width). A peptide solution in 0.1 % TFA/acetonitrile (2:1, [v/v]) with a concentration of approximately 100 pmol/µl and a solution of the matrix molecule 4-hydroxy- α -cyano cinnamic acid in the same solvent system (20 mg/ml) were prepared and mixed together in 1:1 proportion. 0,5 µl of the obtained solution was placed onto the stainless steel MALDI target. The solvent was left to evaporate before the sample holder was inserted into the spectrometer. The peptide molecules were embedded into the matrix by a co-crystallizing process. Pulsed laser irradiation caused desorption and ionization of the analyte, the matrix molecules, and their adducts, respectively.

4.1.5 Amino acid analysis

ASA was performed on an Alpha-Plus II analyzer from Pharmacia/LKB (Germany) in a lithium citrate buffer system according to the method of Spackman, Stein and Moore¹³⁰.

2 mg of peptide were hydrolyzed for 24 h at 110 °C in 2 ml of 5.7 N HCl, in the presence of 100 µl thioglycolic acid and a small amount of phenol. The solution was removed in vacuum, the residue was washed with deionised water, and dried in vacuum. This procedure was repeated 3 times and then the residue was analyzed.

4.1.6 White light interferometry

The investigations of the topography of the polymer surfaces were carried out on a Wyko NT2000 white light interferometer from Veeco (Cambridge, England). All measurements were performed in a vertical scanning interferometer (VSI) modus with a 25x objective and a field of view (FOV) of 1.0. An area of 185 μm x 243 μm was analyzed every time.

4.1.7 X-ray photoelectron spectroscopy

All XPS were recorded on a Krotos AXIS HSi165 Ultra spectrometer using a monochromatic AlK α X-ray source (1486.6 eV). Binding energies were determined in reference to the C_{1s} component, set at 285.0 eV. The concentric hemispherical electron energy analyzer is equipped with a multi-channel detector operating in a constant energy analyzer mode at an electron take-off angle of 55° with respect to the sample normal, which results in an information depth of approximately 6 nm. A linear baseline was used for background subtraction and Gaussian functions were used for peak fitting. Atomic percentages were determined from peak areas, while taking into account their Scofield factors.

4.1.8 Attenuated total reflection-infrared spectroscopy

IR spectroscopic measurements were carried out by means of a 710 Fourier transform infrared (FTIR) spectrometer from Nicolet (Germany). Spectra were recorded in air in attenuated total reflection (ATR) mode, while using a Ge crystal. The angle between the surface of the sample, placed on the front and back side of the internal reflection element (IRE), and the beam was of 45°. A mirror scanning speed of 3.2 mm/s was used.

4.1.9 Raman spectroscopy

Raman spectra were measured on a Raman spectrometer RFS 100/S from Bruker Optik GmbH (Germany). The spectrometer is equipped with a broad-range quartz beamsplitter and a Bruker Optics' patented frictionless interferometer with ROCKSOLID™ alignment, which provides high sensitivity and stability. The diode-pumped, air-cooled Nd:YAG laser source (1064 nm) is completely software controlled. The standard configuration provides a spectral range of 3600 – 70 cm⁻¹ (Stokes shift) and - 100 - - 2000 cm⁻¹ (anti-Stokes shift). The excitation wavelength of 1064 nm was provided by the Nd:YAG laser source, adjustable between 200 – 500 mW. The spectral resolution was 4 cm⁻¹.

4.1.10 Contact angle measurements

Contact angles were measured by the captive bubble method on a G402 system from Krüss (Germany). The samples sized 1 cm x 2 cm were fixed with a double side adhesive tape to a glass slide and immersed in ultra-pure water. A micro-liter syringe was used to place air droplets of 0,5-1,0 µl on the film surfaces from below. The angle between the film surface and the air droplet was measured by means of a goniometer. Contact angle measurements were carried out on 4 samples for each modification step at room temperature. 10 measurements were performed at different places on the sample surface to exclude modification inhomogenities. Afterwards the average and the standard deviation values were calculated.

4.1.11 Zeta potential measurements

Analysis of the electro-kinetic properties of unmodified and modified PVDF surfaces was carried out on a Electro Kinetic Analyzer EKA from Paar (Austria). For each sample type, two polymer foils of the same sample were prepared on sample holders and placed at both ends of the measuring cell. A

10^{-3} M electrolyte solution of KCl was used. The zeta potential of each sample was measured in a pH range from 3 to 10.

4.1.12 Determination of microsphere size

Measurements of microsphere size distribution were performed on a particle size analyzer Mastersizer 2000 with a simple dispersion unit Hydro 2000 from Malvern (United Kingdom). The instrument is equipped with a Helium/Neon and a diode-laser (wavelengths 632.5 and 450.0 nm, respectively). The measuring range is from 0.02 μm to 2000 μm . A microsphere dispersion in water was placed in the simple dispersion unit and stirred at 1200 rpm. The dispersion was pumped in a closed loop circuit between the simple dispersion unit and the measuring-cell in order to achieve a homogeneous distribution. The results of the measurements were analyzed using the particle size analyzer software 2.00.002b1 version.

4.2 Chemicals and materials

Chemicals

All the chemicals used in the preparation of 3-butyl-5-(bromomethylene)-2(5H)-furanone were purchased from Fluka (Germany) and used without further purification. The amino acid derivatives were purchased from Novabiochem (Germany), and the resin 4-(2',4'-dimethoxyphenyl-Fmoc-aminomethyl)-phenoxyethyl-polystyrene (200-400 mesh, substitution: 0,3-0,6 mmol/g) from Bachem (Germany). All the chemicals and reagents employed in the synthesis of RIP-NH₂ were purchased from Merck (Germany). Acrylic acid (Acc) was obtained from Fluka (Germany), distilled under reduced pressure and kept under nitrogen until use. N-Ethyl-N'-(3-dimethylaminopropyl)-carbodiimid-hydrochlorid (WSC·HCl) and N-hydroxysuccinimide (NHS) were purchased from Sigma-Aldrich (Germany).

Solvents

Solvents of the quality “pro analysi” were purchased from Fluka (Germany). Dimethyl formamide (DMF) was distilled prior to use in the SPPS of RIP-NH₂.

Polymers

PDLLA Resomer R208, batch no. 260316 (average M_w 180.000) was obtained from Boehringer Ingelheim KG (Germany). Sylgard[®]184 silicone elastomer kit was purchased from Dow Corning (Germany). The kit consists of two liquid components:

Component A (prepolymer): vinyl-terminated poly(dimethyl siloxane)

Component B (cross-linking agent): methylhydrogen siloxane/dimethyl siloxane copolymer

PVDF SOLEF[™]1008 granulate was purchased from Solvay Adv. Polym. (Germany).

Buffers

Phosphate buffered saline (PBS)-buffer

For the preparation of PBS buffer (pH 7.4) powder from Sigma-Aldrich was used. A packet of powder was dissolved in 1 l deionized and degassed water, or PBS buffer was prepared using the following method:

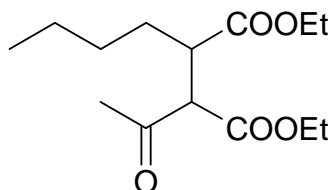
0.01 M disodium hydrogenphosphate dihydrate, 0.14 M sodium chloride, and 0.01 M potassium chloride were dissolved in deionized and degassed water, the pH was adjusted to 7.4 with NaH₂PO₄·H₂O.

Materials

Silica gel 60H (for column chromatography) was purchased from Merck (Germany). Silica gel (F₂₅₄) plates (2 mm) for preparative thin layer chromatography were purchased from Analtech, Inc. (USA).

4.3 Preparation of 3-butyl-5-(bromomethylene)-2(5H)-furanone

4.3.1 Preparation of diethyl 2-acetyl-3-butylbutanedioate



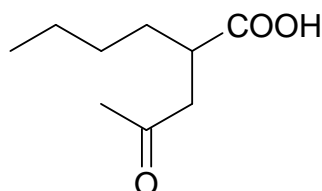
Sodium (0.51 g, 0.02 mol) was dissolved in 10 ml of absolute ethanol (placed in a 50 ml three-necked flask). Ethyl acetoacetate (2.60 g, 0.02 mol) was added to the resulting solution of sodium ethoxide in ethanol under stirring and the mixture was heated to reflux. Ethyl-2-bromohexanoate (4.46 g, 0.02 mol) was added over 2 h and heating was continued until the solution became neutral (ca. 8 h). The reaction mixture was cooled to room temperature, the precipitate of sodium bromide (NaBr) was filtered off, and the solution was evaporated to yield a pale yellow oil. The crude product was purified by flash column chromatography using ethyl acetate/petroleum (1:4, [v/v]) as the solvent system. The diester was obtained as a colorless oil (3 g, 56 %).

$^1\text{H-NMR}$ (CDCl_3) δ (ppm): 0.88, t, J 7.8 Hz, CH_3 ; 1.26, m, $\text{CH}_3\text{CH}_2\text{CH}_2\text{CH}_2$ and $\text{CO}_2\text{CH}_2\text{CH}_3$; 1.52, m, $\text{CH}_3\text{CH}_2\text{CH}_2\text{CH}_2$; 2.26 and 2.30, 2 x s, COCH_3 ; 3.8, m, CH; 3.87 and 3.91, 2 x d, J 10.3 Hz, CH; 4.15, m, $\text{CO}_2\text{CH}_2\text{CH}_3$.

$^{13}\text{C-NMR}$ (CDCl_3) Isomer A δ (ppm): 14.18, $\text{CH}_3\text{CH}_2\text{CH}_2\text{CH}_2$; 14.47 and 14.55, $\text{CO}_2\text{CH}_2\text{CH}_3$; 22.84, $\text{CH}_3\text{CH}_2\text{CH}_2\text{CH}_2$; 28.79, $\text{CH}_3\text{CH}_2\text{CH}_2\text{CH}_2$; 30.11, COCH_3 ; 30.12, $\text{CH}_3\text{CH}_2\text{CH}_2\text{CH}_2$; 44.25, CH; 60.79 and 61.04, $\text{CO}_2\text{CH}_2\text{CH}_3$; 61.77, CH; 167.92 and 174.16, $\text{CO}_2\text{CH}_2\text{CH}_3$; 201.45, CO. $^{13}\text{C-NMR}$ (CDCl_3) Isomer B δ (ppm): 14.18, $\text{CH}_3\text{CH}_2\text{CH}_2\text{CH}_2$; 14.37 and 14.55, $\text{CO}_2\text{CH}_2\text{CH}_3$; 22.80, $\text{CH}_m\text{CH}_2\text{CH}_2$; 29.18, $\text{CH}_3\text{CH}_2\text{CH}_2\text{CH}_2$; 29.86, $\text{CH}_3\text{CH}_2\text{CH}_2\text{CH}_2$; 30.71, COCH_3 ;

44.38, CH; 61.34, CH; 61.97 and 62.02, CO₂CH₂CH₃; 168.27 and 173.93, CO₂CH₂CH₃; 201.78 CO.

4.3.2 Preparation of 2-(2-oxopropyl)hexanoic acid (pathway A)



Diethyl-2-acetyl-3-butylbutanedioate (2.71 g, 0.001 mol) was stirred overnight at room temperature with aq. sodium hydroxide (1.25 M, 50 ml). The solution was acidified with H₂SO₄ 2 M, extracted with diethyl ether (3x30 ml), the extracts were washed with water (40 ml), dried over magnesium sulphate (Mg₂SO₄) and evaporated. The residual oil was dissolved in benzene/toluene (25 ml) and the solution was refluxed for 1 h. Evaporation of the solvent gave 2-(2-oxopropyl)hexanoic acid as a pale yellow oil. (87 % when the decarboxylation reaction was carried out in benzene, 80 % when the decarboxylation reaction was carried out in toluene).

¹H-NMR (CDCl₃) δ (ppm): 0.90, t, *J* 7.6 Hz, CH₂CH₂CH₂CH₃; 1.31, m, CH₂CH₂CH₂CH₃; 1.53-1.65, m, CH₂CH₂CH₂CH₃; 2.17, s, COCH₃; 2.52, m, CH; 2.88, m, CH₂; 9.2, br s, CO₂H.

¹³C-NMR (CDCl₃) δ (ppm): 13.86, CH₃; 22.52, CH₃CH₂CH₂CH₂; 29.11, CH₃CH₂CH₂CH₂; 30.02, CH; 31.37, CH₃CH₂CH₂CH₂; 39.95, COCH₃; 44.66, CH₂; 181.39, CO₂H; 207.00, CO.

4.3.3 Preparation of 2-(2-oxopropyl)hexanoic acid (pathway B)

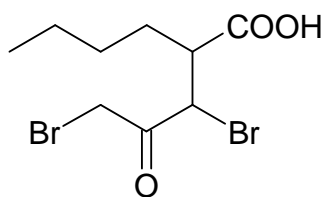
Diethyl-2-acetyl-3-butylbutanedioate (2.71 g, 0.001 mol) was stirred overnight under reflux with hydrochloric acid (6 N, 12 ml). The solution was extracted with

diethyl ether (3x30 ml), and the extracts washed with H₂O (40 ml) and dried over magnesium sulphate (Mg₂SO₄). Removal of the solvent gave 2-(2-oxopropyl)hexanoic acid as a pale oil (90 %).

¹H-NMR (CDCl₃) δ (ppm): 0.90, t, *J* 7.2 Hz, CH₂CH₂CH₂CH₃; 1.31, m, CH₂CH₂CH₂CH₃; 1.53-1.64, m, CH₂CH₂CH₂CH₃; 2.17, s, COCH₃; 2.52, m, CH; 2.89, m, CH₂; 10.2, br s, CO₂H.

¹³C-NMR (CDCl₃) δ (ppm): 13.86, CH₃; 22.52, CH₂; 29.11, CH₂; 30.02, CH; 31.37, CH₂; 39.94 COCH₃; 44.64, CH₂; 181.46, CO₂H; 206.96, CO.

4.3.4 Preparation of 2-(1,3-dibromo-2-oxopropyl)-hexanoic acid

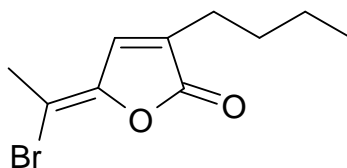


A solution of bromine (1.64 g, 10.23 mmol) in dry dichloromethane (5 ml) was added dropwise to a solution of 2-(2-oxopropyl)hexanoic acid (1 g, 3.10 mmol) in dry dichloromethane (30 ml) containing 33 % [v/v] hydrobromic acid in acetic acid (3 drops). The reaction mixture was warmed at 50 °C for 0.5 h, then refluxed for 1 h, and cooled to room temperature. The resulting solution was washed successively with water (10 ml), aqueous sodium metabisulfite (Na₂S₂O₃ 0.5 M, 10 ml) and brine (saturated NaCl solution) (10 ml) and dried over sodium sulphate (Na₂SO₄). Removal of the solvent gave the crude bromo acid as a pale yellow oil, which was used without further purification.

4.3.5 Alternative way for the preparation of 2-(1,3-dibromo-2-oxopropyl) hexanoic acid

Bromine (2.06 g, 0.016 mol) was added to a solution of 2-(2-oxopropyl)hexanoic acid (1 g, 0.006 mol) in dry diethyl ether (3 ml) within 4 h while keeping the temperature at -5 °C. Then the mixture was poured into water (25 ml) and extracted with diethyl ether (3x20 ml). The combined extracts were washed with saturated sodium bicarbonate (NaHCO₃) (20 ml), dried over sodium sulphate (Na₂SO₄) and evaporated. Short-path ball-tube distillation (140°C/0.01 Torr) was performed.

4.3.6 Preparation of 3-butyl-5-(bromomethylene)-2(5H)-furanone



Phosphorus pentoxide (1.5 g, 283.89 g/mol) was added with stirring to a solution of 2-(1,3-dibromo-2-oxopropyl) hexanoic acid (2 g, 6.33 mol) in dry dichloromethane (50 ml) while stirring. The mixture was heated under reflux while stirring for 2 h, and cooled to room temperature. The resulting mixture was filtered through a celite pad and the filtrate was treated with 1,4-diazabicyclo[2.2.2] octane (DABCO) (0.16 g, 1.44 mmol). The mixture was stirred at room temperature for 2 h and filtered. The filtrate was washed successively with dilute hydrochloric acid (2 N, 10 ml), brine (20 ml), dried over magnesium sulphate (Mg₂SO₄) and evaporated to dryness. The crude product was purified by preparative thin layer chromatography (TLC) using ethyl acetate. hexane, 1:10 [v/v] as a solvent system. The 3-butyl-5-(bromomethylene)-2(5H)-furanone was obtained as a pale yellow oil.

$^1\text{H-NMR}$ (CDCl_3) δ (ppm): 0.93, t, J 7.2 Hz, $\text{CH}_2\text{CH}_2\text{CH}_2\text{CH}_3$; 1.37, m, $\text{CH}_2\text{CH}_2\text{CH}_2\text{CH}_3$; 1.58, m, $\text{CH}_2\text{CH}_2\text{CH}_2\text{CH}_3$; 2.33, t, J 7.3 Hz, $\text{CH}_2\text{CH}_2\text{CH}_2\text{CH}_3$; 5.98, s, 5-CHBr; 7.07, s, CH.

$^{13}\text{C-NMR}$ (CDCl_3) δ (ppm): 13,88, $\text{CH}_2\text{CH}_2\text{CH}_2\text{CH}_3$; 22,4, $\text{CH}_2\text{CH}_2\text{CH}_2\text{CH}_3$; 25,46, $\text{CH}_2\text{CH}_2\text{CH}_2\text{CH}_3$; 30,90, $\text{CH}_2\text{CH}_2\text{CH}_2\text{CH}_3$; 104,24, CHBr; 129,28, CH; 133,96 C; 151,87 C; 168,19, CO

4.4 Preparation of PDLLA films loaded with active agent

PDLLA (Resomer® R 208) was dissolved in chloroform in a concentration of 100 g/l, the active agent was added and the resulting solution was poured onto glass plates (ca. 0.15 ml of solution per cm^2). The solvent was allowed to evaporate overnight at room temperature. The glass plates were covered for dust protection. The thickness of the films was 12 μm and their diameter was 24 mm. The ratio between PDLLA and 2-(2-bromoethyl)-2,5,5-trimethyl-1,3-dioxane was 247.5 mg/12.5 mg and between PDLLA and 3-butyl-5-(bromomethylene)-2(5H)-furanone was 247.5 mg/2.5 mg.

4.5 *In vitro* release experiments

In vitro release studies were performed in triplicate under sink conditions. The experiments were carried out in 50 ml centrifuge vessels filled with 30 ml of deionized water in an incubator at 37°C, shaking at a frequency of 200 min^{-1} . At defined time points the aqueous medium was decanted and replaced with fresh deionized water. The amount of active agent released was determined by UV/Vis-spectrophotometry at 213 nm for 2-(2-bromoethyl)-2,5,5-trimethyl-1,3-dioxane and at 287 nm for 3-butyl-5-(bromomethylene)-2(5H)-furanone.

4.6 Synthesis, isolation and purification of RIP-NH₂

The synthesis of RIP-NH₂ (YSPWTNF-NH₂) was performed in a shaking and suction device constructed at the German Wool Research Institute. The device consisted of a pump, a suction flask and a sintered glass funnel vessel, shaking at an angle of 120° with a frequency of 50/min.

4.6.1 Coupling of the first amino acid (Fmoc-Phe) to the resin

Per equivalent of resin 3 equivalents of Fmoc-Phe, 3 equivalents of diisopropylcarbodiimide (DIC) and 3 equivalents of 1-hydroxybenzotriazole (HOBt) were used. Fmoc-Phe, DIC, and HOBt were dissolved in DMF and the resulting solution was added to the resin. The reaction mixture was shaken overnight. The resin was then washed six times with DMF and dried in vacuum.

4.6.2 Determination of resin loading by Fmoc cleavage

After the attachment of the phe-derivative, the resin substitution was assessed by treating a known quantity of Fmoc-loaded resin with piperidine in methylenchloride and measuring spectrophotometrically the amount of dibenzofulvene (DBF)-piperidine adduct released¹³¹.

10 mg of dried resin were rotated for 30 min in 1 ml piperidine/methylenchloride (1:1, [v/v]). Then the resin was filtered and washed with methylenchloride. The filtrate was evaporated in vacuum, and the residue dissolved in 25 ml of methylenchloride. The absorbance of this solution was measured at 300 nm. The resin loading (0.44 mmol/g) was calculated by means of the Lambert-Beer law.

4.6.3 Capping procedure

A capping step was performed in order to block the non reacted linker amino functions prior to coupling the second amino acid.

The resin was shaken for 10 minutes with a solution of 200 μ l acetic anhydride (Ac_2O) (5 eq) and 200 μ g N,N-diisopropylethylamine (DIPEA) (1 eq.) in 5 ml of DMF. Then the resin was washed 5 times with DMF and dried in vacuum. To remove Fmoc-protecting groups the resin was treated 2 times for 10 min with a solution of 20 % [v/v] piperidine in DMF, then washed 6 times with DMF and dried in vacuum.

4.6.4 Activation of the amino acids and coupling reactions

In relation to the loading of the resin 3 equivalents of Fmoc-amino acids were employed. The coupling of Fmoc-Asn(trt)OH was effected by use of the (O-(benzotriazol-1-yl)-N,N,N',N'-tetramethyluronium tetrafluoroborate TBTU/HOBt procedure, all the other amino acids were coupled using the DIC/HOBt procedure. DIC procedure: 3 equivalents of Fmoc amino acid, 3 equivalents of HOBt and 3 equivalents of DIC were dissolved in DMF and added to the resin. Then the reaction mixture was shaken for 30 min.

TBTU/HOBT procedure: 3 equivalents of Fmoc amino acid, 3 equivalents of HOBt, and 3 equivalents of TBTU were dissolved in DMF and added to the resin. Then the reaction mixture was shaken for 30 min.

4.6.5 Kaiser test

The completeness of each coupling reaction was monitored by the ninhydrin test developed by Kaiser, which is based on the formation of dark blue products as a result of the interaction between ninhydrin and the free amino groups of the amino acids¹³²

To perform the test the following solutions were required:

Solution 1: 500 mg ninhydrin in 10 ml ethanol

Solution 2: 8 g phenol in 2 ml ethanol

Solution 3: 0.2 ml of 0.001 M aqueous potassium cyanide solution in 10 ml pyridine.

After each coupling reaction a few resin beads were transferred into a small glass tube and washed 3-4 times with DMF. A drop of each of the prepared solutions was added and the mixture was heated to 110 °C for 5 min.

A positive test result is indicated by blue resin beads. The test was not performed for proline which, being a secondary amino acid, yields a different reaction.

4.6.6 Coupling protocol for Fmoc- solid-phase peptide synthesis

Each coupling cycle was performed according to the standard protocol for Fmoc-SPPS depicted below.

- | | |
|--------------------------|---------------------------------------|
| 1) Wash | 6 x 1 min with DMF |
| 2) Removal of Fmoc group | 2 x 10 min with 20% piperidine in DMF |
| 3) Wash | 6 x 1 min with DMF |
| 4) Coupling | reaction time 30 min |
| 5) Wash | 6 x 1 min with DMF |
| 6) Kaiser test* | |
| 7) Wash | 6 x 1 min with DMF |

*If negative proceed.

4.6.7 Cleavage of RIP-NH₂ peptide from the resin

The resin was washed with methanol, dried and transferred into an other vessel. A solution of TFA/TES/H₂O (95:2.5:2.5, [v/v/v]) containing tryptamine was prepared and added to the resin (0.5 g resin/ 5 ml solution of TFA/TES/H₂O

containing 100 mg of triptamine). After gently stirring the suspension for 4 h, the resin was removed by suction filtration and washed with TFA and methanol. The filtrates were combined and the crude peptide was precipitated by adding the 8-10 fold volume of cold *t*-butyl methyl ether. Then the suspension was centrifuged. After re-suspension steps with fresh *t*-butyl methyl ether and subsequent centrifugation, the ether was carefully decanted.

4.6.8 Purification of RIP-NH₂ by means of column chromatography (ion exchange chromatography and reverse phase medium pressure liquid chromatography)

IEC and RP-MPLC were performed using an Ultrarac fractions collector and a UV-detector Uvicords from LKB (Sweden) and a Duramat pump from (CfB) ProMinent (Switzerland).

Ion exchange chromatography was carried out using a SP-sephadex column from Pharmacia (Sweden). The crude peptide was dissolved in a solution of 10 % [v/v] isopropanol in 0.01 M NaH₂PO₄·2H₂O (pH 3) and applied to the column. A gradient of 0-0.5 M NaCl was applied over 3 h. All fractions of the main part of the first peak of the IEC procedure were collected. After reducing the volume of the solution in vacuum a RP-MPLC was performed. As reverse phase material C₁₈-modified silica was used. A linear gradient of 5-30 % [v/v] isopropanol in 0.1 % [v/v] aqueous TFA was applied over a period of 3 h at a flow rate of 3 ml/min in a pressure range of 2-4 bar

4.7 Modification of PVDF surfaces

4.7.1 Preparation of PVDF foils

The preparation of PVDF-foils was performed with a melting press from SPECAC (United Kingdom). 2 g of PVDF granulate was placed between two steel plates covered with aluminum foil. The plates were placed in the press and heated to

200 °C for 5 min. Finally the films were pressed with a pressure of ca. 12 t. The formed films were cooled to room temperature and cleaned by Soxhlet extraction with hexane/ethanol (79:21, [m/m]).

4.7.2 Plasma treatment

Plasma treatments were carried out with a custom-made “microwave” plasma unit. The hexagonally shaped reactor chamber (volume = 0.012 m³), made of stainless steel, contained an H-plane horn antenna as microwave coupler for the transmission of the MW power. The horn antenna is directly connected via a 3-stub tuner, H-plane waveguide bend and isolator to the magnetron. The apparatus is equipped with a commercially available air-cooled microwave head, operating at 2450 MHz and connected to a thyristor regulated power supply with a between 5 % and 100 % (600 W) adjustable performance. The microwave power passes through the quartz disc (d = 20 cm) and the plasma through the microwave coupler, which is placed on the top of the quartz window at its geometrical centre. Process gas is supplied to the discharge region through a side port, localized at the side panel of the recipient. Gas pressure is measured by two sensors, one between the vacuum pump unit and the vacuum chamber, and a second one between the vacuum chamber and the gas outlet valve. Both are connected to a total pressure gauge and controller TPG 300 (Liechtenstein). The system is evacuated by a turbo molecular pump backed by a rotary vane vacuum pump TRIVAC-B/D4B (Germany). The chamber was evacuated before each experiment to pressures below 10⁻⁴ mbar. Experiments were carried out in argon gas with 99.99 % purity. The working pressure is controlled by adjusting the gas flow by a mass flow controller (Brooks Instruments, USA), which is also connected to the TPG.

The plasma treatment conditions were as follows: frequency: 1 kHz; pressure: 2x 10⁻¹ mbar; power: 400 W for PVDF films; treatment time: 60 s for PVDF films; flow rate: 20 sccm. After plasma treatment, the recipient was evacuated to 5x10⁻⁵ mbar, and nitrogen, ambient air, and oxygen respectively was introduced into the chamber.

4.7.3 Graft copolymerisation of acrylic acid

Plasma treated PVDF foils were exposed to air for 20 min and then immersed in an aqueous solution containing 20 % [v/v] of AAc monomer. After sparging with nitrogen for 20 min to remove dissolved oxygen, the reaction tubes were sealed and placed in a 90 °C water bath to initiate the graft-co-polymerization. The reaction was terminated when the solution viscosity increased. The PAAc-grafted PVDF foils were rinsed with distilled water for 24 h to remove non-reacted monomers and non-immobilized AAc polymers. The successfully coated PVDF samples were stored in distilled water until use.

4.7.4 Quantification of the carboxyl group content of PVDF-g-PAAc surfaces by means of toluidine blue staining

PVDF-PAAc foils (surface = 8 cm²) were placed in a 12 well plate and incubated overnight at room temperature with 10 ml of a 10⁻⁴ M NaOH aqueous solution containing 5 · 10⁻⁴ M of TB. Then, each foil was washed several times with 10⁻⁴ mol/l NaOH solution. The dye was desorbed from the foils by treatment with 10 ml of 50 % [v/v] acetic acid solution for 30 min at room temperature. The dye content was obtained by measuring the optical density of the solution at 620 nm by means of an UV-Vis spectrophotometer. The carboxyl group content of the grafted PAAc was obtained from a calibration plot.

4.7.5 Quantification of the carboxyl group content of PVDF-g-PAAc surfaces by means of pH-titration

PVDF-g-PAAc foils were immersed in a titrated 0.1 M sodium hydroxide solution for 2 h. Aliquots of this solution were then titrated with 0.1 M hydrochloric acid. Accuracy requires controlled conditions such as the use of boiled deionized water to avoid undesired carbonation, titrated solutions (Titrisol®) and automatic burette.

4.7.6 Covalent immobilization of RIP-NH₂

The carboxyl-end groups of the grafted PVDF samples were activated with 0.2 M N-ethyl-N'-(3-dimethylaminopropyl)-carbodiimid-hydrochlorid (WSC·HCl) and 0.1 M N-hydroxysuccinimide (NHS) in distilled water for 20 min at room temperature. After briefly rinsing with ultrapure water, the films were incubated for 2 h in solutions of RIP-NH₂ of two different concentrations; 20 µg/ml, 10 µg/ml in carbonate buffer (pH 9.4). Finally the films were washed 2 times with buffer, 2 times with water, dried and sterilized by gamma radiation, with an intensity of 18 kG.

4.7.7 Quantification of immobilized model peptide YRGDS by radioactive labeling with ¹²⁵Iodine

Reagents and buffers

- Radioactive iodide solution

Na¹²⁵I solution IMS30 from Amersham Europe Inc. (Freiburg, Germany); 1 mCi (37 MBq; 0.45 nmol) in 10 µl 0.1 M NaOH.

- PBS (pH 7.4):

Cf. 4.2 Buffers.

- Substrate solution

10 µg, 50 µg, and 100 µg YRGDS were dissolved in 1 ml PBS.

- Chloramine-T solution

1 µg, 5 µg, and 10 µg chloramine-T trihydrate solved in 1 ml PBS.

- BSA solution

Solution of 10 % (w/w) BSA ice-cooled, 1 % (w/w) NaI, and 0.01 % (w/w) NaN₃ in water.

- TCA solution

Ice-cooled solution of 10 % trichloro acetic acid in water.

Preparation protocol

100 µl of substrate solution were placed in a silanized counter vial (3.5 ml). After the addition of 1 µl Na¹²⁵I solution (0.1 mCi; 3,7 MBq; 45 pmol) to the substrate solution the reaction was started by adding 5 µl chloramine-T solution under stirring (miniaturized stirrer).

Determination of the entrapment rate of radioactive ¹²⁵I: the peptide was precipitated with TCA. A glass capillary was dipped first into the iodination mixture and then into 200 µl of BSA solution. After vigorously mixing 10 µl were taken and mixed with another 200 µl of BSA solution. Afterwards, the peptide/BSA mixture was precipitated with 2 ml of ice-cooled TCA solution. After centrifugation the supernatant and the precipitate were measured separately by the gamma-counter COBRA II Auto-Gamma from Packard (Germany).

Separation of radio-labelled peptide from non-bound iodine was achieved by gel-filtration using a Sephadex® G-25 column NAPTM5 from Pharmacia Biotech AB (Sweden). The column was previously equilibrated with PBS as an elution media. The labelled peptide was kept at -20 °C and used within one week.

Quantification of surface-immobilized ¹²⁵I-labelled YRGDS

YRGDS solutions with three different coupling concentrations used for the immobilization reactions on PVDF-g-PAAc surfaces were adjusted to a minimal activity of 100.000 cpm/500 µl (1.67 kBq/500 µl; 45.0 pCi/500 µl) by adding a defined concentration of ¹²⁵I-labelled YRGDS. In order to measure the activity of the solutions, 500 µl-samples were analyzed on a gamma-counter COBRA II Auto-Gamma from Packard (Germany) within 3 min. After the immobilization reaction the radioactivity of the PVDF samples was measured for 5 min.

4.7.8 Evaluation of the antibacterial properties of PVDF-g-PAAc surfaces covalently modified with RIP by means of picoGreen assay

Foils were placed in a 12 well-plate and incubated with 2 ml of a ca. 10^9 bacteria/ml suspension of *Staphylococcus aureus* (ATCC 29213) in PBS overnight at room temperature. After briefly rinsing with PBS, the foils were placed in a tube containing 1 ml of distilled water. The tubes were sealed and cooked in a water bath for 10 min. 700 μ L aliquot of each sample was incubated for 4 min with 300 μ L of TE-buffer (tris-HCl/ 0.1M EDTA 10:1) and 1 ml of the PicoGreen reagent in the dark at room temperature. The fluorescence of the solution was measured on a fluorescence microplate reader Ultra384 (using standard fluorescein wavelengths of 485 nm for excitation and 520 nm for emission.) The fluorescence value was converted into a DNA amount using a calibration curve prepared with a λ -DNA standard.

4.8 Preparation of microspheres

4.8.1 Preparation of Kathon® 910 SB-loaded PDMS microspheres and unloaded PDMS microspheres

The preparation of Kathon® 910 SB-loaded PDMS microspheres and unloaded PDMS microspheres was performed in a 1000 ml glass-reactor equipped with a heating jacket and a vacuum sealed stirrer unit from HWS (Germany). The reactor was tempered by means of a cold-thermostat DC30 K20 from Thermohaake (Germany) and the pressure was regulated by means of a membrane-pump VAC 503 with a vacuum controller V800 from Buechi (Germany).

The microspheres were prepared according to the o/w solvent evaporation method and using the Sylgard® 184 silicone elastomer-kit from Dow Corning (Germany) as base material.

For the preparation of Kathon® 910 SB-loaded silicone microspheres an amount of 11.08 g of the base polymer silicone elastomer Sylgard® (component A), 1.108 g of the cross-linking agent (component B) and 0.313 g of Kathon® 910 SB* were dissolved in 31 ml of chloroform. This Kathon® /polymer solution (oil phase) was slowly added over 10 min to 550 ml of 4 % [w/v] aqueous PVA-solution (average $M_w = 61.000$) (water phase). The two phases were stirred at 380 rpm at room temperature and atmospheric pressure for 90 min, then under reduced pressure (200 mbar) for 60 min and finally at 50 °C and atmospheric pressure for a further 30 min. The formed microspheres were recovered by vacuum filtration, washed several times with deionized water and dried under vacuum. 90 % of the particles (microspheres) had a size smaller than 125 µm, 50 % smaller than 70 µm and the remaining 10 % a size smaller than 31 µm.

4.9 Investigation of the biocidal properties of Kathon® 910 SB-loaded PDMS microspheres

4.9.1 Agar diffusion hole test and dilution test

The tests were performed at the department of hygiene research of Henkel KGaA (Germany).

5 Literature

- ¹Lawrence J.R., Korber D.R., Hoyle B.D., Costerton J.W., Caldwell D.E., *J. Bacteriol.*, **173**, (1991), 6558
- ²Parsek M.R., Greenberg E.P., *Proc. Natl. Acad. Sci. USA*, **97**(16), (2000), 8789
- ³Costerton J.W., Lewandowski Z., Caldwell D.E., Korber D.R., Lappin-Scott H.M. *Annu. Rev. Microbiol.*, **49**, (1995), 711
- ⁴Kolter R, and Losick R., *Science*, **280**, (1998), 226
- ⁵Costerton J.W., Stewart P.S., Greenberg E.P., *Science*, **284**, (1999), 1318
- ⁶Nickel J.C., Ruseska I., Wright J.B., Costerton J.W., *Antimicrob. Agents Chemother.*, **27**, (1985), 619
- ⁷Elder M.J., Stapleton F., Evans E., Dart J.K., *Eye*, **9**, (1995), 102
- ⁸Brown M.R., Allison D.G., Gilbert P., *J. Antimicrob. Chemother.*, **20**, (1988), 777
- ⁹Dankert J., Hogg A.H., Feijen J., *CRC Crit. Rev. Biocompat.*, **2**, (1986), 219
- ¹⁰Finberg R.W., Moellering R.C., Tally F.P., Craig W.A., Pankey G.A., Dellinger E.P., West M.A., Joshi M., Linden P.K., Rolston K.V., Rotschafer J.C., Rybak M.J., *Clin. Infect. Dis.*, **39**(9), (2004), 1314
- ¹¹Pankey G.A., Sabath L.D., *Clin. Infect. Dis.*, **38**(6), (2004), 864
- ¹²Mulligan M.J.; Cobbs C.G., *Infect. Dis. Clin. North Am.*, **3**(3), (1989), 389
- ¹³Luellmann H., Mohr K., Wehling M., *Pharmacologie und Toxicologie*, Thieme Edition, Stuttgart, (2003)
- ¹⁴Green DW., *Expert Opin. Ther. Targets*, **6**(1), (2002), 1
- ¹⁵Koch A.L., *Clin Microbiol. Rev.*, **16**(4), (2003), 673
- ¹⁶Goessens W.H., *Eur. J. Clin. Microbiol. Infect. Dis.*, **12**, (1993), 9
- ¹⁷Wiese A., Gutschmann T., Sevdal U., *J. Endotoxin. Res.*, **9**(2), (2003), 67
- ¹⁸Hancock R.E.W., Patrzykat A., *Current Drug Targets-Infectious Disorders*, **2**, (2002) 79
- ¹⁹Tsubery H., *Biochemistry*, **39**, (2000), 11837
- ²⁰Tsubery H., *J. Med. Chem.*, **43**, (2000), 3085
- ²¹Novac O., Guenier A.S., Pelletier J., *Nucleic Acids Research*, **32**(3), (2004), 902
- ²²Carter A.P., Clemons W.M., Brodersen D.E., Morgan-Warren R.J., Wimberly B.T., Ramakrishnan V., *Nature*, **407**, (2000), 340

- ²³Hansen J.L., Ippolito J.A., Ban N., Nissen P., Moore P.B., Steitz T.A., *Mol. Cell*, **10**, (2002), 117
- ²⁴Stratton C.W., *Emerging Infectious Diseases*, **9**, (2003), 10
- ²⁵Yamada T, Nagata A., Ono Y., Suzuki Y., Yamanouky T., *Antimicrob. Agents Chemoter.*, **27**(6), (1985), 921
- ²⁶Bjelaković G., Stojanović I., ielaković G.B., Pavlović D., Kocić G., Daković-Milić A., *Medicine and Biology*, **9**, (2002), 201
- ²⁷Lyndal York J., Enzymes. Classification, kinetics and control. In: Devlin MT. Wiley-Liss. (Textbook of biochemistry with clinical correlations). New York, (1997)
- ²⁸Dessen A., Di Guilmi A.M., Vernet., Dideberg O., *Curr. Drug Targets Infect Disord.*, **1**(1), 2001, 63
- ²⁹Hotta K., Yamamoto H., Okami Y., Umezawa H., *J. Antibiot*, **34**(9), (1981), 1175
- ³⁰Tally FP, Malamy MH, Scand., *J. Infect. Dis. Suppl.*, **35**, (1982), 37
- ³¹Mohd-Zain Z., Turner S.L., Cerdeno-Tarraga A.M., Lilley A.K., Inzana T.J., Duncan A.J., Harding R.M., Hood D.W., Peto T.E., Crook D.W., *J. Bacteriol.*, **186**(23), (2004), 8114
- ³²Gorman S.P., Jones D.S., Report, Business briefing: medical device manufacturing and Technology, (2002), Medical Devices Group, School of Pharmacy, Queen's University Belfast
- ³³Road I., Buzaid A., Rhyne J., Hachem, Darouiche R, *Clinical Infectious Diseases*, **25**(1), (1997), 149
- ³⁴Leung J.W., Lau G.T., Sung J.J., Costerton J.W., *Gastrointest. Endosc.*, **38**, (1992), 338
- ³⁵DiTizio V, Ferguson GW, Mittelman MW, Khoury AE, Bruce AW, DiCosmo F, *Biomaterials*, **19**(20), (1998), 1877
- ³⁶Gottenbos B., van der Mei H.C., Klatter F., Nieuwenhuis P., Buscher H.J., *Biomaterials*, **23**, (2002), 1417
- ³⁷Roderick G. Flemming, Christopher C. Capelli, Stuart L. Cooper, Richard A. Proctor. *Biomaterials*, **21**, (2000), 273
- ³⁸Nagamune H., Maeda T., Ohkura K., Yamamoto K., Nakajima M., Kourai H., *Toxicol In Vitro*, **14**, (2000), 139
- ³⁹Vacheethasanee K., Marchant R.E., Student Research Award in the Ph. D. Degree Candidate Category, World *Biomaterials Congress 2000*, Kamuela, H I, May, 15-20, 2000, 302

-
- ⁴⁰Jansen B., Kohnen W., *J. Ind. Microbiol.*, **15**, (1995), 391
- ⁴¹Kwok C.S., Wan C., Hendricks S., Bryers J.D., Hobett T.A., Rather B.D., *Journal of Controlled Release*, **62**, (1999) 2989
- ⁴²Schierholz JM, Steinhouser H., Rump A.F.E., Berkels R., Pulver G., *Biomaterials*, **18**, (1997), 839
- ⁴³Tatsuo T., *Macromol. Mater. Eng.*, **286**, (2001), 63
- ⁴⁴Telford G., Wheeler D., Williams P., Tomkins P.T., Appleby P., Sewell H., Stewart G.S.A., Bycroft B.W., Pritchard D.I., *Infection and Immunity (Infect Immun)*, **66**, (1998), 36
- ⁴⁵Dong Y-H., Wang L-H., Xu J-L., Zhang H-B., Zhang X-F, Zhang L-H., *Nature*, **411**, (2001), 813
- ⁴⁶David J. Stickler, Nicola S. Morris, Robert J. C. McLean, and Clay Fuqua. *Applied and Environmental Microbiology*, **64**(9), (1998), 3486
- ⁴⁷Davies D.G., Parsek M.R., Pearson J.P., Iglewski B.H., Costerton J.W., Greeberg E.P., *Science*, **280**, (1998), 295
- ⁴⁸DeLisa M.P., Bentley W., *Microbial Cell Factories*, (2002), 1
- ⁴⁹Nealson KH, Platt T, Hastings JW., *J Bacteriol.*, **104**, (1970), 313
- ⁵⁰Nealson KH, Hastings JW., *Microbiol Rev.*, **43**, (1979), 496
- ⁵¹de Kievit T.R., Iglewski B.H., *Infection and Immunity*, **68**, (2000), 4839
- ⁵²Pearson J.P., Van Delden C., Iglewski B.H., *Journal of bacteriology*, **181**(4), (1999), 1203
- ⁵³de Nys, R., Wright A.D., Koenig G.M., Sticher O., *Tetrahedron*, **49**, (1993), 11213
- ⁵⁴Maximilien R., de Nys R., Holmstrom C., Gram L., Givskov M., Crass K., Kjelleberg S., Steinberg P., *Aquat. Microb. Ecol.*, **15**, (1998), 233
- ⁵⁵De Nys R., Dworjanyn S., Steinberg P.D., *Mar. Ecol. Prog. Ser.*, **162**, (2002), 79
- ⁵⁶Manefield M., de Nys R., Kumar N., Read R., Givskov M., Steinberg P., Kjelleberg S., *Microbiology*, **145**, (1999), 283
- ⁵⁷Givskov M., de Nys R., Manefield M., Gram L., Maximilien R., Eberl L., Molin S., Steinberg P., Kjelleberg S., *Journal of bacteriology*, (1996), 6618
- ⁵⁸Manefield M., (Bovbjerg Rasmussen T., Henzter M., Andersen J. B., Steinberg P., Kjelleberg S., and Givskov M., *Microbiology*, **148**, (2002), 1119
- ⁵⁹Ren D., Sims J.J., Wood T.K., *Environmental Microbiology*, **3**(11), (2001), 731
- ⁶⁰Ren D., Sims J.J., Wood T.K., *Letters in Applied Microbiology*, **34**, (2002), 293

- ⁶¹Baveja J.K., Nordon R.E., Hume E.B.H., Kumar N., Willcox M.D.P., Poole-warren L.A., *Biomaterials*, (2004), 5013
- ⁶²Hume E.B.H, Baveja J.K., Muir B., Schubert T.L., Kumar N., Kjelleberg S, Griesser H.J., Thissen H., Read R., Poole-Warren L.A., Schindhelm K., Willcox M.D.P., *Biomaterials*, **25**, (2004) 5023
- ⁶³Gov Y., Bitler A., Dell' Acqua G., Torres J.V., Balaban N., *Peptides*, **22**, (2001), 1609
- ⁶⁴Giacometti A., Cirioni O., Gov Y., Ghiselli R., Del Prete M.S., Mocchegiani F., Saba V., Orlando F., Scalise G., Balaban N., Dell' Acqua G. *Antimicrobial Agents and Chemotherapy*, (2003), 1979
- ⁶⁵Balaban N., Gov Y., Bitler A., Boelaert J.R., *Kidney International*, **63**, (2003), 340
- ⁶⁶Balaban N., Giacometti A., Cirioni O., Gov Y., Ghiselli R., Mocchegiani F., Viticchi C., Del Prete M.S., Saba V., Scalise G., Dell' Acqua G., *The Journal of Infectious Diseases*, **187**, (2003), 625
- ⁶⁷Dell' Acqua G., Giacometti A., Cirioni O., Ghiselli R., Saba V., Scalise G., Gov Y., Balaban N., *Journal of Infectious Diseases*, **190**, (2004), 318
- ⁶⁸Dong Y.-H, Xu J.-L., Li X.-Z, Zhang L.-H., *Proc. Natl. Acad. Sci.*, **97**, (2000), 3526
- ⁶⁹Manny A.J., Kjelleberg S., Kumar N., de Nys R., Read R.W., Steinberg P., *Tetrahedron*, **53**, (1997), 15813
- ⁷⁰Beechan C.M., Sims J.J., *Tetrahedron Letters*, **19**, 1649
- ⁷¹N. Kumar, Read R.W., Synthesis of cyclic compounds, PQ8419, (2002)
- ⁷²Zimmer R., Collas M., Roth M., Reißig H.-U., *Liebigs Ann. Chem.*, (1992), 709
- ⁷³Colombo P., Bettini R., Santi P., Peppas N.A., *Pharmaceutical Science and Technology Today*, **3**, (2000), 198
- ⁷⁴Khare A., Peppas N.A., *J. of Biomaterial Science and Polymer Education*, **4**, (1993), 275
- ⁷⁵Ritger P.L., Peppas N.A., *J. of Controlled Release*, **5**, (1987), 37
- ⁷⁶Merrifield R.B., *J. Am. Chem. Soc.*, **85**, (1963), 2149
- ⁷⁷Jakubke H.-D., *Peptide: Chemie und Biologie*, Spektrum Akadem. Edition, Heidelberg, (1996)
- ⁷⁸Gutte B., Merrifield R.B., *J. Am. Chem. Soc.*, **91**, (1969), 501
- ⁷⁹Atherton E., Fox H., Harkiss D., Logan C.J, Sheppard R.C., Williams B.J., *J. Chem. Soc., Chem Commun.*, (1978), 537

- ⁸⁰Meienkofer J., Waki M., Heimer E.P., Lambros T.J., Makofske R.C., Chang C.D., *Int. J. Pept Prot. Res.*, **13**, (1979), 35
- ⁸¹Knorr R., Trzeciak A., Bannwarth W., Gillessen D., *Tetrahedron Lett.*, **30**, 1989, 2739
- ⁸²Gude M., Ryf J., White P. D., *Letters in Peptide Science*, **9**, (2002), 203
- ⁸³Le Nguyen D., Castro B., *Pept. Chem.*, **231**, (1998), 231
- Coste J., Le Nguyen D., Castro B., *Tetrahedron Lett.*, **31**, (1990), 205
- ⁸⁴Barlos K., Gatos D., Koutsogianni S., *J. Peptide Res.*, **51**, (1998), 194
- ⁸⁵Karas M., Hillenkamp F., *Anal. Chem.*, **60**, (1988), 2299
- ⁸⁶Hillenkamp F., Karas M., Beavis R.C., Chait B.T., *Anal. Chem.*, **63**, (1991), 1193
- ⁸⁷Wang R., Chait B.T., *Curr. Opin. Biotechnol.*, **5**, (1994), 77
- ⁸⁸Beavis R.C., Chait B.T., *Anal. Chem.*, **62**, (1990), 1836
- ⁸⁹Stults J.T., *Curr. Opin. Struct. Biol.*, **5**, (1995), 691
- ⁹⁰Strupat K., Karas M., Hillenkamp F., *Int. J. Mass Spectrom. Ion Processes*, **111**, (1991), 89
- ⁹¹Beavis R.C., Chait B.T., *Rapid Commun. Mass Spectrom.*, **3**, (1989), 432
- ⁹²Beavis R.C., Chaudhury T., Chait B.T., *Org. Mass Spectrom.*, **27**, (1992), 156
- ⁹³Juhasz P., Costello C.E., Biemann K., *J. Am. Soc. Mass Spectrom.*, **4**, (1993), 399
- ⁹⁴Gobom J., Nordhoff E., Mirgorodskaya E., Ekman R., Roepstorff P., *J. Mass Spectrom.*, **34**, (1999), 105
- ⁹⁵Winston R.L., Fitzgerald M.C., *Anal Biochem.*, **262**, (1998), 83
- ⁹⁶Brockman A.H., Dodd B.S., Orlando R., *Anal Chem.*, **69**, (1997), 4716
- ⁹⁷Blackledge J.A., Alexander A., *J. Anal Chem.*, **67**, (1995), 843
- ⁹⁸Zhang H. Y., Caprioli R.M., *J. Mass Spectrom.*, **31**, (1996), 690
- ⁹⁹Vorm O., Roepstorff P., Mann M., *Anal. Chem.*, **66**, (1994), 3281
- ¹⁰⁰Kussman M., Nordhoff E., Rahbek-Nielsen H., Haebel S., Rossel-Larsen M. Jakobsen L., Gobom J., Mirgorodskaya E., Kroll-Kristensen A., Palm L., Roepstorff P. *J. Mass Spectrom.*, **32**, (1997) 593
- ¹⁰¹Perkins J.R., Smith B., Gallagher R.T., Jones D.S., Davis S.C., Hoffman A.D., Tomer K.B., *J. Am Soc. Mass Spectrom.*, **4**, (1993), 670
- ¹⁰²Billeci T.M., Stults J.T., *Anal. Chem.*, **65**, (1993), 1709
- ¹⁰³Amado F.M.L., Dominigues P., Santa-Marques M.G., Ferrer-Correia A.J., Tomer K.B., *Rapid Commun. Mass Spectrom.*, **11**, (1997), 1347

- ¹⁰⁴Kratzer R., Eckerskorn C., Karas M., Lottspeich F., *Electrophoresis*, **19**, (1998), 1910
- ¹⁰⁵Grinnell F., *Int. Rev. Cytol.*, **53**, (1978), 65
- ¹⁰⁶Baier R.E., *Science*, **168**, (1968), 1360
- ¹⁰⁷Schaffer G. H., *American Machinist & Automated Manufacturing*, **132**, (1988), 17
- ¹⁰⁸Klee D., Ademovic Z., Bosserhof A., Hoecker H., Maziolis G., Erli H-J, *Biomaterials*, **24**, (2003), 3663
- ¹⁰⁹Clochard M.-Cl., Bègue J., Lafon A., Caldemaison D., Bittencourt C., Pireaux J-J., Betz N., *Polymer*, **45**, (2004), 8683
- ¹¹⁰Tamura N., Shinohara K., *Prep Prog Polym Phys Japan*, **6**, (1963), 265
- ¹¹¹elbert JN, Wagner BE, Pointdexter EH, Kevan L., *J Polym Sci, Polym Phys Edn*, **13**, (1975), 825
- ¹¹²Suryanarayana D., Kevan L., *J. Am Chem Soc*, **104**, (1982), 6251
- ¹¹³Betz N., Petersohn E., le Moel A., *Radiat Phys Chem*, **47**, (1996), 411
- ¹¹⁴Benes P., Paulenova M., *Colloid and Polym Sci*, **251**, (1973) 766
- ¹¹⁵Van Wagenen RA, Coleman DL, King RN, Trioro P., Brostrom L., Smith LM, Gregonis DE, Andrade JD, *J. Colloid Interface Sci.*, **84**, (1981),155
- ¹¹⁶Samal RK, Iwata H., Ikada Y., *Physicochemical Aspects of Polymer Surfaces: Mittal, KL, (Ed) Plenum, New York*, **2**, (1983),801
- ¹¹⁷Kang ET, Tan KL, *Macromolecules*, **29**, (1996), 6872
- ¹¹⁸van Delden C.J., Bezemer J.M., Engbers G.H.M.,Feijen J., *J. Biomater. Sci. Polymer Edn.*, **8**(4), (1996), 251
- ¹¹⁹Lahiri J., Isaacs L., Tien J., Whitesides M., *Anal. Chem.*, **71**, (1999), 777
- ¹²⁰Blotta I., Prestinaci F.,Mirante S., Cantafora A., *Ann. Ist. Super Sanità*, **41**(1), (2005), 119
- ¹²¹Singer V.L., Jones J.J., Yue S. T., Haugland R. P., *Analytical Biochemistry*, **249**, (1997), 228
- ¹²²Hack S.P., Christie M.J., *Crit. Rev. Neurobiol.*, **15**(3-4), (2003), 235
- ¹²³Auger-Messier M., Arguin G., Chaloux B., Leduc R., Escher E., Guilenette G., *Mol. Endocrinol.*, **18**(12), (2004), 2967
- ¹²⁴Montastruc JL, Galitzky J, Berlan M, Montastruc P., *Therapie*, **48**(5), (1993), 421

-
- ¹²⁵Conde-Salazar L., Flis M., Gonzales M.A., Guimaraens D.; Rev. Esp. Alergol. Immunol. Clin., **13**, (1998), 268
- ¹²⁶Laopaiboon L., Smith R. N., S, Hall, J.; J. of Applied Microbiology, **91**, (2001), 93
- ¹²⁷Al-Maaich A., Flanagan D.R., *J. Control. Release*, **70**(1-2), (2001), 169
- ¹²⁸Fu X., Ping Q., Gao Y., *J. Microencapsul.*, **22**(1), (2005), 57
- ¹²⁹Zhu KJ, Jiang H.L., Yasuda H., Ichimaru A, Yamamoto K., Lecomte P., Jerome R., *J. Microencapsul.*, **22**(1), 25
- ¹³⁰Spackman D.H., Stein W.H., Moore S., Anal. Chem., **30**, (1958), 1190
- ¹³¹Sheppard R.C., J. Pept. Sci., **9**, (2003), 545
- ¹³²Kaiser, Colescott R.L., Bossinger C.D., Cook P., Anal. Biochem, **34**, (1970), 595

Curriculum Vitae

Personal Details

Name	Carla Terenzi
Date of Birth:	29 th December, 1973
Place of Birth	Penne (Pescara), Italy
Nationality:	Italian

Education

09/1979-06/1987	Elementary school, Città S. Angelo (PE), Italy
09/1987-07/1992	Gymnasium, Pescara, Italy
10/1992-10/1999	Master studies in Pharmaceutical Chemistry and Technology at the University of Perugia, Italy
11/1999-04/2000	Practical training in a pharmacy in Perugia, Italy
06/2000	Qualification to exercise the profession of pharmacist at the University of Perugia, Italy
01/2002-05/2006	Doctoral studies (Ph.D. work) under the supervision of Prof. Dr. rer. nat. Hartwig Höcker at the Chair of Textile and Macromolecular Chemistry, RWTH Aachen, Germany. „Novel strategies for the inhibition of biofilm formation on polymer surfaces“
10/2004-12/2004	Visiting researcher at the Ian Wark Research Institute, Adelaide, Australia

Work Experience

03/2001-10/2001	Research assistant at the Pharmaceutical Institute, Pharmaceutical Chemistry Poppelsdorf, University of Bonn
-----------------	--